

EDWARDS AQUIFER STORAGE ASSESSMENT
KINNEY COUNTY TO HAYS COUNTY, TEXAS

by

S. D. Hovorka, S. C. Ruppel, A. R. Dutton, and Joseph Yeh

assisted by

S. S. Parthasarathy, R. A. Johns, and Martina Blüm

Prepared for
Edwards Underground Water District
under Contract No. 93-04-F0

Bureau of Economic Geology
W. L. Fisher, Director
The University of Texas at Austin
Austin, Texas 78713-7508

December 1993

EDWARDS AQUIFER STORAGE ASSESSMENT
KINNEY COUNTY TO HAYS COUNTY, TEXAS

by

S. D. Hovorka, S. C. Ruppel, A. R. Dutton, and Joseph Yeh

assisted by

S. S. Parthasarathy, R. A. Johns, and Martina Blüm

Prepared for
Edwards Underground Water District
under Contract No. 93-04-F0

Bureau of Economic Geology
W. L. Fisher, Director
The University of Texas at Austin
Austin, Texas 78713-7508

December 1993

CONTENTS

Abstract.....	1
Introduction.....	2
Geologic Setting	4
Methods	9
Stratigraphic Model.....	9
Log Acquisition.....	10
Log Calculation of Porosity.....	11
Measurement of Porosity in Core.....	16
Neutron- and Resistivity-Log Calibration of Cored Wells.....	16
Porosity Calculation from Wells with Scaled Curves.....	22
Porosity Calculation from Wells with Unscaled Curves.....	24
Use of Barometric Efficiency to Estimate Aquifer Storativity.....	27
Theory.....	28
Analysis Technique	32
Results	33
Stratigraphic Model.....	33
Platform Cycle Types	34
Subtidal low-energy cycles.....	34
Subtidal low- to high-energy cycles.....	38
Subtidal low-energy to Intertidal/supratidal cycles.....	38
Subtidal high-energy to Intertidal/supratidal cycles.....	39
Hypersaline cycles	39
Maverick Basin Facies	43
Facies Relationships.....	45
Log-Based Correlation	47

Porosity Description from Core and Thin Section.....	50
Intergranular Porosity in Grainstones.....	50
Intercrystalline Porosity in Dolostone.....	52
Solution-Enhanced Intergranular/Intercrystalline Porosity	52
Fracture- and Solution-Enhanced Fracture Porosity	55
Cavernous Porosity Produced by Gypsum or Carbonate Dissolution	58
Intraclastic Porosity in Breccia.....	58
Porosity/Permeability Relationships.....	59
Porosity Calculation.....	60
Porosity Distribution	67
Analysis of Water-Level Response to Atmospheric Pressure Changes.....	73
Discussion.....	79
Additional Studies.....	85
Conclusions	87
Acknowledgments.....	89
References	89
Glossary.....	96

Figures

1. Location of the Edwards aquifer study area.....	5
2. Geologic setting of the Edwards aquifer study area.....	6
3. Stratigraphy of the Edwards Group.....	7
4. Specific conductance map used to estimate R_{wa} in resistivity log porosity calculations.....	23
5. Cumulative frequency plots of representative calibrated porosity logs	25
6. Idealized barometric efficiencies and water-level fluctuations.....	29
7. Typical fluctuations in water level and barometric pressure.....	30

8. Idealized high-frequency cycle.....	35
9. Typical grainstones and tidal-flat facies	36
10. Representative depositional fabrics	40
11. Representative depositional fabrics	44
12. Systems tract interpretation of the Edwards Group on the basis of examination of cores and outcrops.....	46
13. Log cross section showing representative logs and the stratigraphic units that were identified regionally.....	48
14. Diagenetic enhancement of porosity.....	51
15. Diagenetic enhancement of porosity.....	53
16. Diagenetic enhancement of porosity.....	56
17. Calculated (scaled neutron and unscaled resistivity) and measured porosity, USGS Randolph FM 1604 well, AY 68-30-807	61
18. Calculated (unscaled neutron and resistivity) and measured porosity, USGS Castle Hills, AY 68-29-910.....	62
19. Calculated (unscaled neutron and resistivity) and measured porosity, TWDB TD-3 well, TD 69-39-504	63
20. Calculated (unscaled neutron and resistivity) and measured porosity, USGS Sabinal well, YP 69-37-402.....	64
21. Calculated (unscaled neutron and resistivity) and measured porosity, TWDB YP-4 well, YP 69-42-709	65
22. Correspondence of core-calibrated neutron and resistivity logs.....	66
23. Northwest-southeast porosity cross section B-B', Bexar County.....	69
24. North-south porosity cross section C-C', Medina County	70
25. East-west porosity cross section D-D' along the length of the aquifer.....	71
26. Records of atmospheric pressure and water-level hydrographs used to estimate barometric efficiency.....	75
27. Records of atmospheric pressure and water-level hydrographs used to estimate barometric efficiency.....	76
28. Records of atmospheric pressure and water-level hydrographs used to estimate barometric efficiency.....	77

Tables

1. Well data base.....	12
2. Plug porosity and permeability.....	17
3. Calculation of specific storage and storativity in the Edwards aquifer on the basis of barometric efficiency and log-based porosity measurements.....	74

Plates (In pocket)

1. Locations of wells used in this study	
2. Isopach of the lower part of the Edwards aquifer (Walnut-Kalner-lower Devils River-West Nueces-McKnight interval)	
3. Isopach of the upper part of the Edwards aquifer (Person-Georgetown-upper Devils River-Salmon Peak interval)	
4. Isopach of the entire Edwards aquifer used in the model	
5. Average porosity in the lower part of the Edwards aquifer (Kalner-lower Devils River-West Nueces-McKnight interval)	
6. Average porosity in the upper part of the Edwards aquifer (Person-upper Devils River-Salmon Peak interval)	
7. Average porosity in the entire Edwards aquifer	
8. Estimated total Edwards pore volume in porosity (percent) times feet	

ABSTRACT

The distribution of water in the Edwards aquifer was assessed using a core- and log-based stratigraphic study that included 200 neutron and resistivity logs and 300 porosity and permeability plug analyses. The Kainer, Person, Devils River, West Nueces, McKnight, and Salmon Peak Formations of the Edwards Group were investigated during this study. The aquifer extends over 3,111 mi² (8,004 km²) and thickens toward the south from approximately 500 to 780 ft (150 to 240 m). In the Edwards outcrop, the aquifer thins northward because of erosion and decreased saturated thickness. Porosity data were interpolated between wells to create a three-dimensional cell-based model of porosity.

Porosity distribution reflects both the depositional rock fabric and later diagenesis. Small-scale vertical variations in porosity are the result of facies changes caused by high-frequency cyclicity in the depositional environment. Vertical facies stacking influences the amount of dolomitization and diagenetic enhancement of porosity. Subtidal facies deposited during major sea-level highstands are generally undolomitized and exhibit low porosity (4- to 12-percent porosity). Grainstones at cycle tops in the Kainer, Person, and Devils River Formations are typically high-porosity intervals with high depositional porosity that may have additional solution enlargement of pores and pore throats (20- to 42-percent porosity). Dolomitized subtidal facies have very high porosity in intervals with stacked tidal-flat cycles because of preferential dolomite dissolution.

The average porosity of the Edwards aquifer in the study area is 21.7 percent. Variation in average porosity reflects depositional environment and possibly structural and hydrologic influence on secondary porosity development and cementation. Low porosity is characteristic of the West Nueces and McKnight Formations of the Maverick Basin. The overlying Salmon Peak Formation has moderate to high porosity. In the Devils River, Kainer, and Person Formations, local high and low porosity is encountered in structurally complex areas that may be related to variable ground-water flow rates and chemistry and consequent variations in pore enlargement or cementation. A high-porosity area is found in southern Medina and

southwestern Bexar Counties on both sides of the saline–freshwater interface known as the bad water line.

The total water-filled pore volume of the Edwards aquifer within the study area is 215 million acre-feet. The volume in the unconfined part of the aquifer, above the 1984 potentiometric surface, which is among the lowest ever recorded, is 6.9 million acre-feet.

Storativity of the confined part of the aquifer was estimated using barometric efficiency and net porosity. Barometric efficiency was calculated by comparing water-level hydrographs in nine observation wells with atmospheric pressure changes. The storativity calculated using this method averages 2.6×10^{-4} . This approach has the potential for quantifying variations in storativity throughout the confined Edwards aquifer but must be verified by comparison with results of aquifer tests. Such data will improve prediction of how water levels will respond to withdrawal of water from the aquifer.

INTRODUCTION

The prolific Edwards aquifer in South-Central Texas is a geologically complex water resource that has been heavily developed. The Edwards aquifer at present is the sole source of water for the city of San Antonio, Texas, and is the main water resource for agriculture and industry in Bexar, Medina, and Uvalde Counties, Texas. Discharge from the aquifer in Comal and Hays Counties, Texas, feeds springs that are attractions for a tourist industry and have been shown to be critical habitat for a number of endangered species. Ground-water production from the Edwards has exceeded recharge during drought years and has the potential to exceed average annual recharge. Prolonged overdraft without some mitigation would temporarily cause water levels to decline, some wells in the upper reaches of the unconfined part of the aquifer to go dry, and discharge at the springs to decrease to a negligible volume. Evaluating the legal consequences and the total social, economic, and ecological benefits associated with aquifer

management decisions requires ongoing efforts to understand the complex hydrogeology of the aquifer and its water resource (Technical Advisory Panel, 1990).

Among the hydrogeologic information needed, for example, to build more detailed models of ground-water flow, are maps of the three-dimensional, geologically controlled distribution of ground water stored in the Edwards aquifer. Previous estimates of storage were made by extrapolating estimated effective porosity throughout the Edwards aquifer on the basis of samples from a few cored wells, and were considered movable water rather than total water in storage (Maclay, 1989). The objective of this study is to improve the estimate of the total water content of the Edwards aquifer by (1) using a large data base of porosity logs, (2) generating new maps of Edwards aquifer thickness and porosity, correlated using updated facies and diagenetic models, and (3) examining the porosity distribution throughout the aquifer. This study used 200 wireline logs of varying quality to measure aquifer thickness and the amount and distribution of porosity at many locations throughout the aquifer. Log response was calibrated by selecting 300 core plugs from representative lithologies at 1-ft (0.3-m) spacing for porosity and permeability analysis. Porosity logs were then interpolated along stratigraphic subdivisions to define the three-dimensional distribution of porosity in the entire Edwards aquifer. The extensive data base of porosity, well log, and stratigraphic information assembled in this study in a Geographic Information System (GIS) can be updated to include results of future well surveys and hydrogeologic investigations.

The question of how much water can be produced from the Edwards was not addressed by this study of the distribution of porosity and in-place water storage. Storativity and permeability are the main physical controls on the amount of water that can be produced from the Edwards aquifer and the amount of water-level decline resulting from that production. The feasibility of estimating aquifer storativity on the basis of the porosity data and water-level hydrographs was considered. The response of water levels in the confined aquifer to changes in atmospheric pressure potentially can provide additional data and insights about the hydrologic properties of the Edwards aquifer. However, to calculate porosity independent of well logs, additional field

data on storativity must be collected through aquifer tests that use one or more observation wells in conjunction with a production well.

GEOLOGIC SETTING

The Edwards aquifer is composed of highly porous limestones and dolostones of the Lower Cretaceous Edwards Group. The southern and eastern limits of the aquifer are marked by the saline–freshwater interface commonly known as the bad water line (fig. 1). The northern limit of the aquifer lies in the outcrop of the Edwards Group where the thickness of the aquifer becomes negligible. The western limit of the study area is the mapped drainage divide near Brackettville, Kinney County, and the northeast edge is the drainage divide near Kyle, Hays County (fig. 1). However, porosity data were generated beyond these boundaries to minimize edge effects and so that new volumes can be calculated as the aquifer boundaries become better known.

The Edwards aquifer lies within the Balcones fault zone (fig. 2). High-angle normal faults and grabens of this system produce a net displacement of 2,000 ft (600 m) down toward the coast (Maclay and Small, 1986). Individual faults have a strong influence on permeability (Senger and Kreitler, 1984; Maclay and Small, 1986; De la Garza and Slade, 1986; Maclay and Land, 1988) and a lesser influence on porosity development.

The depositional setting of the Edwards Group (Smith, 1964; Rose, 1972) strongly affects the amount, type, and distribution of porosity. Cyclic shallow-water carbonates dominate the Person and Kalner Formations of the San Marcos Platform (figs. 2 and 3). The Devils River Formation of the platform margin is dominated by grainstones. In the Maverick Basin, shallow-water subtidal carbonates of the West Nueces Formation are overlain by anhydrite and carbonate of the McKnight Formation (figs. 2 and 3). The upper Edwards equivalent in the Maverick Basin is composed of moderately porous, fine-grained grainstones, packstones, and wackestones of the Salmon Peak Formation.

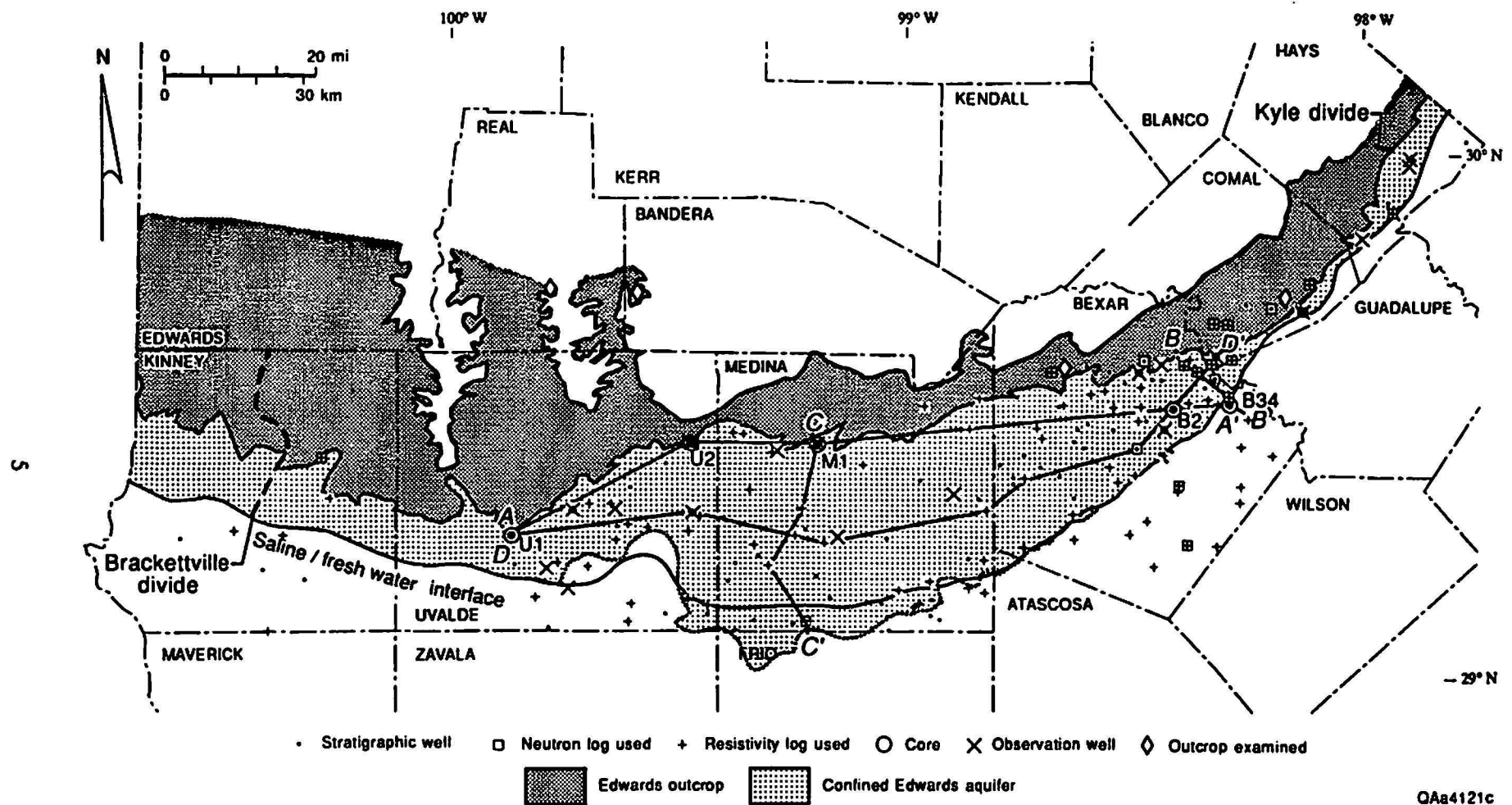


Figure 1. Map of Edwards aquifer study area, showing location of saline–freshwater interface (bad water line) (Brown and others, 1992; Schultz, 1992; Schultz, 1992), confined Edwards aquifer, unconfined Edwards aquifer, updip limit of the Edwards Group, well data base, and cross section lines. Outcrop limits of Edwards Group are from 1:2500,000-scale Geologic Atlas of Texas (Waechter and others, 1977; Proctor and others, 1979; Brown and others, 1983; Proctor and others, 1988). Well locations numbered in plate 1.

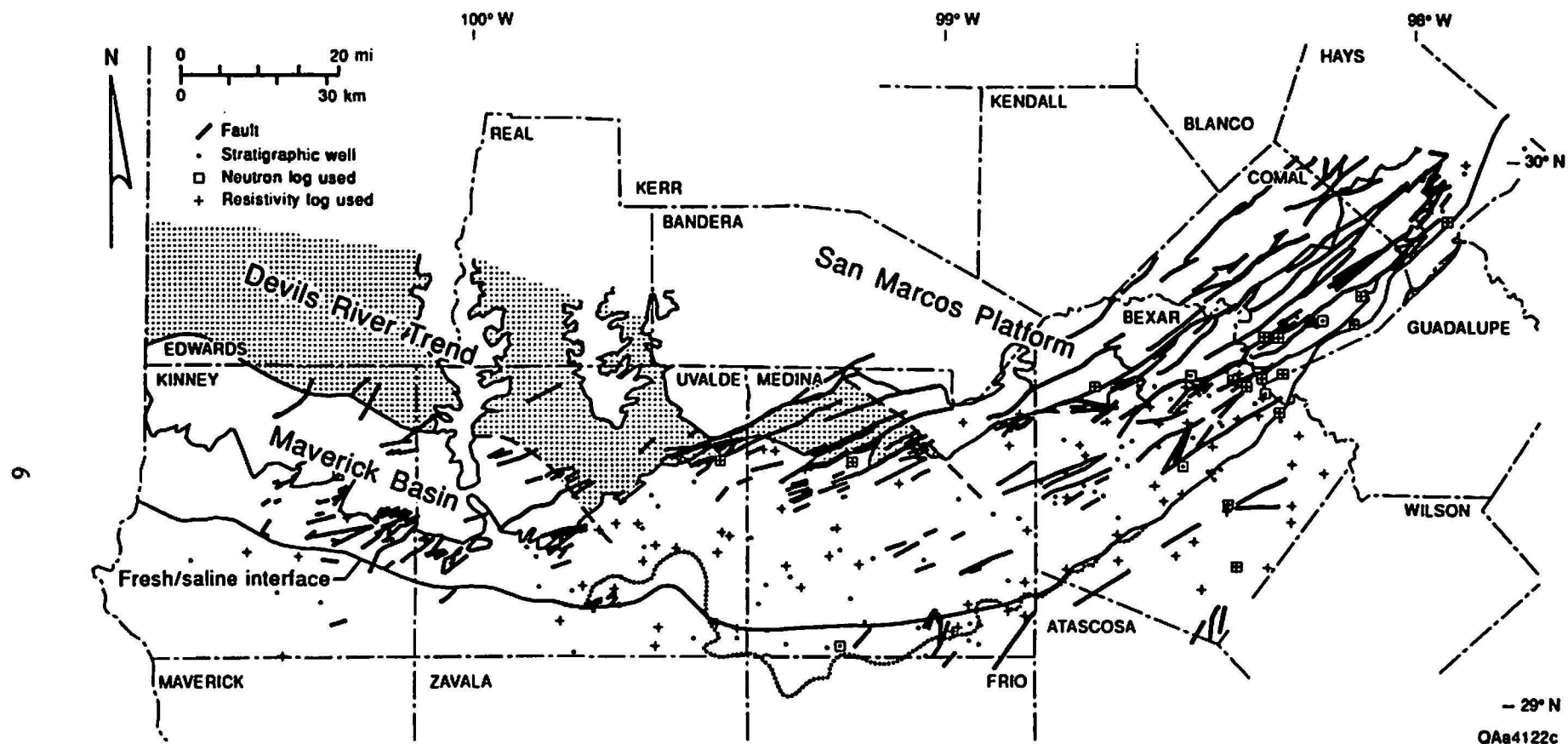


Figure 2. Geologic setting of Edwards aquifer study area, showing location of San Marcos Platform, Devils River trend, and Maverick Basin. Major faults of Balcones Fault system are shown. Saline-freshwater interface (bad water line), updip limit of Edwards Group, and well data base shown for reference.

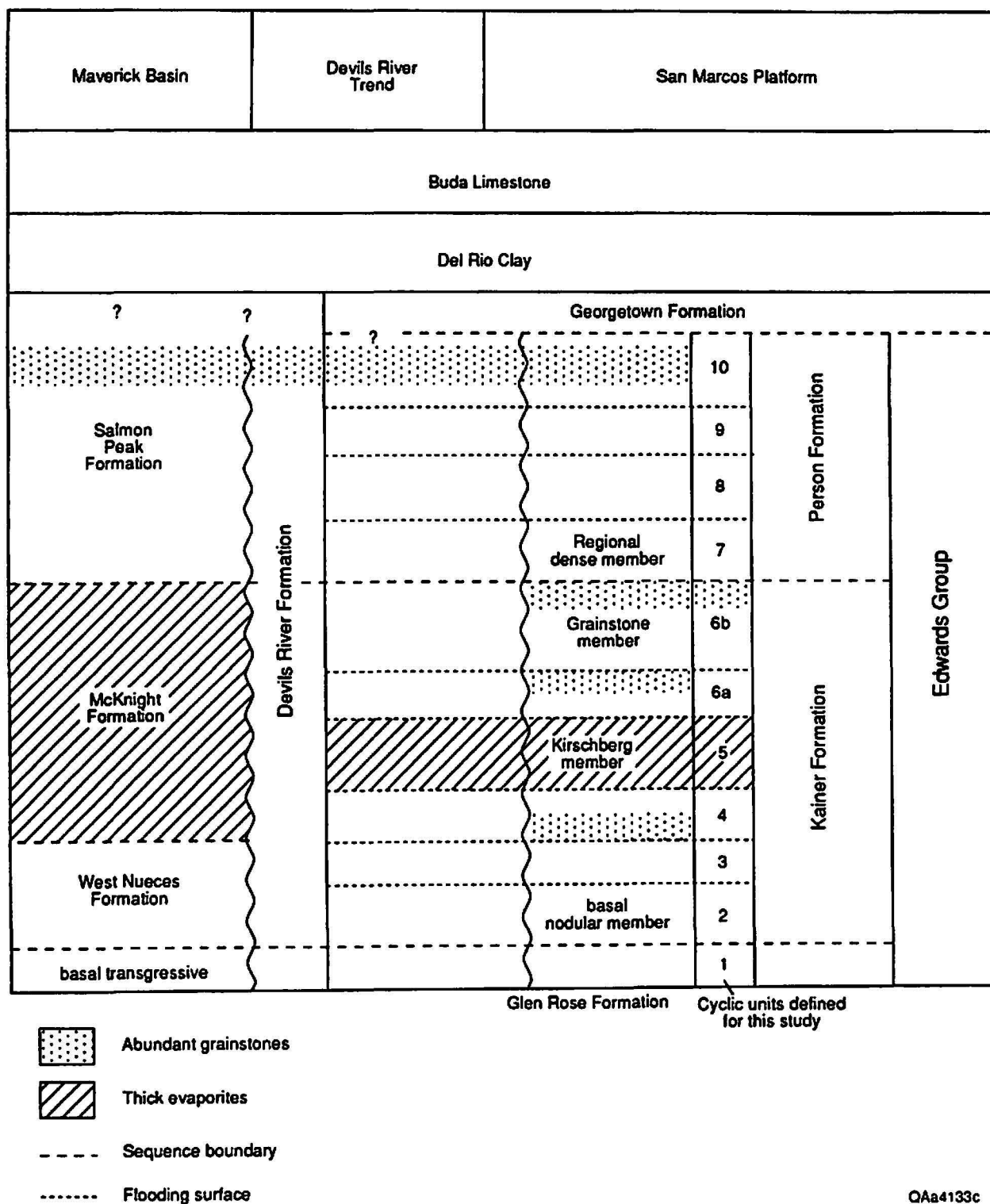


Figure 3. Stratigraphy of Edwards Group. Simplified from Rose (1972) and modified to show preliminary interpretation of major sequence stratigraphic elements.

Recharge occurs where streams cross the Edwards aquifer outcrop (Woodruff and Abbott, 1986). Flow in the aquifer is from highlands in the west (Kinney and Uvalde Counties) toward discharge points at large springs in the east (Hays and Comal Counties). High water usage coincides with metropolitan areas in Bexar County and agricultural areas in Uvalde and Medina Counties (Technical Advisory Panel, 1990).

The interface between fresh water and more saline water, defined where total dissolved solids (TDS) exceed 1,000 mg/L, defines the southern and eastern boundaries of the Edwards aquifer (figs. 1 and 2). The data set used in this porosity study included well logs in southernmost Bexar, Medina, and Uvalde Counties on both sides of the interface (fig. 1). The saline-freshwater interface mapped by Brown and others (1992) was used as a boundary for calculating total volume of fresh water stored in the Edwards aquifer. The location of the interface recently has been resolved in greater detail on the basis of resistivity logs (Schultz, 1992). The log-based analysis identified an area in southwestern Medina and northern Frio Counties where fresh water extends as much as 9 miles (14 km) south of the saline-freshwater interface shown by Brown and others (1992). It also identified an area in south-central Uvalde County where saline water is north of the previously mapped interface (figs. 1 and 2). The validity of the log-based salinity measurements was confirmed by a research well drilled by the EUWD in southern Medina County in the summer of 1993 (John Waugh, personal communication, 1993). The total volume of water contained in the Edwards aquifer bounded by the Brown and others (1992) line is calculated in this report along with the volume of water in the Edwards contained between the Brown and others (1992) and Schultz (1992) lines. As shown by this example, the computer-based porosity model allows recalculation to incorporate additional data from future studies.

METHODS

In this study, the primary method used to assess the amount of water in the Edwards aquifer is log-based measurement of porosity in boreholes, followed by interpolation of these values between boreholes to estimate total porosity in a rock volume. Water-level data from observation wells were used to calculate the barometric efficiency of the aquifer and, using log-based porosity calculations, estimate aquifer storativity.

Interwell porosity interpolations were created using a three-dimensional model built with Stratamodel© Stratigraphic Geocellular Modeling (SGM) software. With this approach, (1) interwell interpolation is facilitated, (2) assessments of total porosity can be upgraded as new data are acquired, and (3) the model can be manipulated readily to examine different aspects of the aquifer. The steps used in data base construction are: (1) log acquisition, (2) stratigraphic model construction, (3) calibration of log porosity, and (4) interwell porosity interpolation.

Stratigraphic Model

The stratigraphic model was used to (1) measure the total thickness of the Edwards aquifer, (2) control interwell porosity interpolation, and (3) guide assumptions made during log calibration.

Seven cores and four outcrops were examined to identify the high-frequency cycles that define the genetic subdivisions of the Edwards Group (fig. 1). A cross section showing correlation of high-frequency cycles and lateral facies changes was prepared. Corresponding genetic subdivisions were identified on geophysical well logs. To update the stratigraphic model of Rose (1972) and incorporate modern concepts of sea-level control on carbonate sedimentation, cycle patterns were examined from the San Marcos Platform toward the Gulf Coast and into the Maverick Basin. Stratigraphic boundaries used for this study, therefore, differ in some areas from previous interpretations. Stratigraphic cross sections were prepared to

subdivide the Edwards Group. The base of the Del Rio Formation, the regional dense member between the Person and Kainer Formations, and the base of the Edwards group were mapped regionally. Higher-frequency cycles were recognized on well logs, but variable porosity development in these cycles precludes tracing them regionally.

In addition to stratigraphic data from logs, elevations of the contacts of the Edwards Group in outcrop were extracted from four sheets of the 1:2,500,000-scale Geologic Atlas of Texas (Waechter and others, 1977; Proctor and others, 1979; Brown and others, 1983; Proctor and others, 1988) to assess the volume of the unconfined part of the aquifer. For volume calculation purposes, a map of approximate water levels as of January 1972 (Klemm and others, 1975) was used to define the upper surface of the unconfined aquifer. In addition, total ground-water volume lying between two potentiometric surfaces mapped by the EUWD (John Waugh, written communication, 1993) in the unconfined part of the aquifer was calculated and compared with net change in storage on the basis of annual recharge and discharge estimates. The lower elevation of the potentiometric surface is represented by the 1984 water levels, which are among the lowest ever recorded. The higher potentiometric surface is represented by 1992 water levels, which are among the highest ever recorded.

Log Acquisition

Resistivity, neutron, sonic, and density logs all show changes in the amount of water-filled porosity in the rocks surrounding the well bore. However, the response of logging devices to changes in water-filled porosity is rarely simple, because it involves variables such as well-bore size, specific conductivity and density of pore fluids, and specific conductivity and density of rocks (Schlumberger, Ltd., 1989). Porosity logs in this study came from various sources, were run in boreholes of variable histories, and as a result are of variable quality for calculating porosity. In this study, the best possible porosity estimates were extracted from a large number of porosity logs with the objective of covering the 3,111 mi² (8,004 km²) aquifer area as

completely as possible within the scope of the study. Of the 200 logs obtained, 125 neutron and resistivity logs were determined to be of good enough quality for porosity calculations. The few available sonic and density logs were not used in this study but should be included to add more detail in future studies.

Logs used in this study were obtained from three sources (table 1): (1) published logs from U.S. Geological Survey (USGS) and Texas Water Development Board (TWDB) studies (Seih, 1975; Maclay and others, 1981; Maclay and Small, 1986), (2) commercial logs from the Surface Casing Division of the Texas Water Commission (TWC), and (3) logs made of Edwards water wells and collected from a variety of other sources by the Edwards Underground Water District (EUWD). No proprietary logs were used. Well locations were extracted from (1) published maps, (2) county property maps with marked well locations from the Surface Casing Division, and (3) data supplied by the EUWD.

Published logs were valuable because many of them were from cored USGS and TWDB research boreholes (fig. 1, plate 1). Many of the TWC logs are from the deeper parts of the Edwards Group south of the bad water line. Logs collected from water wells by the EUWD generally have caliper, gamma-ray, and variously scaled resistivity measurements. Calibration of resistivity curves from these wells is one of the specific tasks performed in this study. Many wells penetrate only the upper part of the aquifer but are very valuable because they provide information directly from its producing intervals. Logs that contained usable porosity information (see Schultz, 1993) were digitized with a sample increment of 1 ft (table 1). Unscaled logs were assigned an arbitrary resistivity or neutron scale. Logs with usable stratigraphic information were reduced to a common scale by digitizing or photocopying.

Log Calculation of Porosity

The steps used to calibrate the logs included: (1) measurement of porosity and permeability from cores using 300 plugs to create core-based porosity logs, (2) calibration of

Table 1. Well data base.

Well no.	Q-no.	Texas no.	Company	Lease or well name	KB	TD	Base Del Rio	Base RDM	Base EDW	Longitude	Latitude	Neut. porosity	Res. porosity	Water-level data	Core
BEXAR 2		AY 6828910	EUWD	Castle Hills Test Hole	750	800	207	413	662	98.4114	29.5178				X
BEXAR 3		AY 6827907	EUWD	City Water Board	920	664	212	439		98.6539	29.5258		X		
BEXAR 4		AY 6827906	EUWD	City Water Board	991	758	284	529		98.6639	29.5236				
BEXAR 5		AY 68281	EUWD	City Water Board	1112	474		138		98.6025	29.5997				
BEXAR 6		AY 68282	SA PWD	Pioneer Aggregate	1010	514	32	211	509	98.5828	29.5864				
BEXAR 7		AY 68284	EUWD	SA Water Supply	1005	374	76	268		98.5942	29.5469		X		
BEXAR 8		AY 68286	Ed. Aq. Study	Morton	910	397	150	311		98.5197	29.5681				
BEXAR 9		AY 6828100	EUWD	Redland Worth Corp.	1045	700	81	261	595	98.5872	29.5922				
BEXAR 10		AY 6828204	EUWD	EUWD Observation Well	1021	523	61	245		98.5533	29.5917				
BEXAR 11		AY 6828500	EUWD	Redland Worth Corp.	885	706	202	381	676	98.5633	29.5539		X		
BEXAR 12		AY 68288--	EUWD	USAA, Church	890	737	242	419		98.5444	29.5219		X		
BEXAR 13		AY 68293	City of SA	Metcalf & Eddy TW #33	925	600	74	321	571	98.3883	29.6022	X	X		
BEXAR 14		AY 68294	City of SA	TW #31	795	740	256	451	731	98.4839	29.5608		X		
BEXAR 15		AY 68299	EUWD	FDIC, Swans Landing #2	728	607	231	465		98.4167	29.5244				
BEXAR 17		AY 6829103	EUWD (Hill Country)	EUWD	953	529		195	454	98.4878	29.5892		X	X	
BEXAR 18		AY 68293--	Ed. Aq. Study	Portland Cement Co.	1040	651	280	465		98.3758	29.6142		X		
BEXAR 19		AY 6829413	EUWD	City of San Antonio	780	406	194	405		98.4592	29.5756				
BEXAR 20		AY 6829506	US Geo. Sur.	Feathercrest (USGS)	788	700	203	421	689	98.4386	29.5742				
BEXAR 21		AY 6829702	Mulsberger Drilling Co.	Mulsberger Wat. Well #1	787	850	441			98.4842	29.5231		X		
BEXAR 22		AY 6829913	SA CWB	Randolph Well #1	822	800	346	547	792	98.3783	29.5303		X		
BEXAR 23		AY 68301	EUWD	Voss Int. (Alamo Cement)	1047	368	237			98.3647	29.6014				
BEXAR 24		AY 68304	EUWD	Jordan Ford	880	548	307	510		98.3422	29.5589				
BEXAR 25		AY 68305	EUWD	Universal City	880	778	312	506		98.3258	29.5681		X		
BEXAR 26		AY 68305E	USGS	Metcalf & Eddy	765	739	251	420	712	98.3208	29.5767	X			
BEXAR 27		AY 68307	EUWD	City of Converse	814	709		697		98.3350	29.5358				
BEXAR 28		AY 6830109	US Geo. Sur.	Fox Run Well #1	947	710	342	581		98.3603	29.5903	X	X		
BEXAR 29		AY 68301--	Edwards Aq.	Portland Cmt. Co. Williams well	926	322	59	243		98.4011	29.6175				
BEXAR 30		AY 6830211	US Geo. Sur.	Seima - EUWD	776	778	221	478	712	98.3278	29.6047	X	X		
BEXAR 31		AY 68305--	Edwards Aq.	Olympia #2	845	618	317	491		98.3231	29.5731				
BEXAR 32		AY 6830616	US Geo. Sur.	Randolph #9	758	950	485	701	990	98.2906	29.5419	X	X		
BEXAR 33		AY 6830700	EUWD	City of Converse	815	654	489			98.3353	29.5361		X		
BEXAR 34		AY 6830807	US Geo. Sur.	Randolph FM 1604 #1	750	1176	593	830	1158	98.2889	29.5267				X
BEXAR 35		AY 68346	EUWD	Cimmaron North Well #2	890	460	488			98.7417	29.4306				
BEXAR 36		AY 68348	EUWD	Texas Research Park	904	677	373	616		98.7953	29.4119				
BEXAR 37		AY 6834904	EUWD	Briggs Ranch	780	1090	629	878		98.7644	29.3861				
BEXAR 38		AY 68351	Edwards Aq.	National Gun Club	1095	804	494	745		98.7456	29.4919				
BEXAR 39		AY 68356	EUWD	R.T.C.	740	566	409			98.6322	29.4561				
BEXAR 40		AY 68357	EUWD	AF Village 11, Well #1	780	817	572	817		98.7392	29.3853		X		
BEXAR 41		AY 68358	Edwards Aq.	Uptmore Develop Well NW	835	730	537			98.7039	29.4064				
BEXAR 42		AY 68359	EUWD	Medina AFB	682	1099	758	1020		98.6619	29.3878				
BEXAR 43		AY 68351--	SA CWB	Anderson Pump Stn #4	961	758	235	486	741	98.7122	29.4819		X		
BEXAR 44		AY 68352--	EUWD	Sea World Inc.	1005	529	364	615	870	98.7008	29.4625		X		
BEXAR 45		AY 68355--	EUWD	Ray Ellison Industries	732	1002	644	913		98.6803	29.3956				
BEXAR 46		AY 68361	City Wat. Bd.	Brookvale	810	810	337	528		98.6236	29.4789				
BEXAR 47		AY 68361	Murch Sports	Wurzbach Wat. Well #3	902	637	340	581		98.6008	29.4894				
BEXAR 49		AY 68364	--	Southwest Research	810	1064	140	406	751	98.6108	29.4431				
BEXAR 50		AY 68368	EUWD	BEXAR Metro. Wat. Dt.	680	1438	876	1127		98.5531	29.4072		X		
BEXAR 51		AY 6836208	EUWD	City Water Board	813.1	779	603			98.5456	29.4794				
BEXAR 53		AY 6837104	City Water Board	Basin Stn. Well #6	720	950	582	820		98.4725	29.4961				
BEXAR 54		AY 6837106	SA CWB	Basin Station #5	710	950	554	799		98.4897	29.4956		X		
BEXAR 55		AY 6837203	US Geo. Sur. (P. Sam Houston)	US Govt. (Dodd Field)	730.81	850	596	724		98.4317	29.4792		X	X	
BEXAR 56		AY 6837402	Pearl Bra. Co.	Water Well #3	661	1157	645	890		98.4933	29.4425	X			
BEXAR 57		AY 68375C2	EUWD	EUWD	620	1149	807	1059		98.4333	29.4294		X		
BEXAR 58		AY 6837519	City Wat. Bd.	Singer Layne	649	1340	925	1140		98.4408	29.4331				
BEXAR 59		AY 6837521	SA CWB	A1	620	1500	985	1224		98.4278	29.4181				

Table 1 (cont.)

Well no.	Q-no.	Texas no.	Company	Lease or well name	KB	TD	Base Del Rio	Base RDM	Base EDW	Longitude	Latitude	Neut. porosity	Res. porosity	Water-level data	Core
BEKAR 61		AY 6837705	SA CWB	Mission Station #12 (new #5)	602	1800				98.4961	29.3911		X		
BEKAR 62		AY 68423	Edwards Aq.	M&E Aquifer Study Well	740	814	646			98.7650	29.3742				
BEKAR 63		TD 68425	EUWD	Wagner	690	1162	975			98.8244	29.3239		X		
BEKAR 64		AY 6842805	EUWD	Liebe	771	2510	1899	2187		98.6308	29.2672		X		
BEKAR 65		AY 68433	Edwards Aq.	Ly DA	720	1660	1410	1661		98.6308	29.3467				
BEKAR 66		AY 6843607	Johnson Drilling Co.	Mitchell #3	612	2145	1591	1869		98.6333	29.3156		X		
BEKAR 67		AY 68449	Phillip Oil & Gas Co.	W-1	553	2124	1605	1876		98.5089	29.2772		X		
BEKAR 68		AY 6845301	US Geo. Sur.	Holt Murphy	610	2100				98.3994	29.3711	X	X		
BEKAR 69		AY 6845901	US Geo. Sur.	CPSB	510	2878	2484	2731		98.3817	29.2564	X	X		
BEKAR 70			Tenneco Oil Company	Virgilia Herrera #1, Wildcat	547	5100	2659	2935	3326	98.4549	29.2147		X		
BEKAR 72			George Parker & C. L. McCune	Tom Goad #1	590	2305	1597	1871	2207	98.4704	29.3026		X		
BEKAR 74			Anderson-Prichard Oil Co.	K. M. Yurri #1	590	4297	1555	1750	2130	98.4019	29.3588		X		
BEKAR 82			Elliot Laub & Hill	Pall Ye Edwards #1	574	2479	1940	2202		98.2652	29.3686		X		
BEKAR 84			Arkansas Fuel Oil	Geo. Burkhardt #1, Wildcat	563	5097	2137	2344	2804	98.2669	29.3379		X		
BEKAR 86			Ralph A. Pair-Jack Woodward Inc	Pauline Lyro #1	602	4800	1657	1880	2220	98.1978	29.4281		X		
BEKAR 87			L. M. Brown Associates	Rudolph Schroeder #1	744	3206	831	1068	1423	98.2501	29.4984		X		
BEKAR 89			Thomas Drilling Co.	Gus Schwinn #1	574	4030	1272	1525	1867	98.2651	29.4452		X		
BEKAR 96			B. M. Jacobs	Dickey Clay Mfg. Co. #1	575	4008	2850	3126	3510	98.3169	29.2539		X		
BEKAR 97		AY 6827512	USGS	AY-1	875	500				98.4694	29.5841	X	X		
BEKAR 98		AY 6829107	USGS	AY-2	577	600				98.2100	29.6100	X			
BEKAR 100	Q7	AY 6837711	Singer Layne Texas Division	SA CWB Mission Pump Sta #7	650	1500	1300			98.5340	29.3780		X		
BEKAR 105	Q51		Bubbran Petroleum	DRE Bubbar #1	725	3600	1800	2082	2447	98.7410	29.2520		X		
O 5		AY 6829209		Encino Park						98.4375	29.6042			X	
COMAL 1		DX 6823202	TWDB	Test Hole DX2	937	404		97		98.2006	29.7111	X			
COMAL 2		DX 68223--	EUWD	Arthur Swan	940	834		212	248	98.2542	29.7175				
COMAL 3		DX 6822800	EUWD	Robert Howey	890	321	149			98.3056	29.6311				
COMAL 4		DX 68228--	EUWD	George McGranahan	865	377	87	318		98.3081	29.6281				
COMAL 5		DX 6823304	EUWD	LCRA	640	958				98.1372	29.7111		X		
COMAL 8/9		DX 6823616	EUWD	A1	616	933	440	660	915	98.1328	29.7042	X	X		
COMAL 10/12		DX 6823617	EUWD	B1	635	916	466	678		98.1344	29.7053	X	X		
COMAL 14/15		DX 6823619	EUWD	Well C1	635	960		807		98.1361	29.7072	X	X		
COMAL 16		DX 68302	EUWD	City of Garden Ridge	865	451	198	429		98.3181	29.6200		X		
COMAL 17		DX 6830200	EUWD	Roy E. Newborn	810	257	56			98.3181	29.6175				
COMAL 18		DX 6822501		DX-1						98.2932	29.6802	X	X		
COMAL 41	Q1	DX 6830312	TWDB	DX-3	715	432	6	184	427	98.2839	29.6132	X	X		
COMAL 43	Q3		TWDB	C. W. Lewis DX-1	908	476	92	245		98.3230	29.6820	X	X		
O 12		DX 6830208	Bracken	Bracken						99.1692	29.6100				
O 17		DX 6823302												X	
HAYS 1		LR 67013	EUWD	City of Kyle	795	634	268	435		97.8922	29.9939		X		
HAYS 2		LR 6701814	EUWD	EUWD Well D	577	775	443	601		97.9308	29.8919		X		
HAYS 3		LR 6701812	EUWD	EUWD Well B	578	891	391	579		97.9294	29.8892		X		
HAYS 5		LR 6701813	EUWD	EUWD Well C	580	921	398	585	884	97.9317	29.8908		X		
HAYS 36	Q9		TWDB	John D. Mullins #4	590	785	8	173	513	97.9420	29.9110				
HAYS 37	Q4		Woodward and Co.	Schubert #1	590	1800	978	1048	1444	97.7680	30.0250				
O 14		LR 6701809		City of Kyle						97.9337	29.8958				
O 16		LR 6709110												X	
O 1		LR 6701303		Kalspel						97.8958	29.9792			X	
KINNEY 1	Q12		Travelers Ins. Co	Bracksville Pms #7	1025	2150	959	1430		100.5913	29.2596				
KINNEY 2	Q11		C. C. Winn	Thompson Payne #1	1075	2287	1042	1640		100.4693	29.2759		X		
KINNEY 4	Q28		Pennsylvania Expls. Co	Dumber Ranch #1	968	5605	2226	2618		100.3922	29.0858		X		
KINNEY 5	Q10		Sutton Drilling Co.	Harrison #1	1238	4290	314	720		100.2595	29.3416		X		
KINNEY 7	Q22		B. R. Wharton & Co.	Belcher #1		2900	1924	2330	2700	100.4897	29.4033		X		
KINNEY 8	Q18		Manor Oil Co	TOFT #1	1121	1603	541	1092		100.3613	29.2690		X		
KINNEY 10	Q14		Leeco Gas & Oil Co	Pauline Franks #1	970	5255	1253	1640	1995	100.3144	29.1852		X		
KINNEY 13	Q27		Phillips Petro. Co.	Hobbs #1	1046	4753	1217	1795		100.4051	29.2023				
KINNEY 14		RP 7038902	TWDB	RP-2	1380	800				100.28					
MEDINA 1		TD 6939504	Texas Water Dev. Bd.	TD3	1021	620	65	328	640	99.1942	29.4503	X	X		X

Table 1 (cont.)

Well no.	Q-no.	Texas no.	Company	Lease or well name	KB	TD	Base Del Rio	Base RDM	Base EDW	Longitude	Latitude	Neut. porosity	Res. porosity	Water-level data	Cnre
MEDINA 2		TD68257	EUWD	Rocky Creek Wr. Co	1270	615		241	543	98.9600	29.5242		X		
MEDINA 3		TD68337	EUWD	Arthur Weiblen	1020	1465	1294			98.9694	29.3819				
MEDINA 4		TD6834105	EUWD	John Persyn	908	1028	716	987		98.8619	29.4811		X		
MEDINA 5		TD6842100	EUWD	Sam Castleberry	762	1257	1082			98.8419	29.3461				
MEDINA 6		TD69373	EUWD	Valdina Farms	1192	572	152	369		99.3808	29.4739		X		
MEDINA 7		TD69381	Edwards Aq. Study	Valdina Farms #2	1100	450		280		99.3569	29.4711		X		
MEDINA 8		TD6938101	US Geo. Survey	Woodward Valdina Farms	1104	600	109	357	584	99.3608	29.4883				
MEDINA 9		TD6938500	EUWD	Dr. John Windrow	1022	728	104	358	651	99.2942	29.4356		X		
MEDINA 10		TD6938601	US Geo. Survey	US Geo. Survey (Seco Creek)	1008	522	94	350		99.2817	29.4372			X	
MEDINA 11		TD69395	EUWD	Gregg Rothe	1030	478	337			99.2039	29.4425				
MEDINA 12		TD69407	EUWD	Pat Stein	900	816	524	773		99.0953	29.4111		X		
MEDINA 13		TD6945600	EUWD	David Ackerman	925	1296	1107			99.4069	29.3094				
MEDINA 14		TD6946100	EUWD	Rene Aelvoet	1080	1360	967	1225		99.3431	29.3633		X		
MEDINA 15		TD6946802	EUWD	Squirrel Creek Ranch	961	1623	1189	1464		99.3331	29.2575		X		
MEDINA 16		TD69474	EUWD	Dr. John Windrow	881	1828	1116	1383	1726	99.2269	29.3269		X		
MEDINA 17		TD69477	EUWD	Charles Collins	870	1734	1322	1637		99.2431	29.2750		X		
MEDINA 18		TD6947400	EUWD	John Bader	889	1722	1180	1459		99.2358	29.3261				
MEDINA 19		TD6947700	EUWD	Timus Harris	935	1815	1406	1689		99.2200	29.2864				
MEDINA 20		TD69555	EUWD	Heart-Bar Deer Farm	759	2378	1879	2194		99.1972	29.1969				
MEDINA 21	Q2		Geo. Parker & McGune	Ganahl Walker #1	700	2252	2012			98.8644	29.2309				
MEDINA 22	Q7		Thomas & Rife	Zedich #1	750	3243	3160			99.0372	29.0939				
MEDINA 23	Q12		Progress Petro.	H. Bendele, Jr. #1	725	3774	2661	2978	3345	98.9698	29.1450		X		
MEDINA 24	Q15		Edmond J. Ford & Hamilton	J. H. Raybourn #1	921	1987	1325	1592		99.3242	29.2369				
MEDINA 26	Q26		Pan Am. Petro. Co.	W. L. Knipp #1	674	5705	2942	3280	3700	98.9256	29.1140				
MEDINA 27	Q31		W. H. Snowden	A. L. Harbort #1	900	4836	1784	2108	2417	99.1796	29.2609		X		
MEDINA 28	Q33		Humble Oil Co.	E. E. Wilson #1	650	7167	2728	3108	3492	99.2462	29.1070				
MEDINA 29	Q44		Edmond J. Ford & Hamilton	Nunley #1	907	5028	1668	1981	2450	99.3910	29.1876				
MEDINA 30	Q45		Hughes & Hughes	Pinchy #1	713	5000	2559	2867	3240	98.8636	29.1748		X		
MEDINA 31	Q46		Progress Petro. Corps. of Tx.	R. Haas #1	681	5700	2627	2950	3320	98.9439	29.1519				
MEDINA 33	Q61		Pan Am. Petro. Corps.	J. Travis Lilly #1	711	3500	2948	3297		98.9461	29.1213				
MEDINA 34	Q62		Tenn. Oil Co. & Perm. United Inc.	John W. Carroll #1	776	4550	2176	2476	2834	98.8296	29.2280		X		
MEDINA 35	Q63		Gulf Oil Corps.	R. F. Richardson #1	871	6955	1472	1791	2240	99.3019	29.2177		X		
MEDINA 38	Q66		Tenneco Oil Co.	E. K. Harper #1	708	4500	2570	2990	3351	99.3319	29.1131				
MEDINA 39	Q68		Tenneco Oil Co.	E. H. Powell #1	750	5100	2710	3021	3390	98.8285	29.1661		X		
MEDINA 40	Q69		Tenneco Oil Co.	Roy Wilson #1	690	4800	2209	2508	2925	99.1667	29.1554				
MEDINA 41	Q72		Tenneco Oil Co.	W. L. Hay #1	876	3900	1422	1704	2160	99.3752	29.2221				
MEDINA 43	Q77		Hughes & Hughes	P. S. Keller #1	721	4700	2354	2630	3020	99.0428	29.2694				
MEDINA 44	Q78		Med-Tex Oil Co.	Robertson #1	700	8001	2680	3000		98.9801	29.1376		X		
MEDINA 50	Q143		Ralph A. Johnston	Howard A #1	792	5006	2382	2691	3035	99.0168	29.1706		X		
MEDINA 51	Q67				710.5		2362	2662	3030	98.9489	29.1870		X		
MEDINA 52		TD6826801	TWDB	TD-1	383	500				98.8400	29.5400		X		
MEDINA 53			EUWD	South Medina Co. Obs. Well #1	672.7	3411	2608	3004	3410	99.2167	29.1108	X			
O 15		TD 69 47 306		City of Hondo						99.1458	29.3504			X	
O 6		TD 6841301	City of Castroville	City of Castroville						98.8958	29.3542			X	
UVALDE 1		YP 6942709	TWDB	Test Well YP-4	1005	700	62	396	683	99.8622	29.2731				X
UVALDE 2		YP 6937402	TWDB	Sabinal Test Hole (Hwy. 187)	1158	700	206	431		99.4725	29.4531	X	X	X	X
UVALDE 3		YP 69367	EUWD	David Bishop	1073	852	260			99.6192	29.3883				
UVALDE 4		YP 69369	EUWD	Chapman Grain Inc.	1185	767	152	380	641	99.5286	29.4133				
UVALDE 5		YP 69399	EUWD	E. B. Mathis	798	801	164			99.1406	29.4031				
UVALDE 6		YP 69419	EUWD	George Ligothy	1047	483	126	462		99.8825	29.2903				
UVALDE 7		YP 69432	EUWD	John Brigman	1098	759	120	411	760	99.6944	29.3358		X		
UVALDE 8		YP 69439	EUWD	Lawrence Priesenbahn	948	1079	796	1077		99.6364	29.2658		X		
UVALDE 9		YP 6943300	EUWD	Maurice Rinkus	1031	837	296	591		99.6475	29.3353		X		
UVALDE 10		YP 6943409	EUWD	EUWD (N. Uvalde)	1055	881	250	500	856	99.7300	29.3239		X		
UVALDE 11		YP 6943605	USGS	Elmer Knippel	978	1275	674	961		99.6344	29.2919			X	
UVALDE 12		YP 69448	EUWD	Moring (4M ranch)	949	1579	867	1130	1533	99.5667	29.2903				
UVALDE 13		YP 6944100	EUWD	Ray Kelly (Knippa)	1043	880	285	555		99.6056	29.3678				
UVALDE 14		YP 6944400	EUWD	Mr. Jess Ward	972	1455	740	1021	1401	99.6103	29.2956		X		

Table 1 (cont.)

Well no.	Q-no.	Texas no.	Company	Lease or well name	KB	TD	Base Del Rio	Base RDM	Base EDW	Longitude	Latitude	Neut. porosity	Res. porosity	Water-level data	Core
UVALDE 16		YP 69455	EUWD	Roberts	935	1368	827	1212		99.4525	29.3128		X		
UVALDE 17		YP 69457	EUWD	Charles Halbardier	910	1657	1055	1294		99.4781	29.2822		X		
UVALDE 18		YP 69459	EUWD	Ferguson Hashknife Ranch	865	1828	1222			98.4153	29.4369				
UVALDE 19		YP 6945400	EUWD	City of Sabin	954	1499	922	1150		99.4694	29.3194		X		
UVALDE 20		YP 6950100	EUWD	Everett Duvall	937	874	606			99.8567	29.2175				
UVALDE 21		YP 6950300	EUWD	Uvalde Equipment Co.	919	161	60			99.7636	29.2206		X		
UVALDE 23		YP 6950803	EUWD	Don Willoughby	938	893	640			99.8108	29.1550		X		
UVALDE 25		YP 6958300	EUWD	General Tire Co.	890	2325	1606	2067		99.7814	29.0972				
UVALDE 26	Q20		Gorman Drilling Co	Woodley #1	760	2483	1915	2233		99.4775	29.1514		X		
UVALDE 27	Q2		Gorman Drilling Co	Woodley #2	759	3688	1955	2249	2698	99.4797	29.1522		X		
UVALDE 28	Q16		Gorman Drilling Co	Woodley #B-1	800	2985	2397	2700	3000	99.4352	29.1246				
UVALDE 31	Q6		Gorman Drilling Co	Woodley #B-11	860	4500	2111	2417	2709	99.4349	29.1419		X		
UVALDE 32	Q32		Intl. Nuclear Corp.	Kincaid Ranch #1	729	2790	1990	2330	2690	99.5277	29.1244				
UVALDE 33	Q33		Intl. Nuclear Corp.	Kincaid Ranch #2	850	4416	1554	1867	2280	99.6024	29.1441		X		
UVALDE 34	Q3		W. J. Steger, ET AL	F. T. Kincaid Ranch #1	856	4015	2186	2590	2890	99.6088	29.1097		X		
UVALDE 38	Q36		Pan Am. Petro. Corp.	Alice T. Houston #1	958	2600	981		1571	99.6975	29.2153				
UVALDE 40	Q4		Ike Howeth	Frank Winslow #1	920	3684	563	870	1216	99.6818	29.2362				
O 13		YP 6943607	Knippa	Knippa						99.6383	29.3264			X	
O 9		YP 6945401	City of Sabin	City of Sabin						99.4681	29.3192			X	
O 10		YP 6950302	City of Uvalde	City of Uvalde						99.7867	29.2103			X	
O 11		YP 6951406	Fred Ehlers	Ehler						99.7408	29.1736			X	

EDW = Edwards Group

EUWD = Edwards Underground Water District

RDM = Regional dense member

SA CWB = San Antonio City Water Board

SA PWD = San Antonio Public Works Department

TWDB = Texas Water Development Board

USGS = United States Geological Survey

neutron and resistivity logs from these wells using plug data, (3) calibration of scaled logs with multiple porosity devices to determine best fit between several different log types, and (4) calibration of unscaled logs by comparison to scaled logs.

Measurement of Porosity In Core

Of the seven cores studied to define stratigraphic subdivisions of the Edwards, core from five wells was examined completely and visible porosity was compared to the porosity recorded on logs. Core plugs 1 inch (2.5 cm) in diameter were removed at approximately 1 ft (30 cm) spacing over intervals of 50 ft (15 m) that were selected for study. The close spacing allowed an accurate match between core and log data that has not been obtained in previous studies of the Edwards. All plugs were oriented with the long axis perpendicular to the core. Core plugs were analyzed for porosity, permeability, and grain density by Core Petrophysics Incorporated of Midland, Texas (table 2). Thin sections were prepared from all core plugs and from representative lithologies along the rest of the cores. To show porosity, thin sections were impregnated with blue epoxy, and the distribution and type of pores were examined and photographed using a transmitted-light microscope.

The plug data were used first to scale porosity logs from the cored wells. Porosity was calculated from commercial logs with standard scales. The successful techniques were applied to wells from which both resistivity and neutron logs were available, then applied to unscaled logs.

Neutron- and Resistivity-Log Calibration of Cored Wells

Calibration of logs from cored wells to the measured porosity was empirical. Plug porosity data were matched to the curves using 3-ft running averages. All logs and plug porosity data were depth corrected to give the best possible inflection point matches. One data set was successively fitted against another until porosity calculations merged toward a single curve.

Table 2. Plug porosity and permeability.

Depth (ft)	Permeability (md)	Porosity (%)	Depth (ft)	Permeability (md)	Porosity (%)
USGS Castle Hills, Bexar County (C-1192) AY 68-28-910			USGS Castle Hills (cont.)		
223.7	0.04	8.9	479.0	296.90	26.1
232.5	0.30	17.7	482.0	44.85	20.1
253.0	199.91	31.4	USGS YP-4 core, Uvalde County (C-6092) YP 69-42-709		
255.0	238.30	34.1	74.0	0.02	8.5
257.0	171.39	30.5	150.0	20.19	25.4
258.0	139.57	32.7	152.0	28.06	27.9
259.0	99.08	31.0	155.0	317.47	29.0
261.0	52.91	27.5	157.0	25.09	26.9
263.0	33.17	25.2	160.0	61.09	26.2
264.0	41.19	28.9	162.0	27.61	28.8
267.0	44.01	28.2	165.0	38.12	29.0
269.0	48.44	28.2	167.0	47.96	30.3
270.0	40.45	28.7	170.0	31.24	28.1
272.0	10.15	22.8	173.0	3.93	17.4
273.0	40.57	32.4	176.0	4.96	22.7
274.0	12.77	25.0	180.0	33.01	27.1
275.0	3.29	16.9	183.0	33.24	28.0
277.0	2.52	15.4	187.0	33.80	28.6
280.0	8.23	16.8	200.0	29.88	27.4
282.0	0.29	8.2	203.0	32.21	26.4
283.0	11.51	7.4	205.0	29.65	27.5
284.0	10.86	10.9	444.0	0.13	3.9
286.0	9.91	16.1	446.0	nd	4.3
287.0	1.09	9.8	453.0	0.05	5.0
288.0	126.19	9.6	455.0	0.12	9.1
290.0	0.25	8.7	501.0	0.06	12.5
291.0	0.07	6.5	513.0	0.08	18.7
292.0	29.34	11.5	539.0	0.01	5.3
293.0	18.56	23.9	593.0	0.04	8.6
294.0	0.09	7.7	625.0	0.01	6.4
295.0	0.17	8.6	629.0	0.17	11.7
298.0	0.05	6.4	646.5	0.06	5.5
396.3	0.03	6.0	661.8	3.67	11.3
400.0	0.03	7.8	USGS TD 69-39-504 core, Medina County (C-6094)		
402.0	0.02	8.5	320.0	0.09	10.8
403.0	0.18	9.6	323.0	0.21	15.3
439.0	0.14	8.0	326.5	0.02	7.4
440.0	0.01	3.2	328.0	0.02	9.6
442.0	4.08	7.6	329.0	0.06	13.4
443.0	39.74	11.4	333.0	2.69	19.9
444.0	1822.19	31.3	335.0	3.53	20.7
446.0	16.90	15.8	336.0	6.21	24.8
447.0	0.03	2.0	338.0	0.52	15.0
449.0	73.83	11.5	350.0	20.26	27.8
450.0	14.10	13.8	351.0	17.09	27.8
451.0	176.77	22.0	356.0	10.00	24.4
453.0	0.01	3.4	357.5	7.31	25.0
455.0	0.03	6.0			
455.0	50.93	20.0			
458.0	0.05	10.8			
463.0	0.04	7.3			
477.0	675.90	26.5			

Table 2 (cont.)

Depth (ft)	Permeability (md)	Porosity (%)	Depth (ft)	Permeability (md)	Porosity (%)
USGS TD 69-39-504 core (cont.)			USGS Randolph FM 1604 #1 (cont.)		
409.0	5.57	21.6	778.0	3.11	14.7
410.0	0.07	5.9	779.0	2.09	17.8
411.0	660.89	17.4	780.0	9.04	23.3
412.0	89.32	12.8	781.0	185.99	21.4
413.0	24.46	16.1	782.0	37.30	28.5
419.5	0.16	9.7	783.0	9.31	21.7
420.0	0.13	7.0	784.0	158.35	31.1
421.0	9.36	11.6	785.0	48.45	23.4
422.5	183.30	8.9	786.0	20.66	27.0
423.5	4.89	6.3	787.0	22.09	22.8
424.0	2.46	8.7	788.0	81.12	27.5
425.0	0.81	8.3	789.0	10.06	21.7
426.0	0.42	4.4	790.0	0.39	12.4
427.0	0.28	5.5	791.0	14.20	21.1
428.0	0.63	6.7	793.0	99.70	35.7
428.5	1.30	7.9	794.0	147.79	37.4
431.0	0.24	4.5	795.0	46.21	36.2
432.0	0.12	4.9	797.0	49.83	38.8
433.0	0.30	4.7	798.4	94.10	38.9
434.0	21.97	21.6	799.5	3.94	19.7
437.0	0.49	5.2	801.0	0.36	11.2
438.0	1.05	8.1	802.0	0.05	5.2
439.0	17.01	9.4	803.0	0.16	11.2
439.5	5.24	8.1	804.0	0.05	8.0
440.0	2.48	8.2	806.8	1.22	25.7
440.5	0.53	8.3	810.8	0.01	5.9
442.0	169.21	21.6	812.5	0.02	7.5
443.0	1.09	8.0	813.0	0.02	7.1
444.0	1.72	10.4	814.5	1.13	7.2
445.0	4.58	7.1	816.4	0.03	5.1
446.0	0.23	4.8	817.0	0.04	6.2
447.0	0.06	3.0	878.0	11.03	19.9
448.0	0.09	5.4	879.0	185.08	21.7
449.0	35.90	19.1	880.0	89.47	25.3
450.0	0.23	2.8	881.0	454.88	24.9
451.0	0.05	1.6	881.8	508.27	24.4
452.0	0.03	2.9	883.3	3202.34	27.1
454.0	0.01	2.8	884.3	3935.46	27.4
457.0	2.02	10.6	885.0	292.85	28.7
458.0	0.09	6.1	886.0	362.95	27.2
459.0	80.89	11.8	887.0	140.98	23.9
			889.0	111.43	28.9
			890.0	236.98	27.5
			892.0	21.08	23.7
			893.0	137.23	27.7
			894.0	9.61	28.6
			895.4	844.93	25.4
			898.0	0.19	24.7
			899.0	115.01	49.8
			900.0	27.23	41.3
			901.0	351.37	39.6
			902.0	16.34	35.4
			903.0	0.49	14.7
USGS Randolph FM 1604 #1, Bexar County AY 68-30-807 (C-00692)					
609.0	0.10	9.0			
611.7	0.15	10.1			
617.0	0.63	18.5			
623.0	0.01	4.9			
773.0	8.48	10.9			
774.5	3.07	15.6			
775.0	6.83	17.1			
777.0	23.61	17.0			

Table 2 (cont.)

Depth (ft)	Permeability (md)	Porosity (%)	Depth (ft)	Permeability (md)	Porosity (%)
USGS Randolph FM 1604 #1 (cont.)			USGS Sabinal (cont.)		
904.0	18.16	24.6	452.0	0.10	4.2
905.0	25.08	36.7	453.0	7.51	21.9
909.0	3.43	17.6	454.5	99.62	17.7
910.0	68.25	31.7	456.0	8.75	18.5
911.2	560.90	37.0	457.0	0.36	9.6
912.0	314.13	38.0	547.0	0.04	2.2
913.0	258.98	29.8	548.0	0.19	12.2
914.0	79.26	42.1	554.0	0.01	4.4
915.0	86.32	40.8	555.0	0.03	4.3
916.0	79.27	37.3	556.0	41.18	7.7
917.0	14.09	16.2	557.0	290.44	7.0
918.0	23.80	17.9	558.5	0.03	4.0
921.0	61.10	30.9	559.0	0.02	4.5
922.0	22.76	28.2	560.0	0.04	5.8
922.9	2.30	19.5	561.0	0.04	5.3
924.0	33.37	27.0	562.0	0.08	6.9
925.0	0.17	12.3	563.0	0.02	4.7
926.0	0.08	13.0	564.0	22.76	19.7
927.0	11.29	24.5	565.0	0.01	3.5
928.0	0.03	8.9	566.0	11.08	9.5
1129.5	0.06	7.7	567.0	600.82	12.5
1131.4	0.05	6.5	568.0	0.02	2.1
1134.2	0.01	2.9	569.5	0.05	6.7
1136.5	0.01	6.1	570.0	0.05	5.9
1147.6	0.02	5.1	571.0	1.16	4.2
USGS Sabinal, Uvalde County YP 69-37-402 (C1819)			572.0	9205.20	16.4
375.0	0.85	14.7	573.0	0.21	7.2
378.0	0.06	7.2	577.0	0.33	10.0
379.0	1.34	16.6	578.0	3.38	5.2
381.0	0.52	14.8	579.0	26.74	7.4
385.0	0.62	12.8	580.0	12.96	8.9
388.0	0.65	8.6	581.0	6.91	4.8
393.0	0.01	3.7	582.0	4805.65	13.3
397.0	0.02	7.3	584.0	2.00	8.7
399.0	0.04	11.4	585.0	0.14	8.7
433.0	0.03	5.2	586.0	1.48	17.1
434.0	0.40	9.4	587.0	26.61	20.6
436.0	0.07	9.1	588.0	0.61	10.4
437.5	0.04	6.7	589.0	0.20	10.1
438.5	0.00	3.8	590.0	0.22	8.4
439.5	nd	2.5	591.0	1.18	10.8
440.5	0.04	7.9	592.0	2.52	13.3
442.0	0.03	4.0	593.0	0.46	12.5
443.0	3.01	7.3	594.0	1.74	14.1
445.0	0.45	6.6	595.0	8.20	12.0
446.0	4.60	9.0	596.0	1.38	16.1
448.0	0.04	4.5	598.0	16.97	20.7
449.0	5.10	8.4	600.0	0.43	12.2
450.0	9.41	8.6	601.0	0.10	6.3
451.0	0.07	6.6	602.0	0.05	5.7
			603.0	344.25	10.1
			604.0	1337.71	23.1
			625.0	0.06	8.4

Table 2 (cont.)

Depth (ft)	Permeability (md)	Porosity (%)
USGS Sabinal (cont.)		
629.5	0.05	8.0
630.7	0.22	7.2
636.4	0.15	7.4
639.5	17.33	10.9
641.5	0.01	6.2

nd = no data

Neutron porosity tools measure the amount of water in pore space. Because they record hydrogen ion content, they also respond to bound water, such as that in clay minerals. In the Edwards aquifer, this effect was ignored because of the generally low clay content; however, in the north part of the aquifer, the apparent porosity of somewhat argillaceous highstand deposits (such as the regional dense member) and some clay-rich karstic breccias may be overestimated.

Most neutron logs in the study area were scaled in counts per second (cps) and therefore required calibration to be used as porosity logs. A borehole size correction for the USGS neutron logs was derived from the USGS YP-4 core. An interval in the Salmon Peak Formation with fairly constant porosity between 25 and 30 percent, as measured in plugs, demonstrated an inverse relationship between borehole size (caliper) and neutron response. Cross plotting allowed derivation of a caliper correction equation:

$$N_{cc} = N + 50(D - 6) \quad (1)$$

where

N_{cc} is neutron caliper corrected,

N = raw neutron in counts per second (cps),

D = caliper diameter in inches, and

6 = the minimum caliper measurement.

Because of scale differences, Schlumberger, Ltd., tables (Schlumberger, Ltd., written communication, 1993) for caliper correction of neutron logs in cps are not directly applicable to this study's logs, but they also showed a simple linear relationship between neutron response and borehole size.

Caliper-corrected neutron-log response was cross plotted against plug-derived porosity to produce a log relationship between measured porosity and log response. This relationship was then used for porosity calculation.

Porosity Calculation from Wells with Scaled Curves

A small number of scaled neutron-porosity logs are available from the study area (table 1). Core is available for one of these, the USGS Randolph FM 1632 well, which allowed the accuracy of the scaled log to be evaluated.

For commercial (Schlumberger, Ltd., or Beeline) resistivity logs, porosity was calculated using the standard equation

$$\phi = 100 \sqrt{\frac{R_{wa}}{R_t}} \quad (2)$$

where

ϕ = porosity (in percent),

R_{wa} = is the resistivity of water, and

R_t = calibrated resistivity value.

This equation assumes that the cementation factor is 2, a conventional value for the Edwards aquifer (Schultz, 1992). R_{wa} is calculated

$$R_{wa} = \frac{10,000}{C} \quad (3)$$

where

C = specific conductance of water in the formation.

Specific conductance was estimated from a revision and extension of the specific conductance map of Schultz (1992). Specific conductance data from wells in the freshwater part of the aquifer north, west, and east of the Schultz (1992) study area were obtained from published data tables (Reeves, 1978; Marquardt and Elder, 1979; Maclay and others, 1980a; Ogden and others, 1985a; Ogden and others, 1985b; Ogden 1986; Brown and others, 1992). The currently mapped bad water line (Brown and others, 1992) was used to constrain contouring in areas with no specific conductance data (fig. 4). Then specific conductance was estimated for wells between data points. Temperature correction is minor because most wells in the study

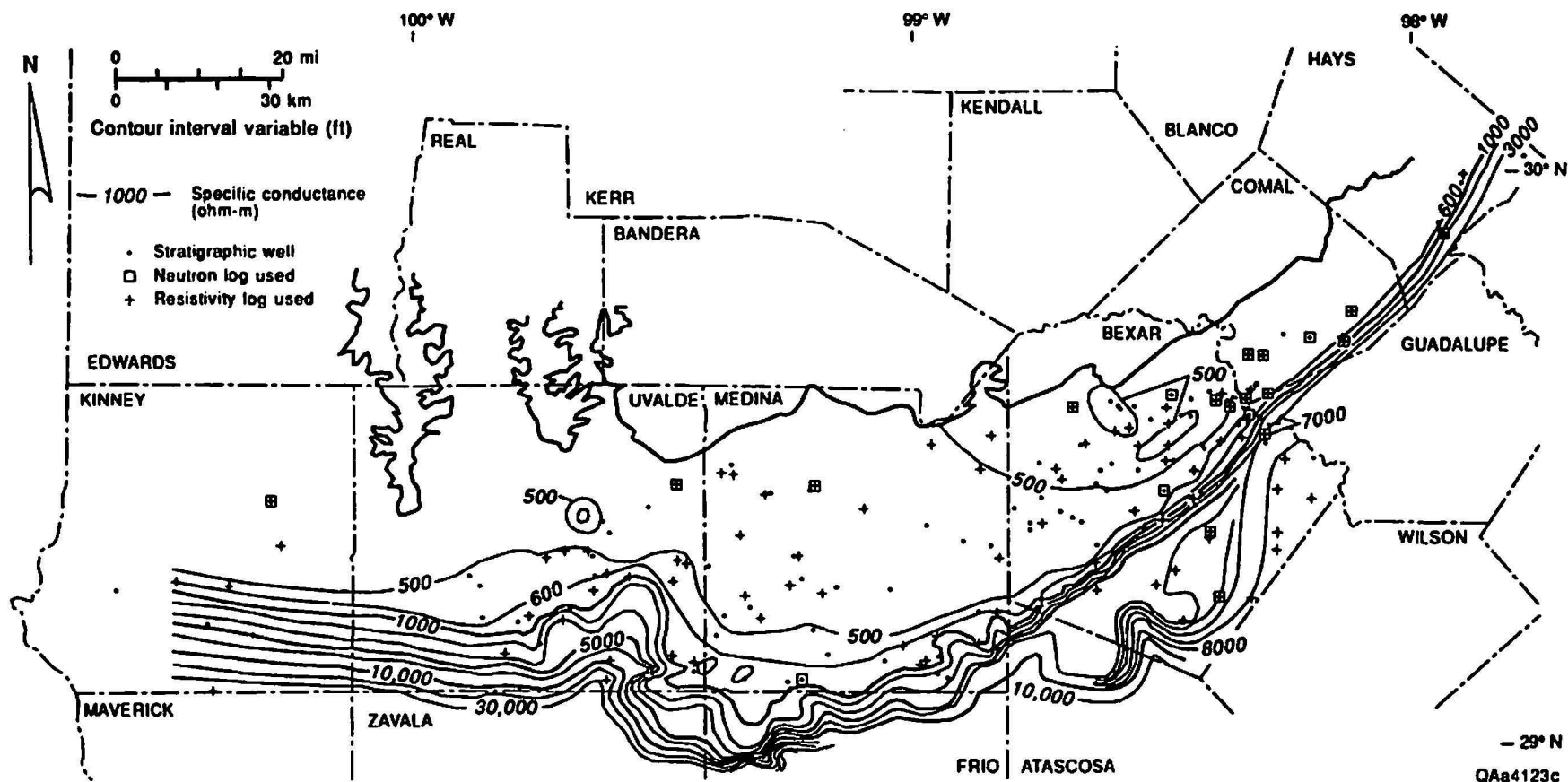


Figure 4. Specific conductance map used to estimate R_{wa} in resistivity log porosity calculations. Contours of Schultz (1992) used in central part of aquifer. Values toward north, east, and west are measured specific conductance (Reeves, 1978; Marquardt and Elder, 1979; Maclay and others, 1980a; Ogden and others, 1985a, b; Ogden, 1986; Brown and others, 1992). Bad water line transferred from Brown and others (1991).

area are shallow. Resistivity was corrected for temperature in parts of the aquifer greater than 1,000 ft (300 m) deep (Schultz, 1992).

Caliper correction failed to improve curve fit between resistivity logs and other logs and plugs, and therefore no correction was applied. The caliper curve varies directly with porosity in most intervals, indicating that the most porous intervals are also friable and subject to caving.

Porosity Calculation from Wells with Unscaled Curves

The high/low correction technique was used for unscaled logs and neutron logs scaled in counts per second (cps). This technique is based on the observation that, although the average porosity is quite variable, the highest and lowest porosities observed in the Edwards are generally consistent. Many of the nondolomitized subtidal facies (Georgetown Formation, the regional dense member, the basal nodular member of the Edwards, and other less regionally traceable transgressive cycle bases) tend to have low porosities. High porosities that have been diagenetically enhanced in grainstones and in leached, calcitized subtidal facies are somewhat more variable but tend to be limited by mechanical strength. Typical calibrated logs and plug data plotted on a cumulative frequency curve generally yield a distribution of 4 to 7 percent porosity at the 5th percentile (0.05) and 30 to 42 percent porosity at the 95th percentile (0.95) (fig. 5). The 1st and 95th percentile values selected for an uncalibrated curve were selected by (1) screening logs to select those where both high and low values are represented, (2) selecting probable high and low values in a comparable calibrated log (same stratigraphic interval and probably similar depositional and diagenetic evolution), (3) calculating a porosity curve for the uncalibrated log using the appropriate equation, and (4) comparing the porosity curve produced in (3) with those previously calculated to test the preceding assumptions.

Calculation of a porosity curve for the uncalibrated resistivity logs used the following steps: (1) selecting the 5th and 99th percentile values of the raw curve values from an interval with well-developed normal cyclic variation in resistivity, (2) calculating the standard resistivity to

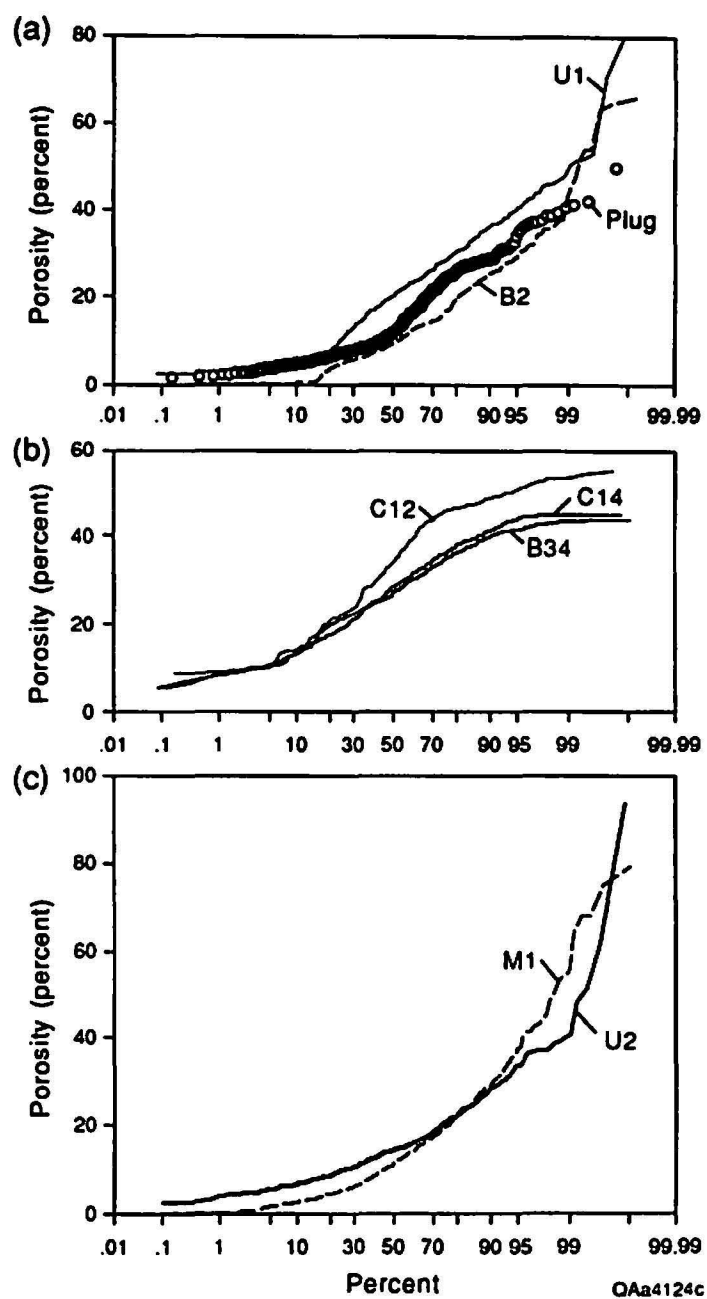


Figure 5. Cumulative frequency plots of representative calibrated neutron porosity logs.

porosity conversion, and (3) scaling the calculated porosity so the 1st and 95th percentile values match the regionally estimated values using the following equations:

$$\phi_r = 100 \left(m \sqrt{\frac{R_{wa}}{R_c}} + b \right) \quad (4)$$

where

ϕ_r = calculated porosity from resistivity, and

$$m = \frac{\phi_1 - \phi_2}{r_1 - r_2} \quad (5)$$

$$b = \phi_1 - mr_1 \quad (6)$$

where

ϕ_1 = the 1st percentile porosity (expressed as fractions of 1) on a nearby calibrated log, typically 0.05,

ϕ_2 = the 95th percentile porosity (as fractions of 1) on a nearby stratigraphically equivalent calibrated log, typically 0.35,

r_1 = the 5th percentile resistivity on the unscaled log,

r_2 = the 99th percentile resistivity on the unscaled log,

$$R_{wa} = \frac{10,000}{C}, \text{ and}$$

C = specific conductance at the well estimated from the contoured map (fig. 4).

These relationships were derived after experimentation with various correction techniques and scaling equations. Many scaled resistivity logs gave porosity distributions that were narrower than the core-data and calibrated-log porosity distributions. When the high/low calibration was applied to these resistivity logs and compared to scaled neutron logs, very good matches in average porosity were generally obtained. After the best estimate of porosity was calculated, some peaks in the porosity log were assigned very high porosities (50 to 100 percent). These intervals typically have bad hole conditions, as shown by large and off-

scale caliper readings. A porosity as high as 100 percent would be the proper value if the borehole intersected a water-filled cavern, so high porosities for narrow intervals were tolerated.

A similar set of high/low calculations was applied to unscaled neutron logs:

$$\log \phi_N = mN + b \quad (7)$$

where

ϕ_N = calculated porosity from unscaled neutron log, and

$$m = \frac{\log \phi_1 - \log \phi_2}{N_1 - N_2} \quad (8)$$

$$b = \log \phi_1 - mN_1 \quad (9)$$

where

ϕ_1 = the 1st percentile porosity on a nearby calibrated log, typically 5 percent,

ϕ_2 = the 95th percentile porosity on a nearby stratigraphically equivalent calibrated log, typically 35 percent,

N_1 = the 5th percentile unscaled neutron log on the unscaled log, and

N_2 = the 99th percentile unscaled neutron log on the unscaled log.

Use of Barometric Efficiency to Estimate Aquifer Storativity

There have been few aquifer tests of the Edwards with observation wells from which storativity might be calculated. The sparse data limit the accuracy of estimates of how much water can be produced from the aquifer for a given amount of water-level decline. The purpose of this task was to determine whether water-level response to atmospheric pressure changes could be used to calculate storativity and porosity. Observing and comparing pressure fluctuations in the atmosphere and the confined aquifer might be a cost-effective method to estimate aquifer properties related to rock elasticity, compressibility of water, porosity, and hydraulic conductivity.

Atmospheric pressure fluctuations associated with passing weather systems, as well as induced by the daily cycle of warming and cooling of the atmosphere, can cause water-level fluctuations in wells penetrating confined aquifers. In response to this change in atmospheric pressure, water will move between the formation and the well until the water column in the well is in equilibrium with the atmosphere. Water levels in wells in confined aquifers fall in response to increases in atmospheric pressure and rise in response to decreases in atmospheric pressure (fig. 6). Because there are generally two atmospheric pressure cycles/day, water levels in aquifers responding to atmospheric pressure changes also show two cycles/day (fig. 7).

Atmospheric pressure changes can also affect water levels in unconfined aquifers. Peck (1960) showed that changes in atmospheric pressure affect the volume of air bubbles trapped in the water table. For example, as atmospheric pressure increases, air bubbles compress and water levels decrease. Peck (1960) also showed that this effect is greatest where the water table resides near land surface.

The difference between water-level fluctuations in confined and unconfined aquifers lies in how the aquifer takes up the change in stress owing to atmospheric pressure: compression of either solids (in a confined aquifer) or entrapped gas (in an unconfined aquifer). However, even water levels in deep unconfined aquifers can respond to atmospheric pressure fluctuations. Weeks (1979) showed that changes in atmospheric pressure almost instantaneously affect water levels in a well in an unconfined aquifer but that resistance to gas flow through the unsaturated zone retards the average effect on the water table.

Theory

If the magnitudes of the atmospheric and water-level pressure fluctuations are known, barometric efficiency, BE , can be calculated as

$$BE = \frac{\Delta h}{\Delta P_a} \quad (10)$$

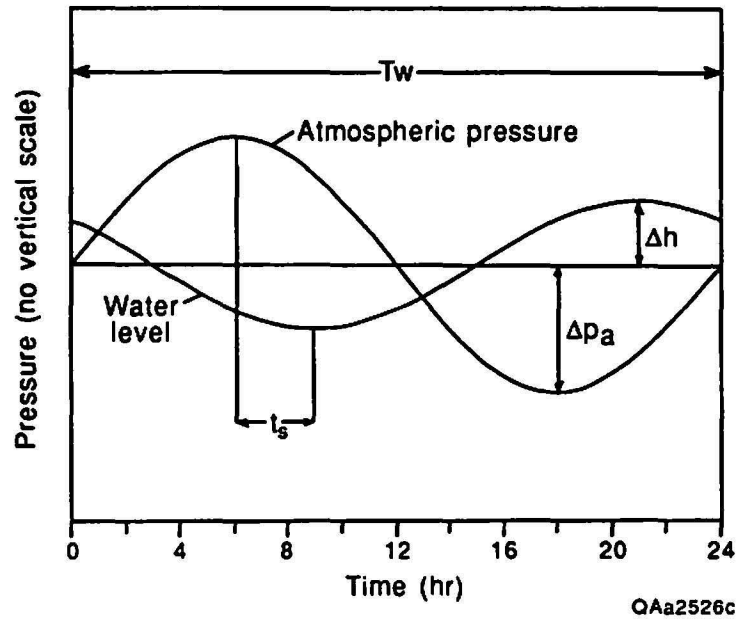


Figure 6. Idealized barometric efficiencies and water-level fluctuations. T_w = wave period, Δh = amplitude of water-level change, Δp_a = amplitude of barometric pressure change, and t_s = phase shift.

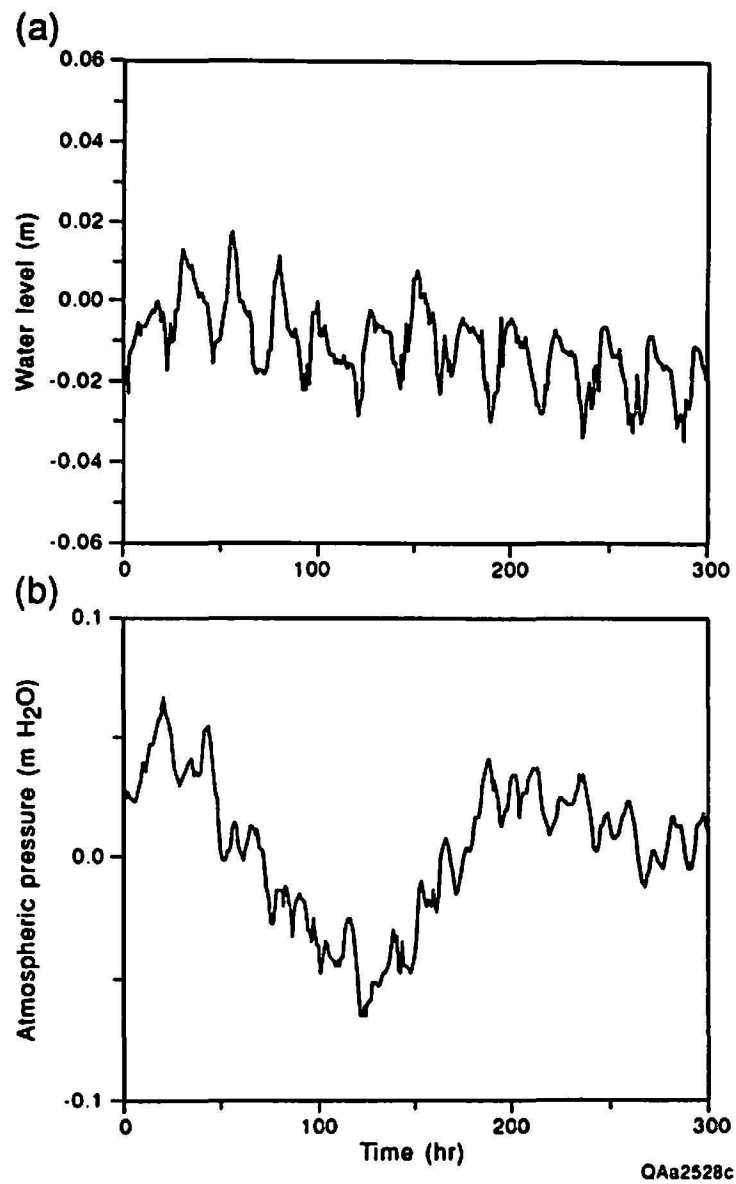


Figure 7. Typical fluctuations in (a) water level and (b) barometric pressure.

where

BE = barometric efficiency (dimensionless),

Δh = amplitude of water-level change (force/unit area), and

ΔP_a = amplitude of barometric pressure change (force/unit area).

Barometric efficiency represents how efficiently the aquifer absorbs atmospheric pressure fluctuation. A value of unity for barometric efficiency indicates that the aquifer is confined and responds completely to the atmospheric pressure change. Barometric efficiency usually falls between 0.20 and 0.75 and can be used to indicate of the degree of aquifer confinement—fully unconfined, unconfined with delayed yield, semi-unconfined, or fully confined (Kruseman and De Ridder, 1983).

Specific storage is the gain or loss of water volume in a unit volume of an aquifer with an accompanying unit change in hydraulic head. Storage is controlled by the compressibility of water and subtle changes in porosity related to aquifer elasticity. Jacob (1940) defined specific storage (S_s) as

$$S_s = \gamma(\alpha + n \beta) \quad (11)$$

where

γ = specific weight of water,

α = bulk compressibility of the aquifer,

n = porosity, and

β = compressibility of water.

It is convenient to refer to the storativity (S) for the entire thickness of an aquifer, calculated as specific storage times saturated thickness.

$$S = b S_s \quad (12)$$

Storativity, therefore, is gain or loss of water volume per unit surface area of a fully saturated aquifer of thickness b with a unit change in hydraulic head.

Barometric efficiency (BE) can also be related to the specific storage of the aquifer (Jacob, 1940)

$$S_s = \frac{n \gamma \beta}{BE} = \frac{n \gamma}{E_w BE} \quad (13)$$

where

E_w = elasticity of water, the reciprocal of compressibility (β).

Barometric efficiency can be estimated from water-level hydrographs and records of atmospheric pressure change (equation 10). Specific weight of water and bulk elasticity can be assumed constant. If the specific storage is known from aquifer test results, then average porosity of the entire completion interval in the well can be calculated from equation (13) and compared to porosity calculated from geophysical logs. In this study, estimates of average porosity are available from analysis of geophysical logs, so equation (13) is used to calculate specific storage from porosity and barometric efficiency.

Water-level trends owing to recharge and discharge must be removed from a hydrograph. Time lag in water-level fluctuations is another potential source of error (Freeze and Cherry, 1979). Because aquifer material resists flow, it takes time for the aquifer to respond to the atmospheric pressure change. Well-bore storage slows response time even more. Large-diameter wells need more time to reach equilibrium than small wells. These resistance and storage effects are expressed as a phase shift in the water levels (fig. 6). This phase shift factor is especially important when analyzing formation of low-permeability and/or large-diameter wells. As time lags and phase shifts are accounted for during analysis, barometric efficiency is correctly estimated (Hvorslev, 1951).

Analysis Technique

The Edwards Underground Water District provided data on water-level and atmospheric pressure fluctuations. Water-level fluctuations had been monitored at 17 wells in the Edwards aquifer at 15-minute intervals for the month of January 1993. All wells except one were

monitored using a float connected to a digital data logger; the other well (AY 68-29-209) was monitored using a pressure transducer and data logger. Atmospheric pressure data for January came from the National Weather Service office at San Antonio, Texas (Station WSFO).

Statistically significant temporal trends in water level were corrected by subtracting from each water-level reading the value calculated by linear-least-squares regression. Data were culled to retain only hourly readings to correlate with the atmospheric pressure data. Segments with a zero mean value were selected from the resulting hydrograph to exclude obvious noise, instrument malfunction, or water-level trends that remained after the linear regression.

The amplitude of the water-level and atmospheric pressure fluctuations can be determined in two ways. Standard deviations of the normalized water levels and atmospheric pressures can be calculated. This method allows a simple and fast approximation of the net effect of the first and second harmonics in the time series, but also includes other time-signal noise. Because daily fluctuations are time series, an alternative method is to employ harmonic (or Fourier) analyses to find mean fluctuation amplitudes for one and two cycles/day in large data sets. The latter approach is more sophisticated and filters out much of the noise in each data set.

RESULTS

Stratigraphic Model

The cyclic pattern of sedimentation predominant in the Edwards Group is the key to (1) stratigraphic correlation in different parts of the facies tract and (2) understanding and predicting the distribution and amount of porosity. The results presented here should be considered preliminary, based on examination of about half of the core and a small fraction of the outcrop data that could be incorporated into such a model.

Platform Cycle Types

Basic cycle types identified in the platform facies of the Person, Kalner, and Devils River Formations are (1) subtidal low-energy cycles, (2) subtidal low- to high-energy cycles, (3) subtidal low-energy to intertidal/supratidal cycles, (4) subtidal high-energy to intertidal/supratidal cycles, and (5) hypersaline cycles. The lithologic character of each cycle type is described in the following paragraphs and summarized in figure 8. Terminology used is that of Lucia (1983) modified from Dunham (1962).

Subtidal low-energy cycles

Subtidal low-energy cycles have a dark, wispy laminated, slightly argillaceous or organic-rich packstone or wackestone at the base (fig. 9a). These rocks typically contain burrows of the flattened *Planolites* type. Cycle bases are commonly grain rich rather than muddy, and in many cases the grains have dark coatings suggesting that they accumulated as a transgressive lag of residual grains. The upper parts of cycles are composed of more rapidly deposited burrowed packstones. *Thalassinoides*-type burrows are abundant, along with local firmgrounds, indicating that the substrate was firmer and more winnowed in response to increased energy resulting from sea-level fall. Whole unbroken shells of caprinid rudists are locally abundant in these cycles. This cycle type is characteristic of the basal nodular member of the Kalner Formation and the lower part of the Person Formation, including the regional dense member. Somewhat similar but more carbonate mud-rich facies with pyrite and glauconite are also found in the Georgetown Formation. Porosity is generally low in this facies, except where it has been dolomitized.

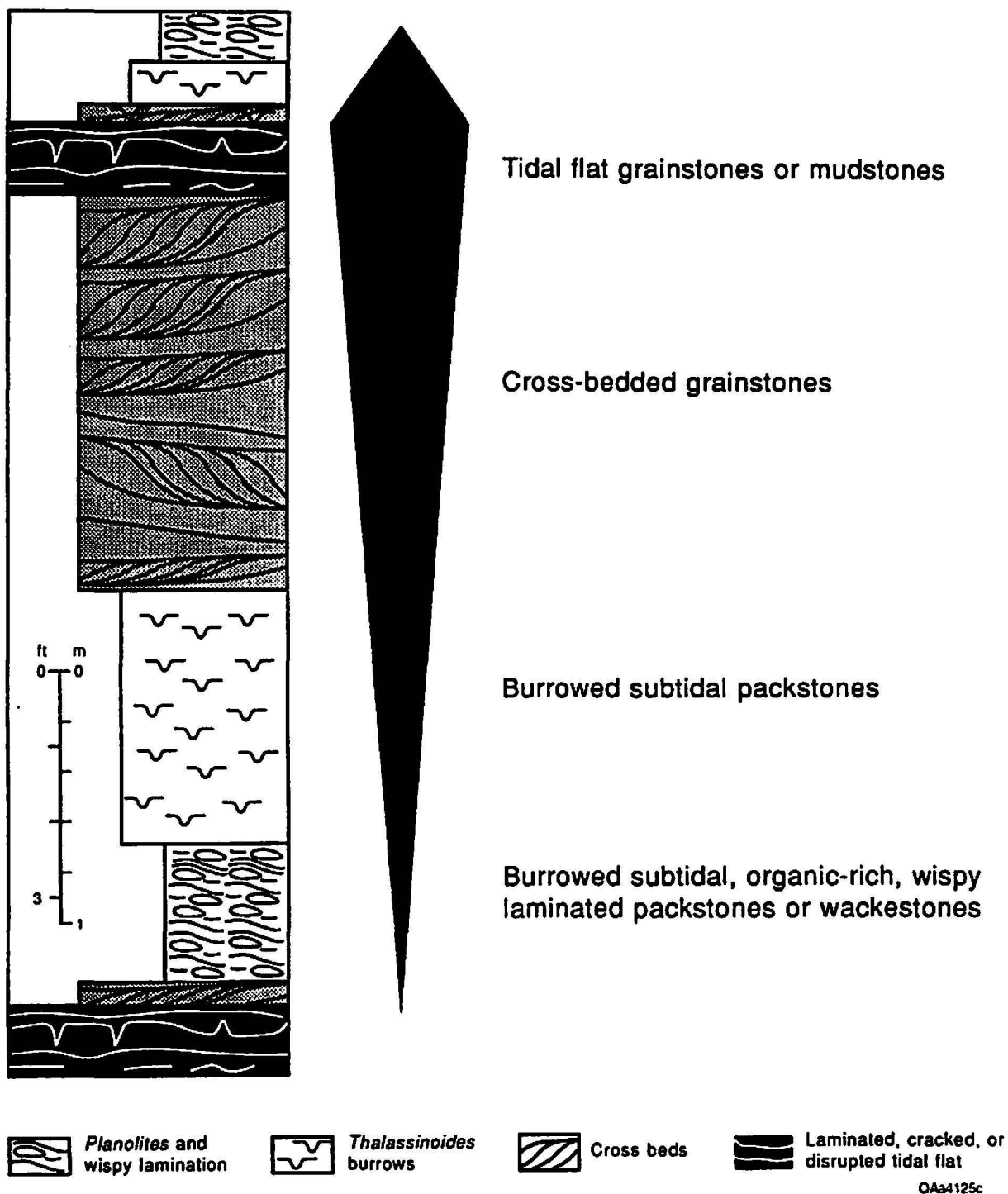
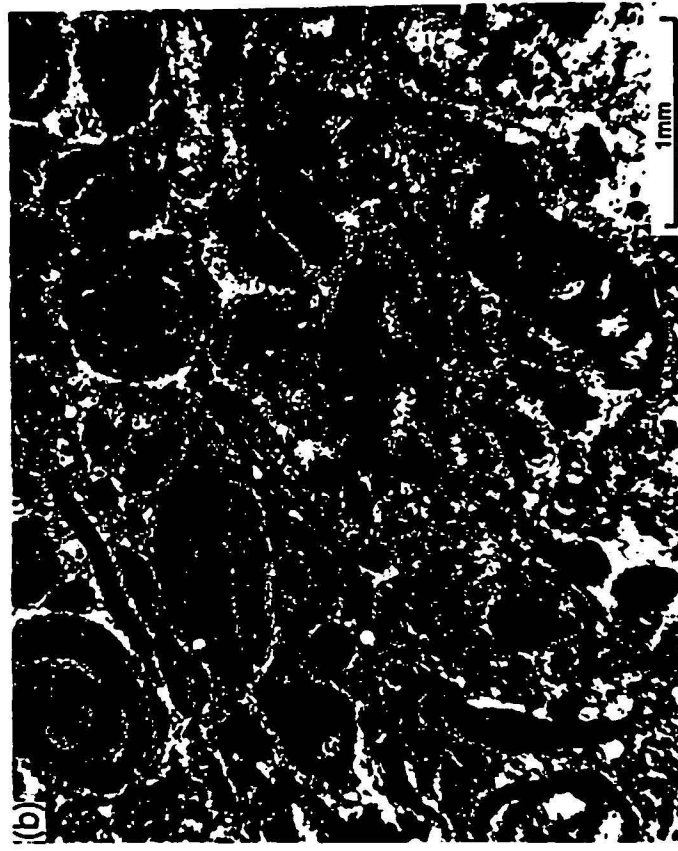
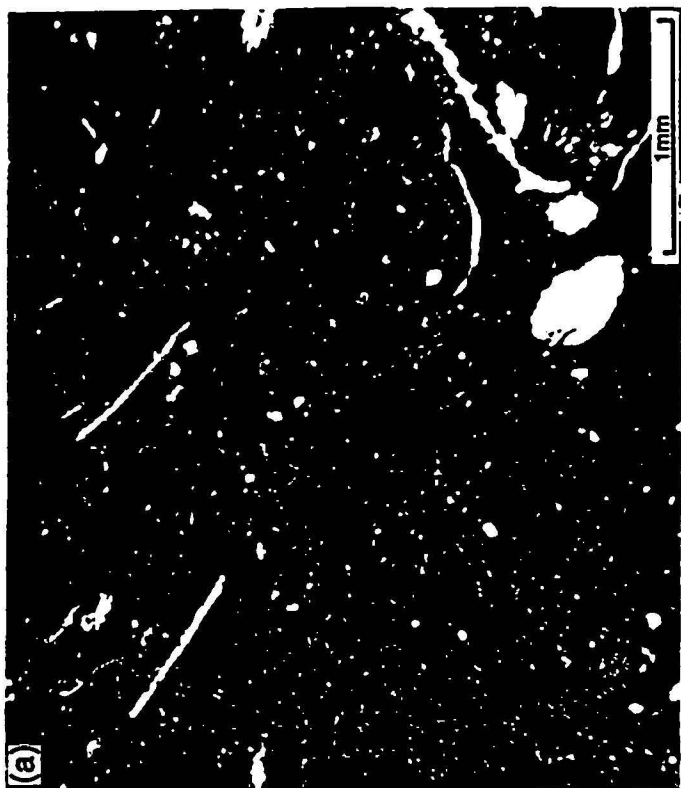
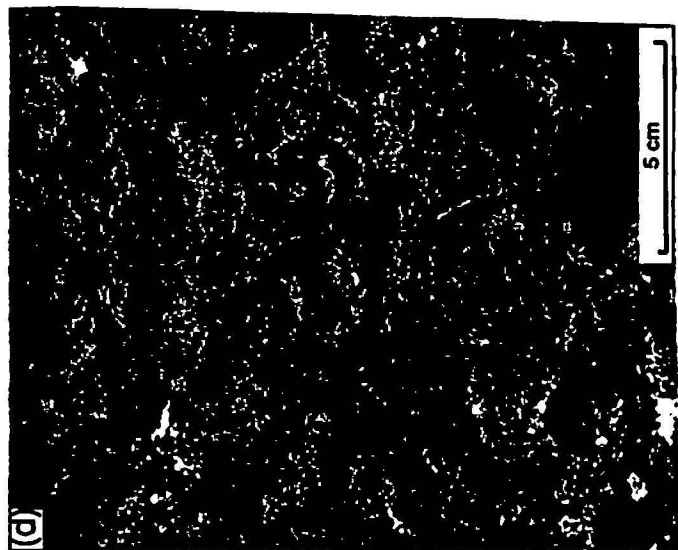
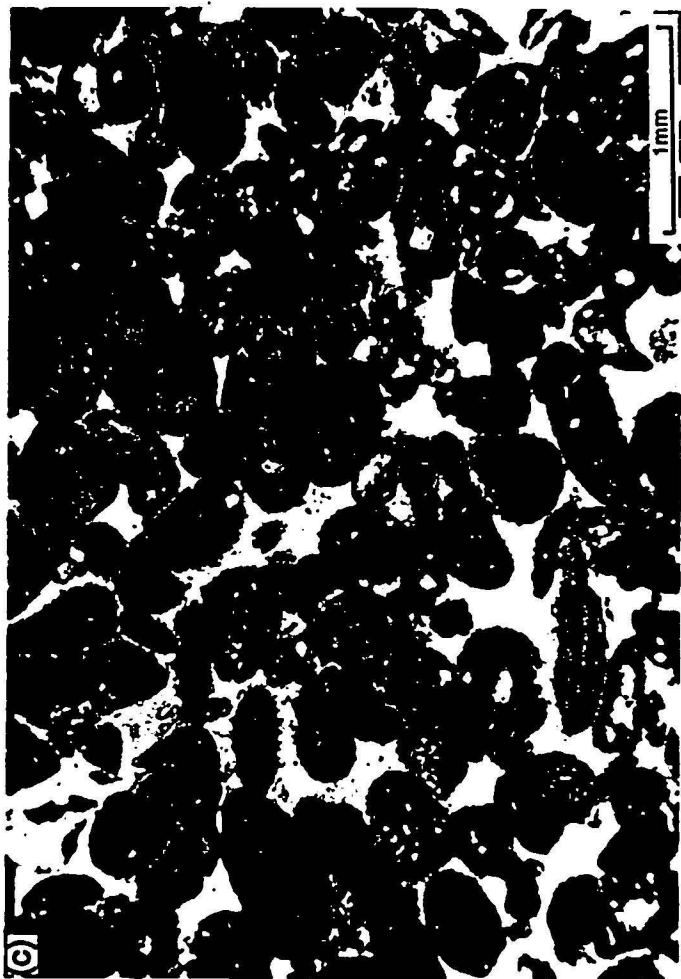


Figure 8. Idealized high-frequency cycle. Black bar shows lower shoaling upward part of cycle overlain by thin, transgressive part of cycle deposited as water depth increased.

Figure 9. Typical subtidal facies. (a) Normal marine, burrowed, slightly pyritic wackestone typical of low-energy conditions during maximum flooding of platform. Porosity is 8.5 percent, permeability 0.02 md. Regional dense member, USGS Castle Hills core, 402 ft. (b) Miliolid/skeletal packstone; compaction has decreased porosity to 3 percent. Grainstone member, upper Kainer Formation, USGS Castle Hills core, 448 ft. (c) Miliolid/peloid grainstone, approximately 15–20 percent primary intergranular porosity preserved. Lower Kainer Formation, TWDB TD-3 core, 604 ft. (d) Caprinid grainstone typical of top of Person. Porosity of interval is about 20 percent. USGS Sabinal core, 230 ft, Devils River Formation.



Subtidal low- to high-energy cycles

Subtidal low- to high-energy cycles are composed of burrowed packstone at their bases and become increasingly grainy upward (fig. 9b). Cycle tops consist of thick (3 to 20 ft [1 to 6 m]) sections of laminated or crossbedded grainstone. The most common grains are plates and fragments of phylloid algae, rudist and oyster shell fragments, ooids and coated grains, and miliolid forams (fig. 9c). Many grainstones are well sorted and range from very coarse to fine grained. Thick (0.2 to 2 inch [0.5 to 5 cm]) carbonate mudstone drapes are interbedded with some grainstones. Many cycle tops show evidence of gradual transgression and deepening in the form of thin units of finer-grained, muddier, and more burrowed beds above the high-energy crossbedded grainstones (fig. 8).

Subtidal low- to high-energy cycles are the most common cycle type in the Kainer, Person, and Devils River Formations. They are prominent in the lower part of the Kainer Formation and in the upper part of the Kainer Formation below the regional dense member in the grainstone member (Rose, 1972). Very coarse-grained rudist grainstones are typical of the top of the Person Formation on the San Marcos Platform and in the Devils River Formation (fig. 9d). Porosity in the packstones is typically low, except where they have been dolomitized. Porosity in grainstones is variable. Some have been wholly or partly cemented and the initial porosity reduced to 12 percent. Elsewhere, moderate to high primary porosity (30 percent) is preserved or the porosity is enhanced by macroscopic or microscopic (chalky) leaching (42 percent).

Subtidal low-energy to intertidal/supratidal cycles

Subtidal low-energy to intertidal/supratidal cycles have initial burrowed packstone facies similar to those previously described. Cycle tops are composed of thin-bedded intertidal or supratidal facies. The subtidal-supratidal contact may be gradational, showing a transition from packstone to burrowed, grain-dominated packstone to grainstone to intertidal grainstone, or it may be sharp with intertidal facies lying directly on subtidal facies. Intertidal facies include

thin-bedded, rippled grainstone interbedded with mudstone (fig. 10a) (tidal channel, washover fans, or other tidal-flat storm deposits) or thick, laminated carbonate mudstone intervals (hypersaline pond). Laminated grainstone with casts of gypsum crystals (hypersaline flat) and finely laminated, fenestral, pisolitic, or mud-cracked carbonate mudstone or grainstone with open or calcite-filled evaporite molds (fig. 10b, c, d) (supratidal-flat, algal-flat, or evaporitic supratidal facies) formed in intertidal to supratidal environments. Many intertidal rocks are composed of fine-grained dolomite. Many of these cycle tops also preserve a thin, transgressive unit composed of grainy packstone or burrowed grainstone above the tidal-flat facies.

Subtidal low-energy to intertidal/supratidal cycles are abundant in the middle part of the Kainer Formation, and they mark thin intervals defining lower-order cycle sets in the Person Formation on the San Marcos Platform. Porosity is low to moderate in intertidal facies, and dolomite and primary textures are well preserved (fig. 10b). Subtidal facies associated with supratidal flats have been intensely dolomitized, and many of them have been replaced by secondary calcite. These units have some of the highest observed porosities (40 percent). These dedolomitized subtidal units have been subjected to intense leaching and may be partly dissolved with only red, muddy residuum or coarse calcite spar remaining in outcrop.

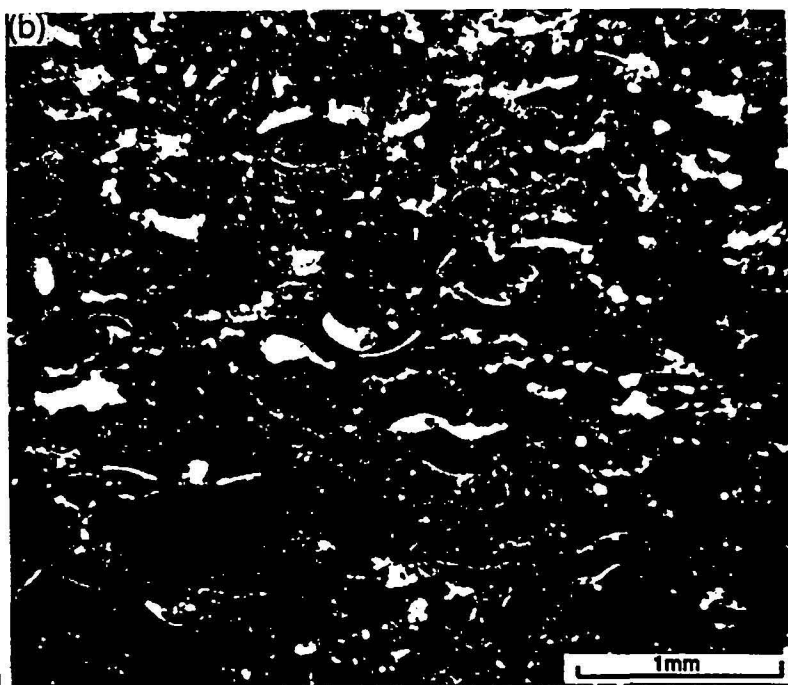
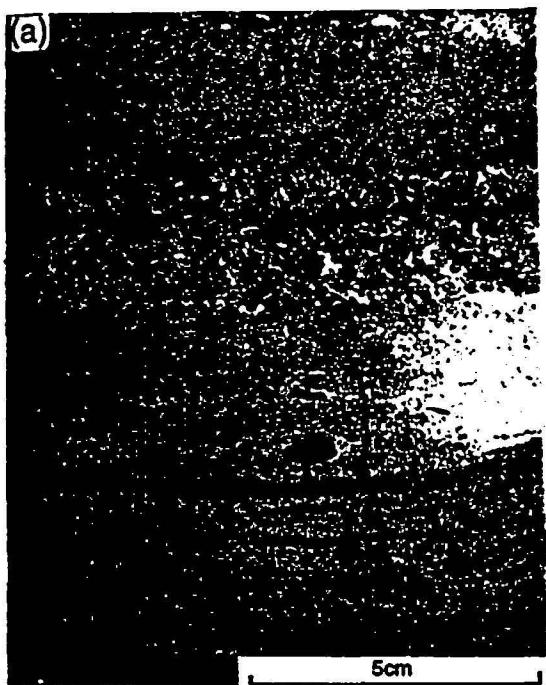
Subtidal high-energy to intertidal/supratidal cycles

These cycles are similar to the upper parts of subtidal low-energy to intertidal/supratidal cycles described above, but they lack the low-energy facies, resulting in tidal-flat rocks that are overlain by grainstone at the base of the next cycle.

Hypersaline cycles

A variety of hypersaline cycles were observed. All gypsum has been dissolved from the Edwards Group in the study area; therefore, its original character and fabric must be deduced from (1) the character of gypsum molds and calcitized gypsum, (2) the position of collapsed

Figure 10. Representative tidal-flat and evaporite facies. (a) Ripple cross-laminated grainy and evaporitic tidal flat, informal member 4 of Kainer Formation. Porosity of interval is about 18 percent. USGS TD-3 core, Medina County, 524 ft. (b) Finely crystalline tidal-flat dolostone is typically well preserved and not calcitized except in near surface or near fault settings. Porosity of sample is 9 percent. Person Formation, USGS Castle Hills core, 318.5 ft. (c) Tidal-flat mudstone, about 5 percent fenestral porosity. Person Formation, USGS Castle Hills core, 318.5 ft. (d) Vuggy porosity created by dissolution of gypsum crystals. In this core, partial replacement of gypsum by calcite has preserved much of gypsum fabric. In other wells, gypsum has dissolved, leaving collapse breccia. TWDB TD-3 core, Medina County, 376 ft.



intervals within cycles, and (3) analogy with preserved gypsum elsewhere in the Edwards Formation and in other stratigraphic intervals. Most of the calcitized gypsum in cores examined in the study area exhibits bottom-growth textures (Warren, 1982; Hovorka, 1992), indicating that gypsum precipitated on the floor of a shallow, gypsum-saturated brine pool rather than in sediments above a water table in a sabkha environment. Thick intervals of relatively pure gypsum with a "chicken wire" or nodular mosaic texture, such as that preserved in the Kirschberg quarry, initially form in a brine pool rather than in a sabkha setting. The significance of this interpretation is that brine pool gypsum forms in subtidal but restricted conditions. Gypsum overlying tidal-flat sequences indicates slight deepening. Many hypersaline cycles, especially those examined in the Devils River Formation, have carbonate grainstone at the base, overlain by as much as 3 ft (1 m) of alternating carbonate and bottom-grown gypsum. Other cycles have thin, supratidal carbonate overlying the gypsum. In some cases the gypsum intervals are preserved only as breccias where subtidal and supratidal carbonate beds within and above the gypsum section have collapsed into the void created by gypsum dissolution. Very coarse calcite spar is present as either pore-filling cement or gypsum replacement. Some excellent pseudomorphs of gypsum crystals are preserved now as calcite (fig. 10d).

Hypersaline cycles are found in the upper Kainer Formation (Kirschberg evaporite member) and in the lower part of the Person Formation (McAllen Ranch breccia of Rose [1972]). Intervals of dissolved evaporite have some of the highest porosity found in the Edwards aquifer, over 50 percent in caves and breccia intervals. In other places, for example the USGS TD-3 core in Medina County, calcite as gypsum replacement and pore-filling cement and red mudstone infill have reduced porosity, and evaporite intervals appear tight on logs as well as in core plug analysis.

Maverick Basin Facies

Cycles in the Maverick Basin are quite different from those on the platform. The West Nueces Formation is characterized by subtidal facies with weakly developed cyclicity (Smith, 1964). Porosity in the West Nueces Formation is low, 5 to 10 percent (fig. 11a). The overlying McKnight Formation has three members: a lower sulfate unit, a middle dark shale, and an upper sulfate unit (Carr, 1987). Deeper in the Maverick Basin in Val Verde County (Boundary Water Commission ID 22 core), preserved sulfates of the McKnight Formation were examined to interpret sulfate residues in Kinney and Uvalde County. Cycles are composed of 3 to 12 inches (10 to 30 cm) of dark *Gryphaea* packstone (organic, argillaceous carbonate) overlain by 3 to 6 ft (1 to 2 m) of bedded, nodular anhydrite (fig. 11b). Relict textures in the anhydrite suggest that it formed primarily as bottom-grown gypsum, with interbedded thin intervals of laminated carbonate. These textures indicate that the gypsum and the carbonate both formed in somewhat deeper water than the Kirschberg and McAllen Ranch evaporites on the platform, but in shallower and less stratified water than the Castile Formation in the Permian of the Delaware Basin (Anderson and others, 1972). The middle McKnight has only a few thin anhydrite interbeds and is composed of dark, argillaceous carbonate.

Dissolution has removed sulfate in much of the McKnight Formation of the study area. Porosities in the McKnight Formation are variable, generally about 5 percent, with irregular high spikes in breccia intervals. The presence of preserved evaporite at fairly shallow depth within this basin is one explanation for salinity variations shown by resistivity logs and presents a major problem in assessing porosities of this interval.

The Salmon Peak Formation overlies the McKnight Formation and is composed of fairly repetitive and homogeneous, burrowed miliolid wackestone, packstone, and grainstone (fig. 11c). Thin, coarser intervals have sharp bases and fine upward, increasing in frequency and thickness upward through the section (fig. 11d). The distinctly coarser miliolid grainstone found

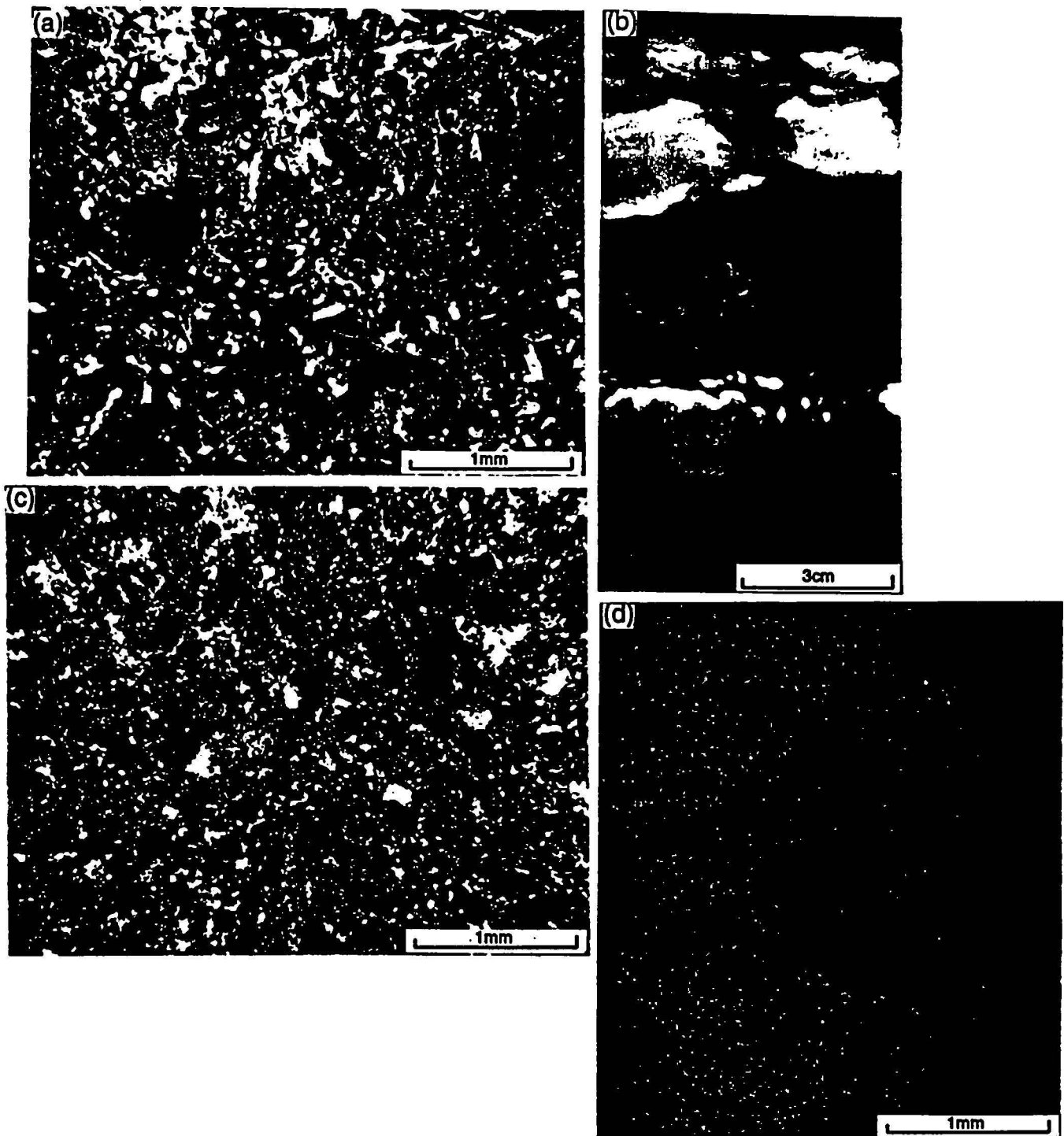


Figure 11. Representative Maverick basin facies. (a) Burrowed skeletal packstone, approximately 5 percent porosity, West Nueces Formation. TWDB YP-4 core, 640 ft. (b) Dark, laminated, organic-rich limestone and bedded, nodular anhydrite, McKnight Formation, International Boundary Commission core ID 22, 692 ft, Val Verde County. Sample from deeper parts of Maverick Basin shows predissolution character of McKnight Formation. In study area, much of original anhydrite has been dissolved, leaving low-porosity limestone and moderate-porosity breccia. (c) Peloid packstone typical of Salmon Peak Formation has 29 percent diagenetically enhanced chalky porosity, 317 md permeability. TWDB YP-4 core, 155 ft. (d) Grainstone-filled channel within finer miliolid grainstone of Salmon Peak Formation. Porosity of interval measured on logs is 30 percent. TWDB YP-4 core, Uvalde County, 633 ft.

at the top of the Salmon Peak Formation may be part of a progradational lowstand tract seen in outcrop (Smith, 1964; C. Kerans, personal communication, 1993).

The Salmon Peak Formation is moderately porous, 25 to 35 percent. The observed textural homogeneity of the deep-water grainstone and packstone was used to correct for resistivity log fluctuations that appear to be caused by high total dissolved solids (TDS) in waters of the lower part of the Maverick Basin.

Facies Relationships

A cross section based on cores (fig. 12) illustrates cycle stacking patterns that define third- or fourth-order relative sea-level fluctuations. Recognition of a sea-level-controlled cycle stacking allows correlation of time-equivalent sections in different parts of the facies tract. Several episodes of platform-wide flooding can be recognized: (1) base Edwards (nodular member)/Walnut Formation (Abbott, 1973), (2) middle Kainer, a thin but laterally persistent flooding surface, (3) regional dense member, (4) middle Person, and (5) base of the Georgetown Formation. These subtidal intervals are minimally dolomitized and have relatively low porosity. Separating these regional third-order highstands are gradual falls in relative sea level where sediment aggraded built toward wave base or into the intertidal zone. Exposure and tidal-flat development favored dolomitization, although the pattern is somewhat complicated by later diagenesis, especially dedolomitization. The mid-Kainer interval has many tidal-flat sequences (fig. 12). The overlying Kirschberg evaporite is interpreted as the product of a period of gradual deepening (backstepping cycles). Hypersaline subtidal evaporite cycles formed in slightly deeper water than the tidal flats. Grainstone cycles of the upper Kainer indicate continued gradual deepening and decreasing hypersalinity. The regional dense member formed during maximum flooding. The Person Formation is more aggradational, because sedimentation had difficulty keeping up with subsidence. This is evident in the paucity of supratidal facies in the Person relative to the Kainer. The muddier facies were ideal environments for rudists, and

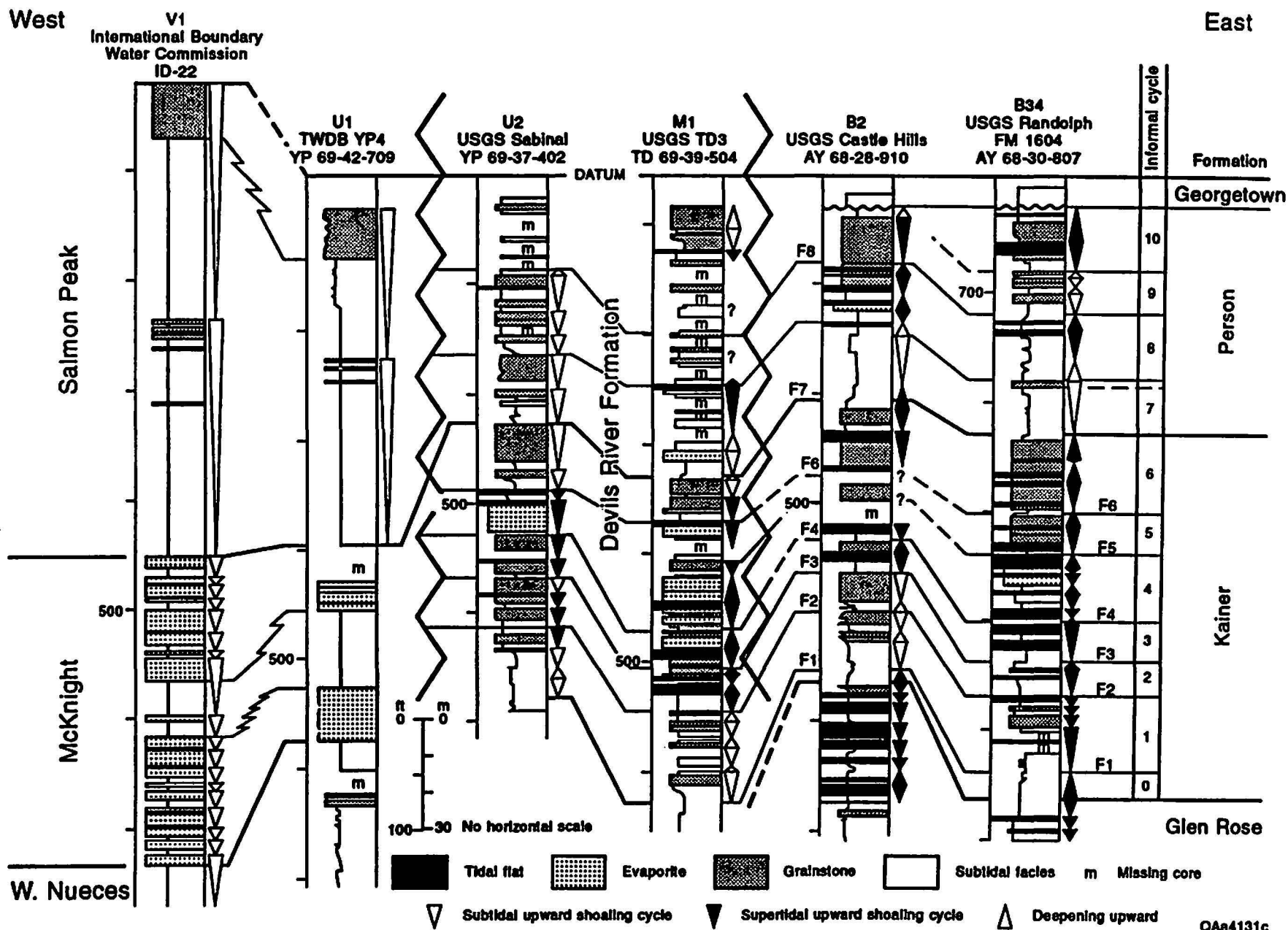


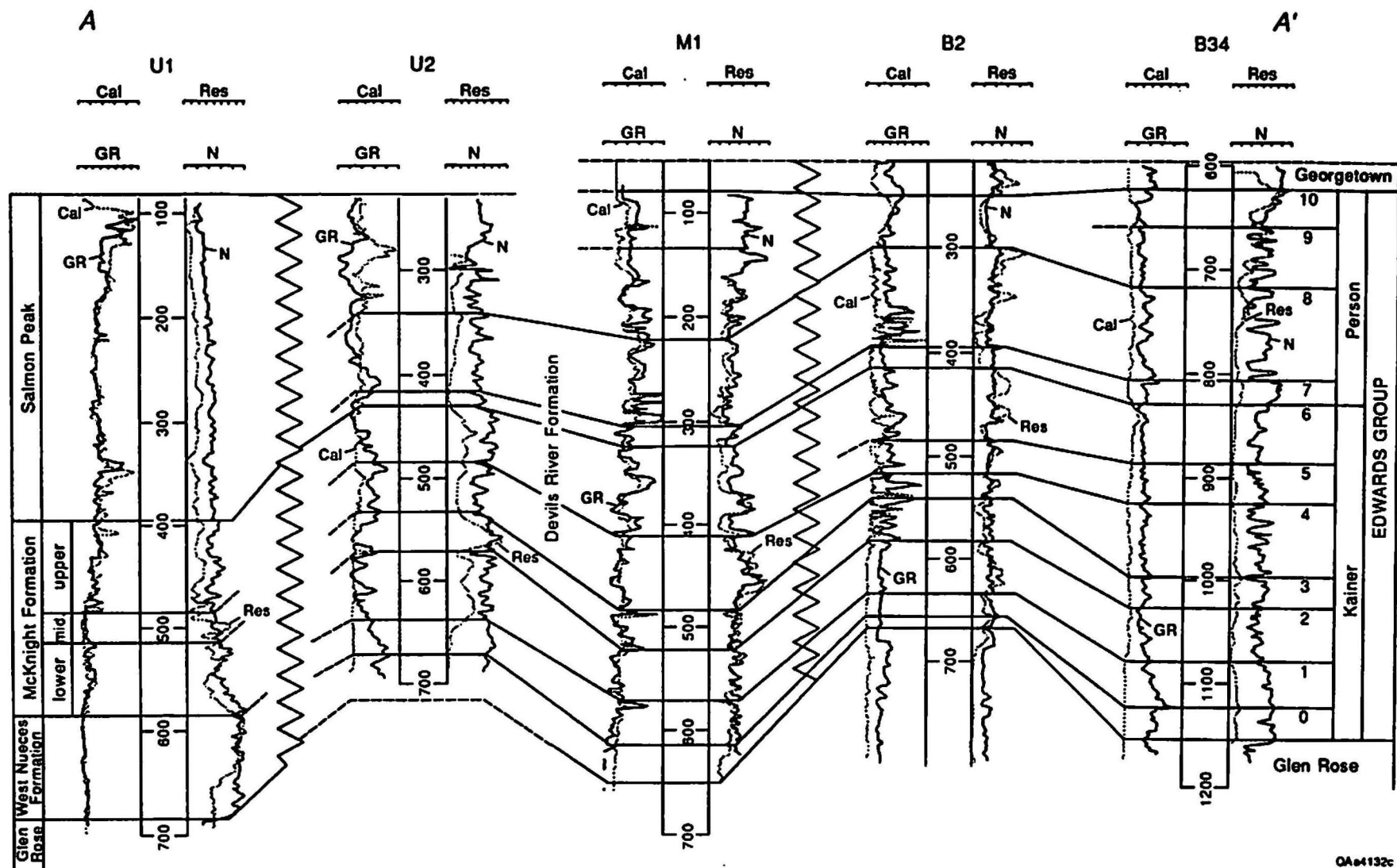
Figure 12. Systems tract interpretation of Edwards Group on the basis of examination of cores and outcrops. Cross section location shown in figure 1. Cycle numbers refer to cycles shown in figure 13.

caprinids and *Toucasia* are abundant. Coarse rudist grainstones are common toward the top of the Person Formation. The regional unconformity at the top of the Edwards Group described by Rose (1972) is not seen clearly in this study. However, textures at the top of the Edwards in two cores (Randolph and Castle Hills) may be evidence of exposure and freshwater diagenesis.

The temporal relationships between the Maverick Basin facies and the San Marcos Platform facies remain problematic. Some previous correlations (Rose, 1972; Sieh, 1975; Miller, 1983) suggested that the argillaceous middle McKnight of the basin correlates with the regional dense member of the platform. An alternative, used here because it keeps unit thickness in the platform and basin more constant, is to correlate the base of Salmon Peak freshening with the basal Person regional dense member flooding event. Resolution of this problem is of minimal significance to the present porosity study, because most of the porosity in the Maverick Basin section is in the Salmon Peak Formation.

Log-Based Correlation

The genetic sequences identified during core descriptions were matched with equivalent log picks, and the log character was traced regionally (fig. 13). The subdivisions are generally similar to those made by Rose (1972), but differ because the units are defined not by the dominant lithology but by tracing the cyclic response of sedimentation to sea-level rise and fall across the platform. In addition, the complex response of logs to depositional facies and diagenetic changes made many of the high-frequency correlations difficult. The Kainer Formation is subdivided into log units 0 through 6; the Person Formation is divided into log units 7, 8, 9, and 10. Unit 0 is a high-gamma-ray, low-porosity unit. It is equivalent to parts of the Walnut, and genetically is a complex, time-transgressive unit recording flooding and cycle backstepping following the post-upper Glen Rose sea-level lowstand. Unit 1 is approximately equivalent to the lower nodular member of the Kainer Formation. Its base is defined at the maximum flooding surface and is a dominantly subtidal progradational unit with low porosity.



QA-1132c

Figure 13. Log cross section showing representative logs and stratigraphic units that were identified regionally. Cross section location shown in figure 1.

Unit 2 is a time-transgressive unit of progradational grainstones, approximately equivalent to the dolomitic member of Rose (1972). Unit 3 is an upward-shoaling progradational set of cycles with thick tidal-flat caps. Unit 4 is an aggradational set of cycles, many containing evaporites equivalent to the Kirschberg. Unit 5 and 6 contain cycles with thick grainstones in the upper parts and exhibit upward-deepening trends and probable backstepping geometries.

The regional dense member at the base of the Person Formation, unit 7, was deposited during maximum flooding. This unit gradually shoals upward into unit 8. Unit 8 is also composed dominantly of subtidal cycles. Unit 9 contains a number of tidal-flat cycles and grainstone on the San Marcos Platform. Unit 10 on the San Marcos Platform contains thick rudist grainstones.

The most reliable log picks on horizons bounding the porous parts of the Edwards aquifer were selected for the stratigraphic model. These are (1) the Glen Rose (unit 0) contact across the entire area; (2) the structural base of the regional dense member (unit 7) on the San Marcos Platform and its interpreted approximate correlative, the base of the Salmon Peak Formation in the Maverick Basin; and (3) the structural base of the Del Rio Formation. These horizons subdivide the Edwards into two units for porosity mapping: a lower Walnut-Kainer-lower Devils River-West Nueces-McKnight interval and an upper Person-Georgetown-upper Devils River-Salmon Peak interval. The thicknesses of these two intervals were mapped and contoured (plates 2, 3, and 4). The thickness of the Edwards Group increases gradually toward the Gulf Coast from a minimum of 500 feet (150 m) to a maximum of 780 feet (240 m) and averages 560 feet (170 m) in the confined part of the study area. Thickness of the saturated, unconfined part of the aquifer decreases rapidly toward the north across the outcrop of the Edwards Group. The structural surface and thickness maps were loaded into Stratamodel SGM® to guide porosity interpolation during three-dimensional modeling.

Porosity Description from Core and Thin Section

Six major categories of high porosity are recognized in the Edwards aquifer:

(1) Intergranular porosity in grainstones, (2) Intercrystalline porosity in dolostone, (3) solution-enhanced intergranular/intercrystalline porosity, (4) fracture- and solution-enhanced fracture porosity, (5) cavernous porosity produced by gypsum or carbonate dissolution, and (6) intraclastic porosity in breccia. In many intervals two or more of these porosity types are found in the same rock. Other porosity types such as moldic pores contribute relatively minor amounts to the total porosity.

Intergranular Porosity in Grainstones

Intergranular porosity in grainstones is depositional porosity that has not been lost during sediment lithification. Grainstones composed of platy phylloid algae fragments, rounded skeletal grains, ooids, or coated grains have normal grainstone porosities of 25 to 35 percent (fig. 9c). However, Edwards aquifer grainstone porosity has been reduced in the depositional environment by the introduction of mud by burrowing and in the subsurface environment by diagenetic processes of cementation or compaction (9b). Gypsum beds and cement have played a complex role both in enhancing and occluding porosity. Very high porosity and permeability were created where a rock of uncertain original composition, possibly a dolomitized grainstone, has been completely replaced by calcite spar with very high intergranular/intercrystalline porosity (fig. 14b). A nearby grainstone has been tightly cemented by sparry calcite (fig. 14a).

Some porosity is found in grainstones composed of complexly shaped fossil shell fragments such as those of the rudist *Toucasia*. It is difficult to assess how much of the porosity in these rocks is accessible. Closed pores within the shell structure may not contribute to permeability, and calcite cement, perhaps derived by dissolution of aragonitic (a mineral variety of CaCO_3) shell material, reduces the porosity and complicates the permeability. In other cases, calcite

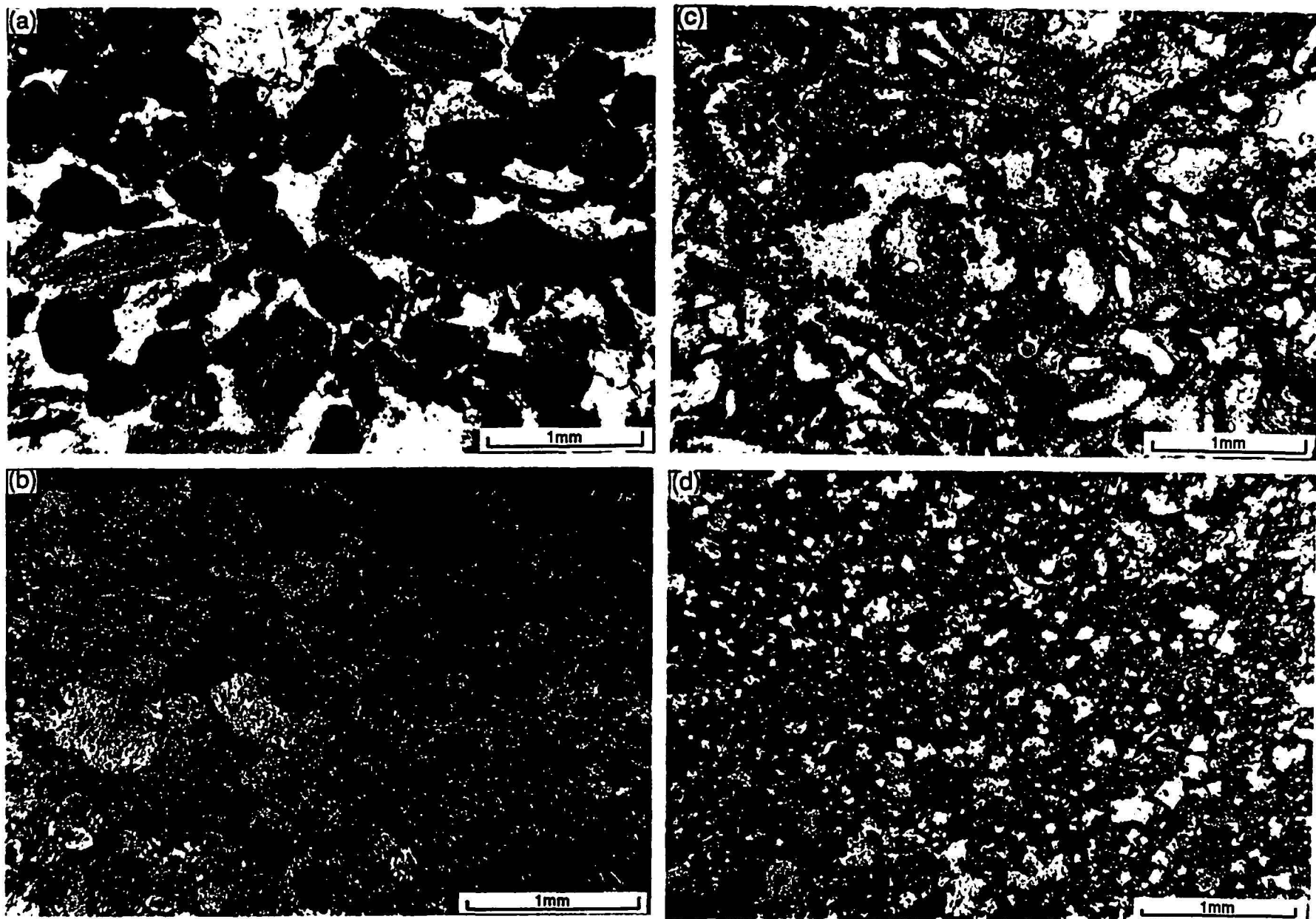


Figure 14. Diagenetic modification of porosity. (a) Calcite-spar-cemented milliolid/skeletal grainstone from same intervals has only 6.9 percent porosity, 0.08 md permeability. USGS Sabinal core, 562 ft. (b) Highly altered grainstone(?) from Kalner Formation below Kirschberg member has 9.5 percent porosity, 11 md permeability. USGS Sabinal core, 566 ft. (c) Upper Person rudist grainstone, 31.4 percent moldic porosity. Permeability of 199.9 md shows that molds are well connected. USGS Castle Hills core, 253 ft. (d) Leached dolomite from subtidal wackestone within interval of thick tidal-flat caps has about 20 percent porosity. TWDB TD-3 core, 551 ft.

dissolution has interconnected moldic porosity, creating moderate porosity and high permeability (fig. 14c). *Toucasia* grainstone porosity ranges from 12 to 25 percent.

Intercrystalline Porosity in Dolostone

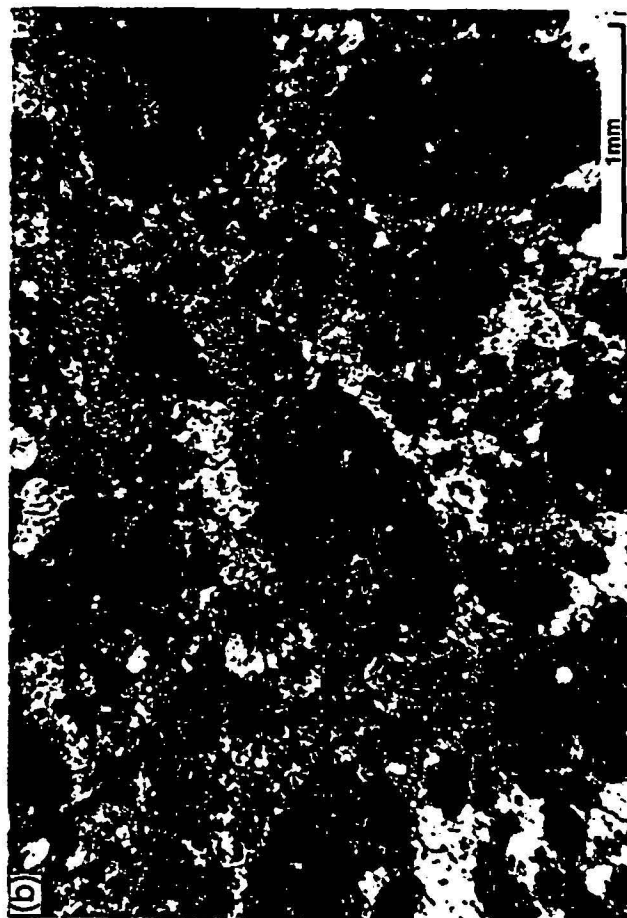
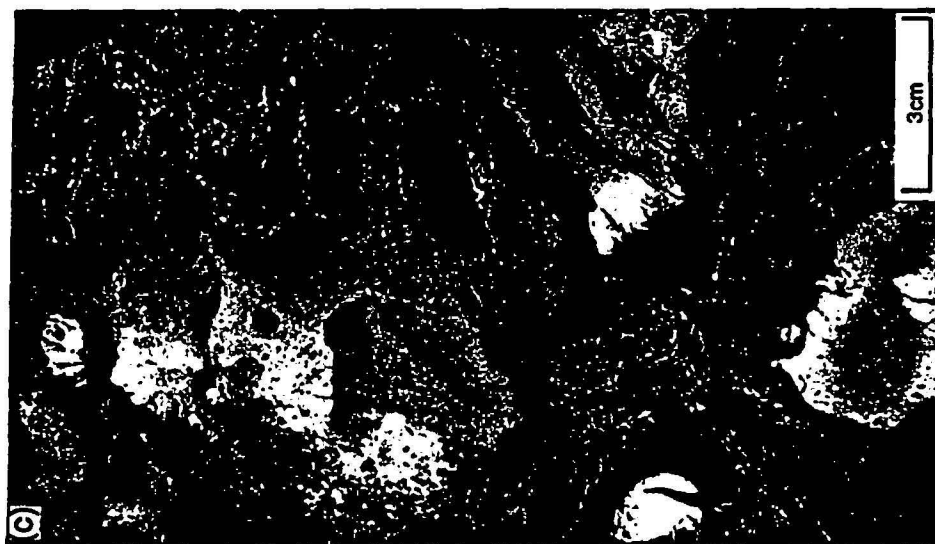
Dolomitization and subsequent dedolomitization has increased the porosity of subtidal mudstones, wackestones, and mud-dominated packstones in some intervals. Without dedolomitization, these carbonate mud-rich rocks would lose most of their porosity during sediment compaction and stabilization. Dolomitization of subtidal sediments appears to be associated with the intervals containing thicker tidal-flat sequences. The association of dolomitized subtidal rocks with tidal flats suggests that hypersaline brines generated on supratidal flats may have contributed to dolomitization of the subtidal sediments. Geochemical studies of Edwards dolomite suggests that there were two episodes of dolomitization, an early episode with hypersaline water and a later episode with fresh to slightly saline water (Ellis, 1986a). Detailed geochemical and petrographic studies needed to document this hypothesis were not part of this research; however, the facies association can be used to explain porosity decreases in more subtidal grainstone facies off the San Marcos Platform.

In most examples in the Edwards aquifer, intercrystalline porosity of subtidal dolostone has been enhanced by partial or complete dolomite dissolution (figs. 14d, 15a). Finely crystalline dolomite in low-porosity supratidal facies has not generally been replaced by calcite.

Solution-Enhanced Intergranular/Intercrystalline Porosity

Solution-enhanced intergranular/intercrystalline porosity is a common cause of high porosity in the Edwards aquifer. Postcementation dissolution has enhanced the porosity of many grainstones and most dolostones (Ellis, 1986a). Grainstone dissolution enlarges pores by dissolving both cement and grains (fig. 15b). This dissolution is probably quite significant in improving permeability because the larger and better interconnected pores have been further

Figure 15. Diagenetic modification of porosity by dolomitization and leaching. (a) Leached dolomite from subtidal, burrowed pellet packstone within interval of abundant tidal flats has 27 percent porosity, 33.4 md permeability. USGS Randolph FM 1604 core, 924 ft. (b) Both grains and cement have been leached from this calcite-spar-cemented grainstone, resulting in about 15 percent porosity. (c) TWDB TD-3 core, 280 ft. Vuggy porosity because of preferential dissolution of dolomitized areas in subtidal wackestones. (d) Bulverde section, Bexar County, Kainer Formation, showing meter-scale cycles. Dark zone is dolomitized subtidal unit that has been intensely altered and partly dissolved.



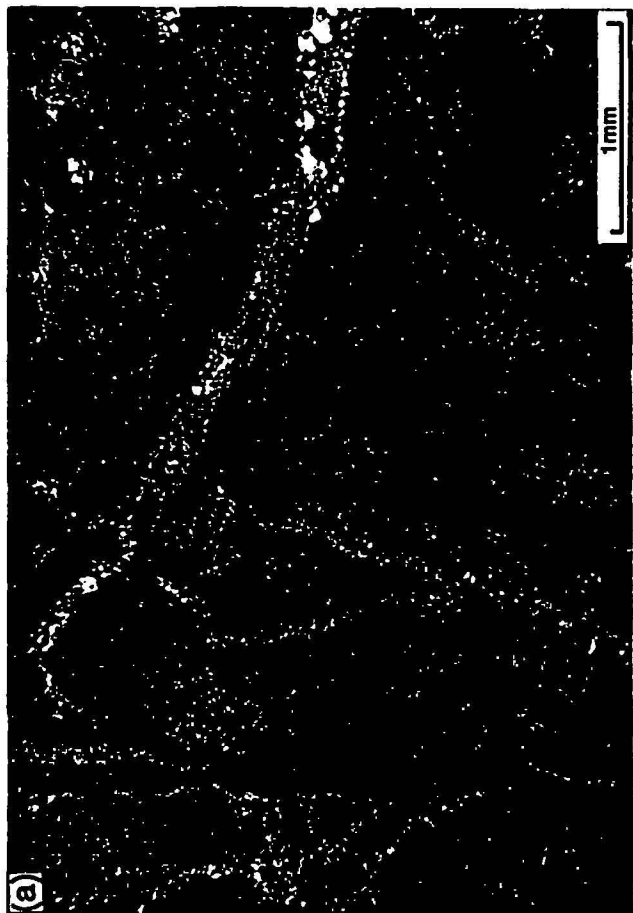
enlarged and connection improved. Calcite dissolution also occurred on a fine scale creating chalky textures. Solution enhancement of permeability is especially important in the freshwater parts of the aquifer (Maclay, personal communication, 1993).

Dissolution of dolomite is a complex process (Abbott, 1974; Ellis, 1986b). Dolomite is out of its stability field in the meteoric magnesium-poor calcium-bicarbonate waters probably introduced into the aquifer at the time of uplift along the Balcones Fault system (Abbott, 1975). These waters have (1) dissolved dolomite, (2) precipitated calcite, and (3) dissolved calcite, resulting in rocks with remnant finely crystalline dolomite outlining former crystals and grains within coarsely crystalline calcite. Large intercrystalline pores are the product of this process in many Edwards Group rocks. Dedolomitization and dolomite dissolution have preferentially attacked dolomitic sections of partly dolomitized subtidal rocks, creating patchy but probably interconnected porosity (fig. 15c, d). Solution-enhanced porosity as high as 42 percent was measured in diagenetically modified dolostone.

Fracture- and Solution-Enhanced Fracture Porosity

Fracture- and solution-enhanced fracture porosity contributes to the total porosity of the Edwards Group. These types of porosity development may have a very strong local and potentially regional effect on permeability (Wermund and others, 1978; Senger and Kreitler, 1984; Maclay and Small, 1986). Closely spaced fractures are typical of low-porosity subtidal rocks, probably because they are more brittle than high-porosity rocks. Many fractures have been partly infilled with calcite cement (fig. 16a); a few have been enlarged by ground water undersaturated with respect to calcite. Some fracturing is the result of dissolution and collapse; however, much Edwards aquifer fracturing probably accompanied Balcones faulting, which probably occurred in the Miocene and resulted in uplift of the Edwards Plateau relative to the Gulf Coast (Ewing and Wilbert, 1991). Fracture intensity may not be represented properly in core, because often recovery is poor in fractured intervals. In the Glen Rose Formation in

Figure 16. Diagenetic modification of porosity by faults, fractures, and karst. (a) Brecciation and fractured low-porosity, subtidal limestone bed within Kirschberg evaporite, Kalner Formation, TWDB TD-3 core, 404 ft. Some fractures are open; others have been cemented by calcite. Fractures contribute only minor porosity but substantive permeability. (b) Vug with travertine infill in interval of calcitized gypsum breccia has only 9.6 percent porosity and 126 md permeability. USGS Castle Hills core, 288 ft. (c) Carbonate dissolution and karst seen in core as missing intervals with red clay and travertine coats on rounded carbonate breccias. Porosity of interval measured by neutron log is 30 percent. USGS Castle Hills well, Person Formation, 274 ft. (d) Highly altered fabric in Person Formation, New Braunfels. This section is north of a major fault system. Limestone, dolomite, and possible evaporite have been replaced by calcite, partly dissolved, with ensuing collapse. Fine-grained subtidal limestone beds are preserved and retain original low (5 percent) porosity. Cave on right side of photograph is a common porosity type in the Edwards.



Bexar County, fracture intensity has been measured in outcrops (Collins, in press) and, between two en echelon faults, is twice that of relatively undeformed areas. The porosity contribution of fractures is small, and fractures are not identifiable on normal logs unless the rock is brecciated and causes breakout of the well bore.

Cavernous Porosity Produced by Gypsum or Carbonate Dissolution

Cavernous porosity produced by gypsum or carbonate dissolution is unquestionably present in the Edwards aquifer (Fieseler and others, 1978) but is difficult to quantify in core and logs. Karst cavities in core appear as intervals with poor recovery containing solution-rounded locally derived carbonate cobbles in a red, argillaceous mudstone (fig. 16c). Flowstone and coarse calcite cements document partial infilling of some karst cavities. Karst cavities appear on logs as high-caliper intervals or higher than average natural gamma-ray response because of the red clay (terra rosa) fills. Resistivity log response is anomalously low.

Intraclastic Porosity in Breccia

Intraclastic porosity in breccia is another porosity type closely related to karst, because when a carbonate or gypsum layer dissolves, a structural configuration that exceeds the mechanical strength of the roof rock is created. Collapse breccia occurs in a wide variety of grain sizes and forms. Two main geometries are noted: stratabound breccias and cave collapse breccia. Stratabound breccias result from dissolution of the more soluble layers (gypsum and dolomite) and collapse of the undissolved interbedded material and variable amounts of the overlying roof (fig. 16d). Because they are continuous over large areas, stratabound breccias are volumetrically the major contributors. Cave collapse breccias form as the arched roof of a cavern spalls and accumulates in a large, irregular pile on the cave floor. Large amounts of overlying material fall into the cave when the roof eventually collapses. Cave collapse breccia can be formed of large rotated blocks of the roof material or of nearly in situ residue of material

remaining after dissolution. Clay, sand, and silt are commonly transported through breccias; they may be deposited and plug the porosity. Breccia porosity cannot be measured using core plugs because of the very large clast size. Log measurement of porosity in breccia intervals is variable, depending on cementation. In some intervals of dissolution breccia, abundant calcite has precipitated. Dissolution of vugs created moderate porosity but high permeability (fig. 16b). Concentrations of transported or residual clay in some of these intervals may produce anomalously high porosity estimates.

In summary, porosity in the Edwards aquifer can be divided into matrix porosity such as intergranular, intercrystalline, and moldic pores, and secondary large pores (touching vug) such as solution vugs, fractures, solution-enhanced fractures, breccia, and caverns. The distribution of porosity is complex as a result of Cretaceous and post-Miocene diagenetic changes to the original porosity of the sediments in the mosaic of carbonate/shelf facies.

Porosity/Permeability Relationships

Permeability and porosity were measured on the same samples (table 2). This study does not undertake interpretation of the permeability data; however, because permeability is a factor in the amount of water available for pumpage, the following preliminary observations are noted. Most of the sample suites analyzed show multiple porosity/permeability relationships. One group of samples had low permeability at moderate porosity, a relationship typical of fine-grained rocks with small pore throats. In the USGS YP-4 core, samples from the Salmon Peak Formation with porosities of 25 to 30 percent have permeabilities between 10 and 100 millidarcies (md), corresponding to fine porosity observed in thin section of these burrowed, fine-grained rocks. Similar porosity/permeability trends were observed in the USGS Randolph core from an area south of the bad water line. The other cores have many samples with high permeability at moderate porosity, exceeding 10 md at porosity of 10 percent, as well as some samples falling on the lower permeability trend. The high-permeability samples generally

correspond to areas where diagenetic alteration, such as replacement of dolomite by calcite or enlargement of pore throats by dissolution, has increased both porosity and permeability.

Porosity Calculation

Porosity was calculated for 125 well logs, including scaled neutron, scaled resistivity, unscaled neutron, and unscaled resistivity (table 1). In the USGS Randolph FM 1604 borehole, porosity measured in core plugs collected at 1-ft (30-cm) spacings matched neutron porosity closely (fig. 17). Similar moderate to good matches between plug porosity and the calibrated log porosity calculated for this study were obtained in other wells (figs. 17 through 21). Porosity derived from scaled neutron logs is considered the most accurate (fig. 22a). Porosity derived from resistivity logs generally had a poorer fit to the plug porosity (fig. 22a). This reflects variation in pore-fluid salinity and measurement of porosity through a larger rock volume, resulting in a smoother and more averaged curve. The effect of higher salinity (and therefore higher specific conductance) can be seen near the base of the borehole in figures 18 and 20. This high salinity may be evidence of cross-formational leakage of higher TDS waters from the Glen Rose Formation as was described in the northern part of the Edwards aquifer by Senger and others (1990). After calibration of the logs, thin intervals with the lowest resistivities had very high (more than 50 percent) calculated porosity (figs. 18 and 20). Some of these might be the product of a bad borehole or poor calibration. These intervals in core from boreholes, however, generally corresponded to zones of poor recovery or to beds of travertine and red clay, suggesting the presence of large karst-related vugs or honeycombed breccia. These high-porosity intervals, therefore, were retained in the data set and the amount of possible error in total water volume was estimated.

Porosity calculated from many commercial resistivity logs produce high-porosity values of 30 to 40 percent but low-porosity values of 15 to 20 percent. The high values are typical of porosity measured using neutron logs and plug analysis, indicating that the logs are properly

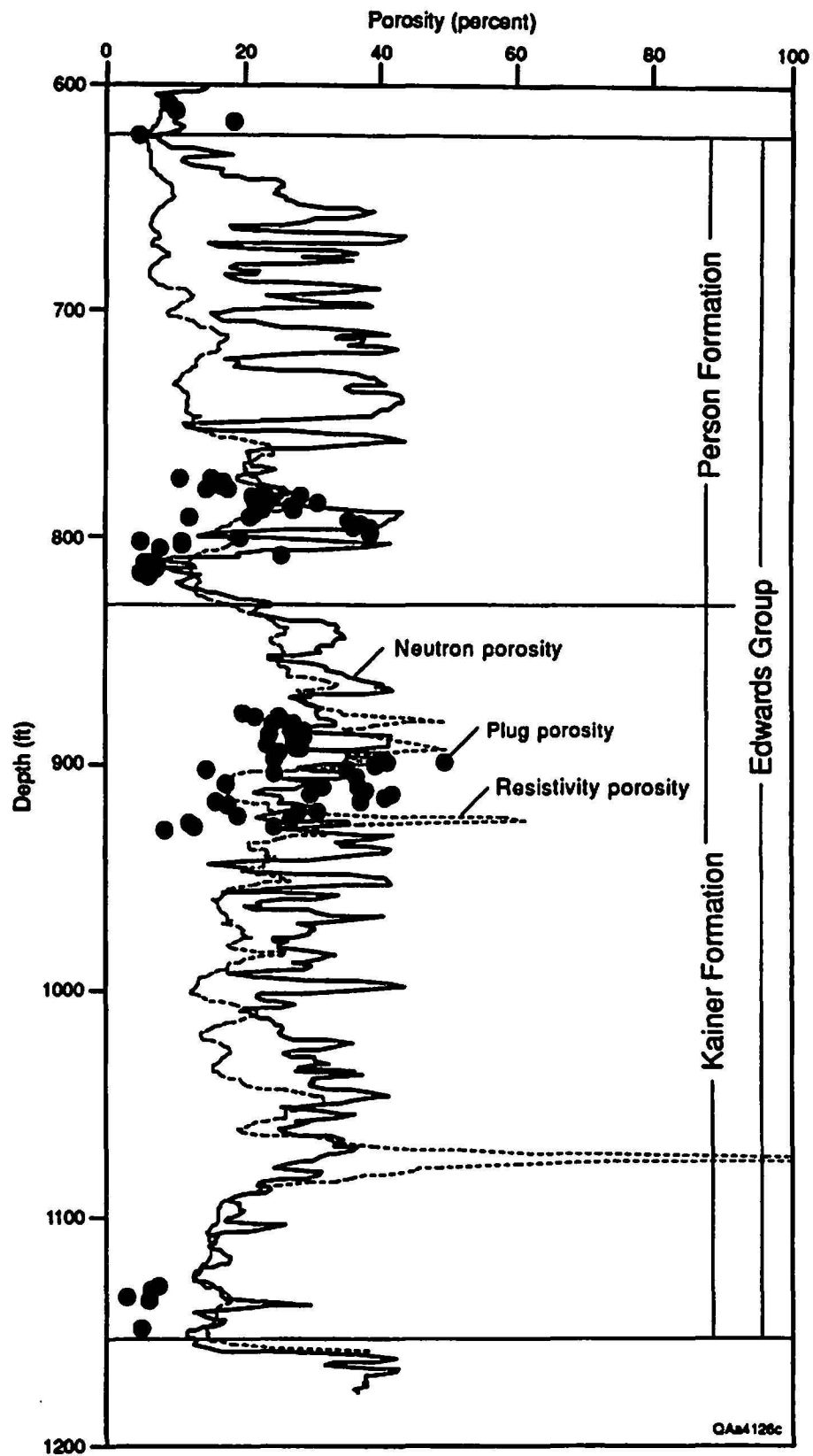


Figure 17. Calculated (scaled neutron, unscaled resistivity) and measured porosity, USGS Randolph FM 1604 well, AY 68-30-807.

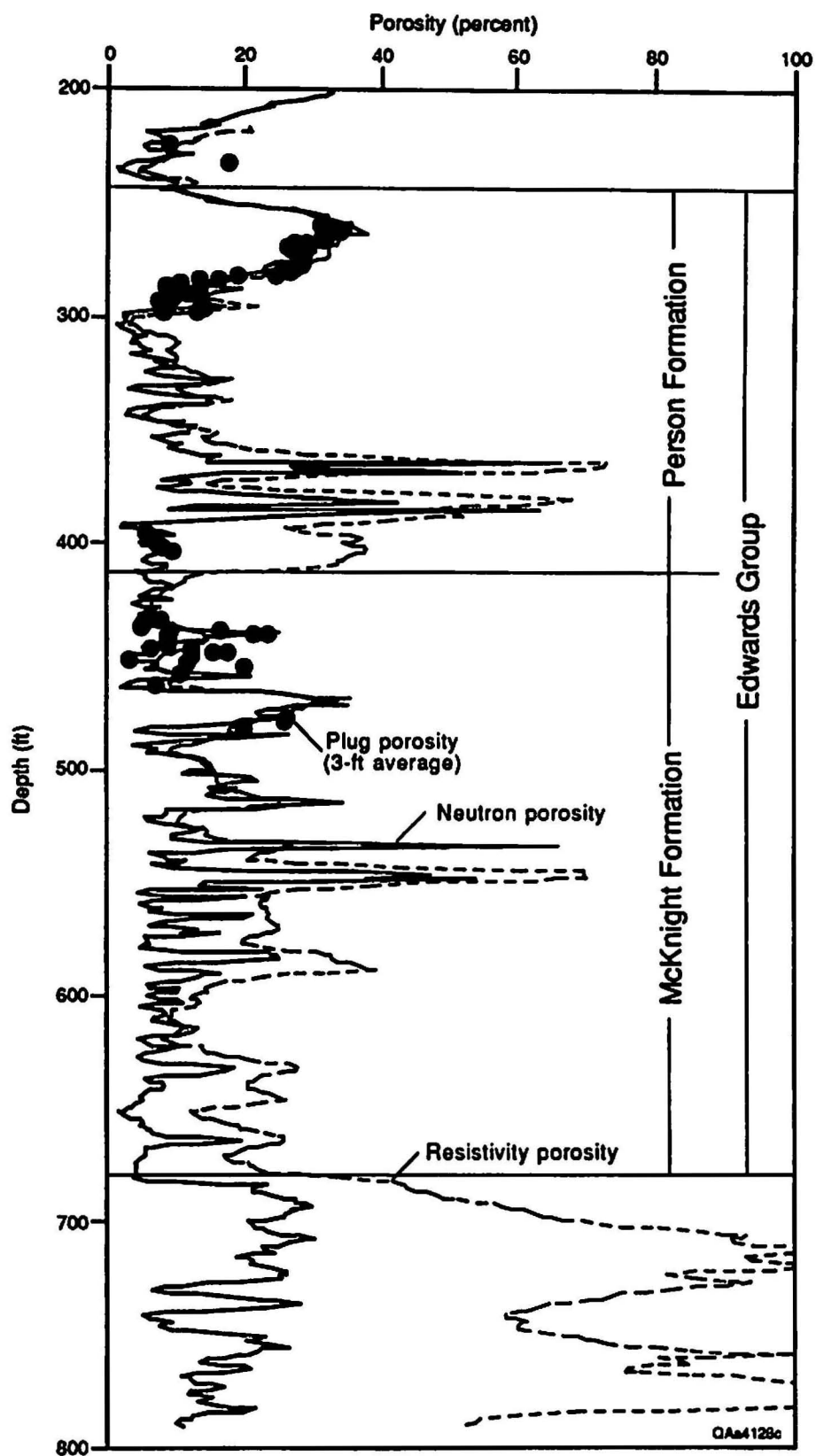


Figure 18. Calculated (unscaled neutron and resistivity) and measured porosity, USGS Castle Hills, AY 68-29-910.

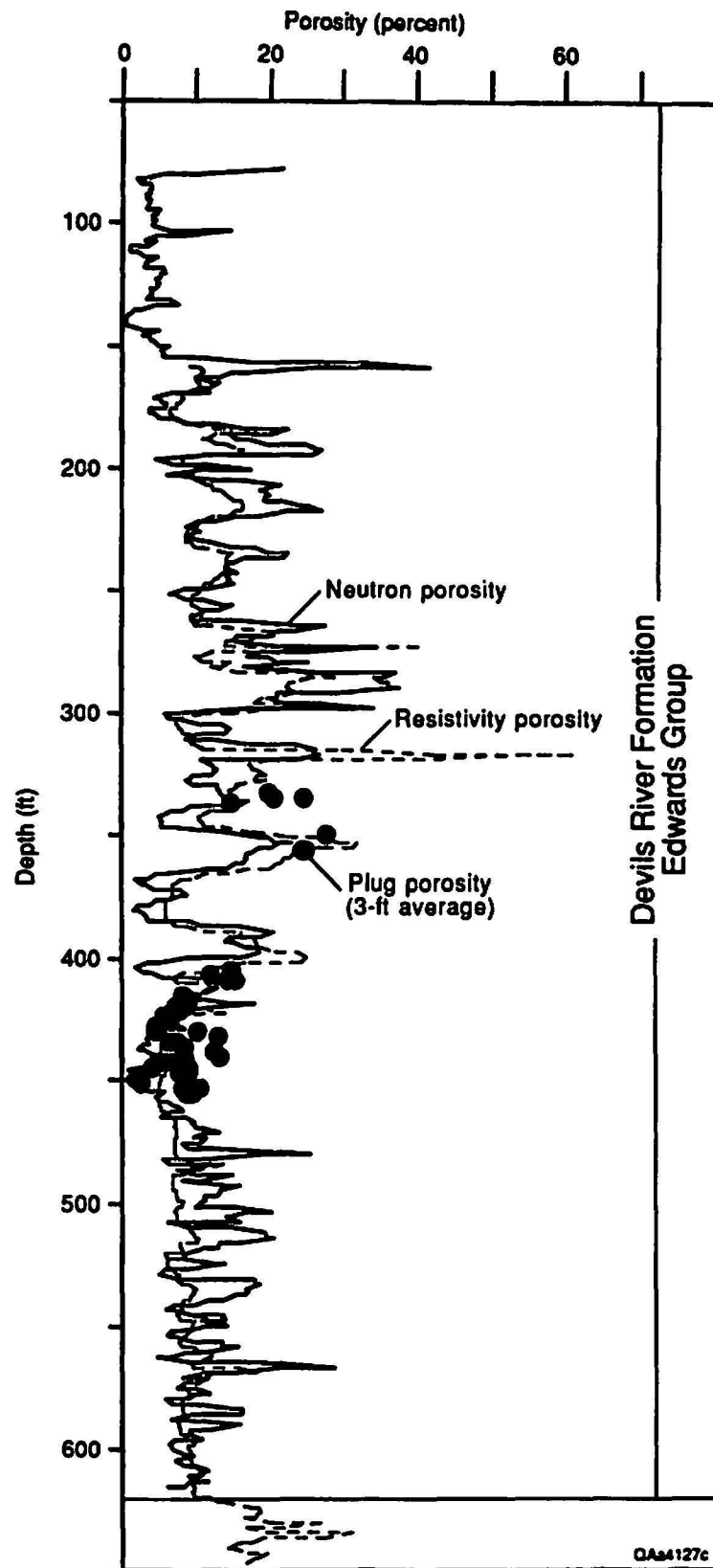


Figure 19. Calculated (unscaled neutron and resistivity) and measured porosity, TWDB TD-3 well, TD 69-39-504.

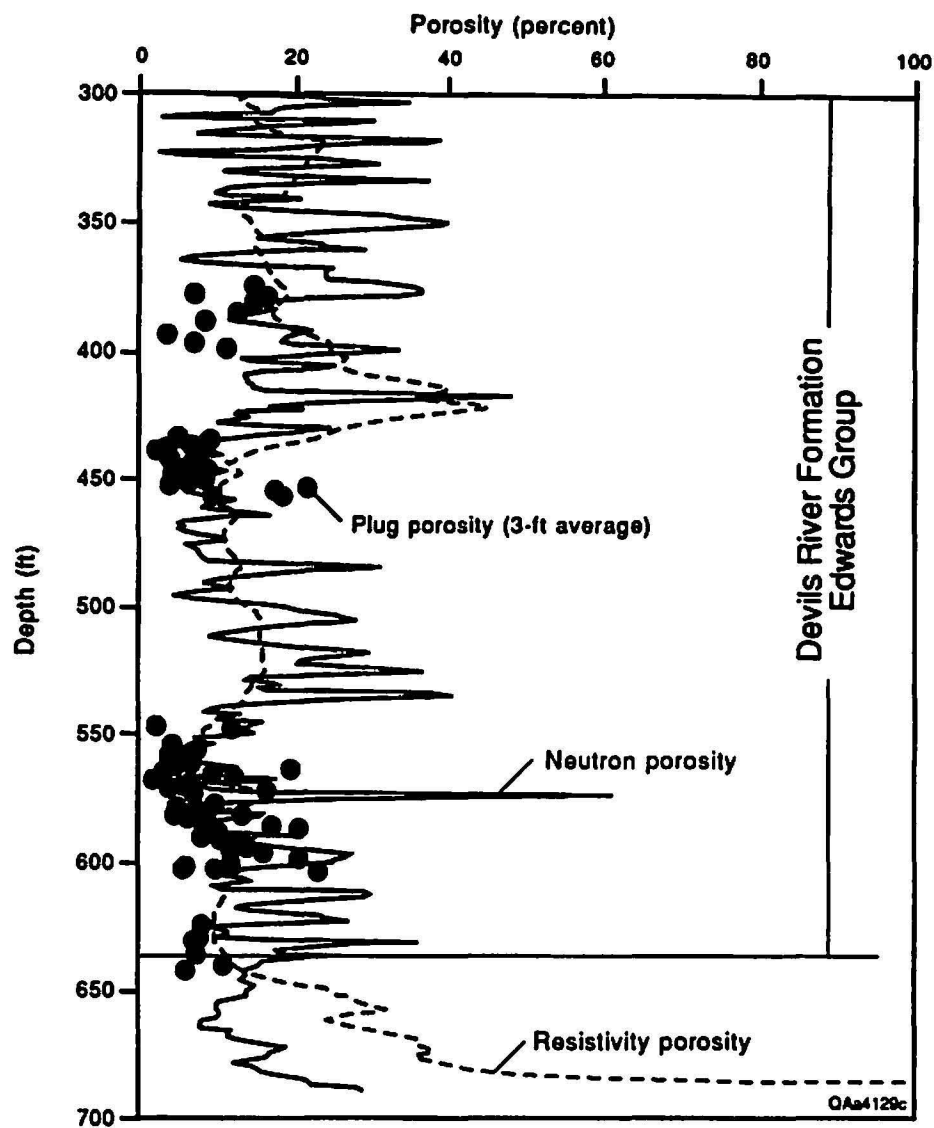


Figure 20. Calculated (unscaled neutron and resistivity) and measured porosity, USGS Sabinal well, YP 69-37-402.

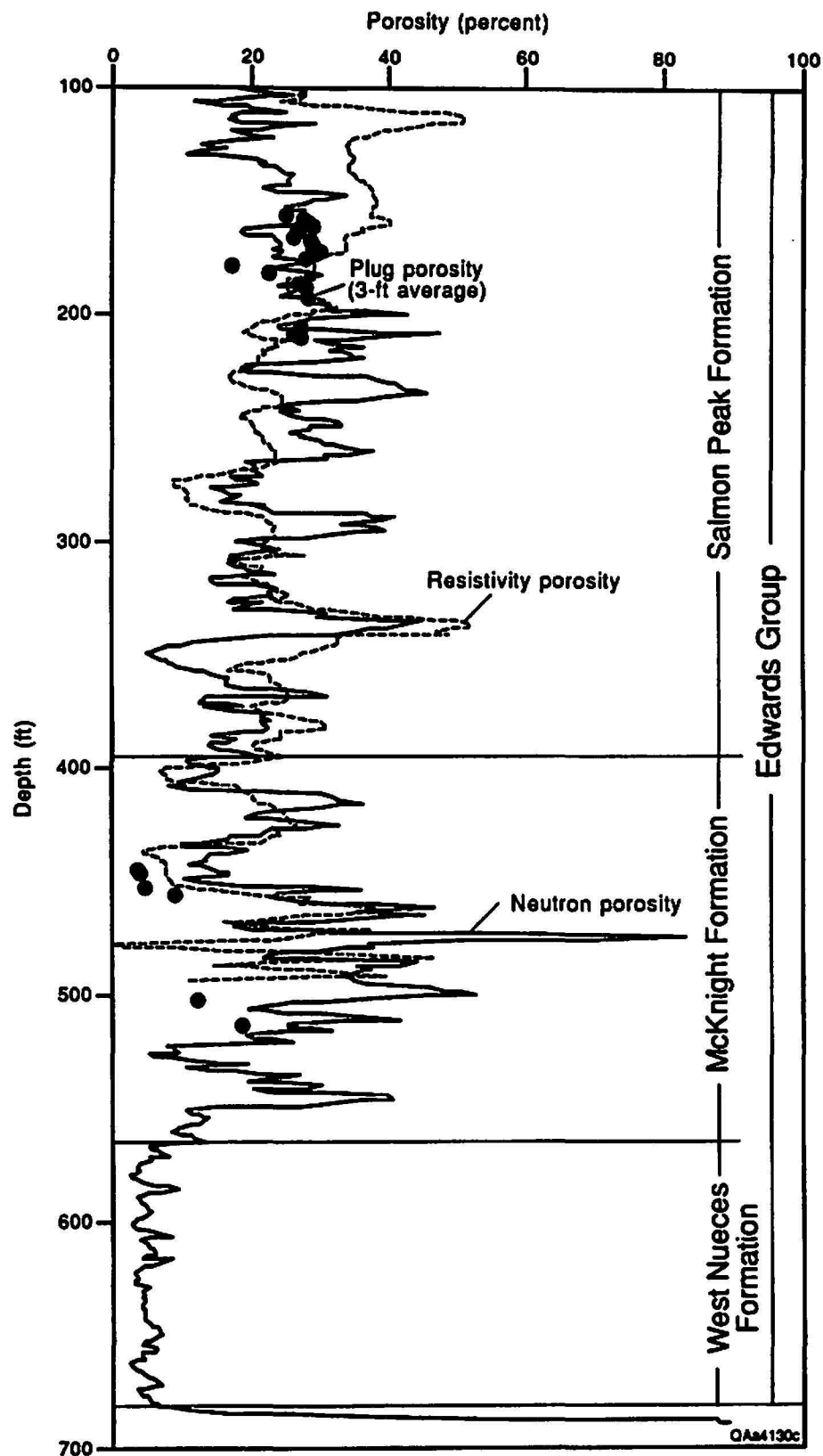


Figure 21. Calculated (unscaled neutron and resistivity) and measured porosity, TWDB YP-4 well, YP 69-42-709.

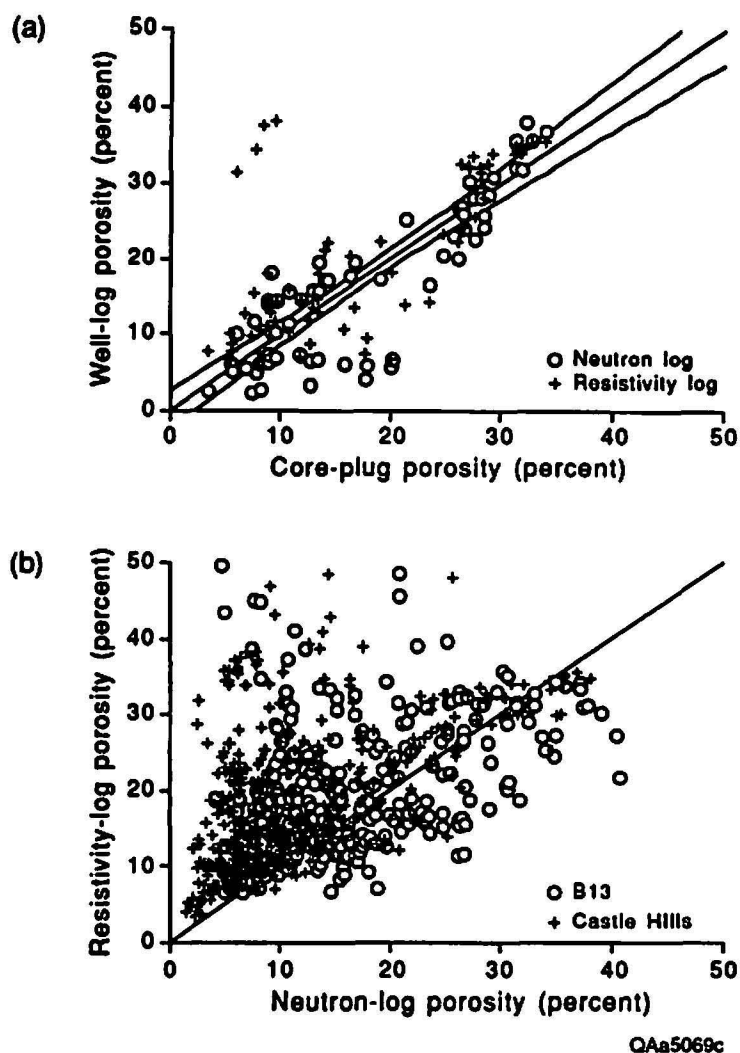


Figure 22. Correspondence of (a) core-calibrated neutron-log and resistivity-log porosity for core from Castle Hills well and (b) neutron-log and resistivity-log porosity from Castle Hills and B13 wells. In (a), correlation coefficient is 0.88 for regressions of neutron-log and resistivity-log porosities against core-plug porosity, discounting the four high values of resistivity-log porosity. Curved lines mark the 95-percent confidence interval of the mean value of neutron-log porosity with a standard error estimate of 5.0 percent. In (b), approximately 50 percent of resistivity-log porosities lie within ± 5 percent of neutron-log porosity and 84 percent lie within ± 15 percent.

scaled and that specific conductance is correct. However, the low values are consistently higher than the low-porosity values (about 5 percent) from neutron logs and plug analysis in the same stratigraphic and hydrologic settings. These high-porosity values in low-permeability units were therefore interpreted as an artifact produced by the presence of more saline pore waters in the low-flow parts of the aquifer or by other variables unaccounted for in the simple porosity equation. These logs were rescaled so that the low porosity units yielded values similar to adjacent wells.

The techniques utilized in this study yielded a fair agreement between neutron and resistivity porosity calculations (fig. 22b). Discrepancies resulting from bad hole conditions or pore-fluid salinity variations are local and not systematic, while average and stratigraphic trends in porosity distribution are reproducible and accurate.

Porosity Distribution

Interwell interpolations of porosity were created using a three-dimensional model built with Stratamodel® Stratigraphic Geocellular Modeling (SGM) software. This software uses stratigraphic horizons to guide interpolation and uses all porosity data entered. The cell sizes generated by this model are 0.5 to 8 ft (0.15 to 2.4 m) in thickness, and 4,104 ft (1,250 m) in horizontal dimensions. The Edwards aquifer is divided into 196 layers. The stratigraphic horizons are first built into the model, and the space between the horizons is subdivided into cells. The attribute, in this case porosity, is then entered as a file, giving a porosity value for each foot. Porosity values are then interpolated using a least-squares regression for each cell in the model, and the interpreted porosity distribution can be viewed in map view, cross section, or block diagram. The results can be exported to other software for contouring or further manipulation.

The vertical porosity distribution is highly variable because of the high-frequency cyclicity. High-porosity (25 to 35 percent) zones 10 to 50 ft (3 to 15 m) in thickness are interbedded

with thinner lower porosity (10 to 20 percent) beds (figs. 23, 24, and 25). Stratiform porous units are prominent in the lower Kalner (unit 3), upper Kalner (unit 6), and upper Person (units 9 and 10). This cyclic porosity can be traced into the Devils River Formation. High-porosity intervals are found at the top of the aquifer in Bexar County; these may be intervals where the porosity in rudist grainstones has been diagenetically enhanced, similar to those observed in the USGS Castle Hills core. Low-porosity units similar to the lower Kalner (units 1 and 2), lower Person (unit 7 and parts of 8), and Georgetown Formations can be traced in many parts of the study area. Porosity in the Salmon Peak Formation and McKnight Formations are less stratigraphically controlled and more blocky, with local high-porosity zones along coarse-grained layers within the Salmon Peak and within breccia zones of the McKnight (fig. 25).

Porosity averaged through the thickness of the aquifer generally shows lateral gradational changes. Minimum average porosity is 16 percent and maximum average porosity is 28 percent in individual wells (plates 5, 6, and 7). The interpolated average porosity of the Edwards Group is 21.7 percent. A large area of low porosity is recognized in the western Maverick Basin part of the lower interval in the West Nueces and McKnight Formations. Porosity in the Salmon Peak Formation of the Maverick Basin is higher toward the outcrop. This may reflect areas of originally coarser-grained sediment or areas where porosity has been increased by near-surface diagenesis. High porosity toward the west and north in Kinney County indicates that the aquifer drainage divide and outcrop boundaries in this area are important in assessing the total resource. The Devils River Formation in central Uvalde County also exhibits high porosity in the upper part and low porosity in the lower unit. This geometry may reflect progradation of platform grainstones into the basin. The stratigraphic variability in porosity may have an impact in the hydrologic behavior in the Knippa Gap area of southern Uvalde County (Maclay and Land, 1988).

As previously mentioned, an area of high porosity lies along both sides of the bad water line in southeastern Medina and southwestern Bexar Counties. This high-porosity zone is within an area of thickening of the Edwards section but does not conform to any known facies

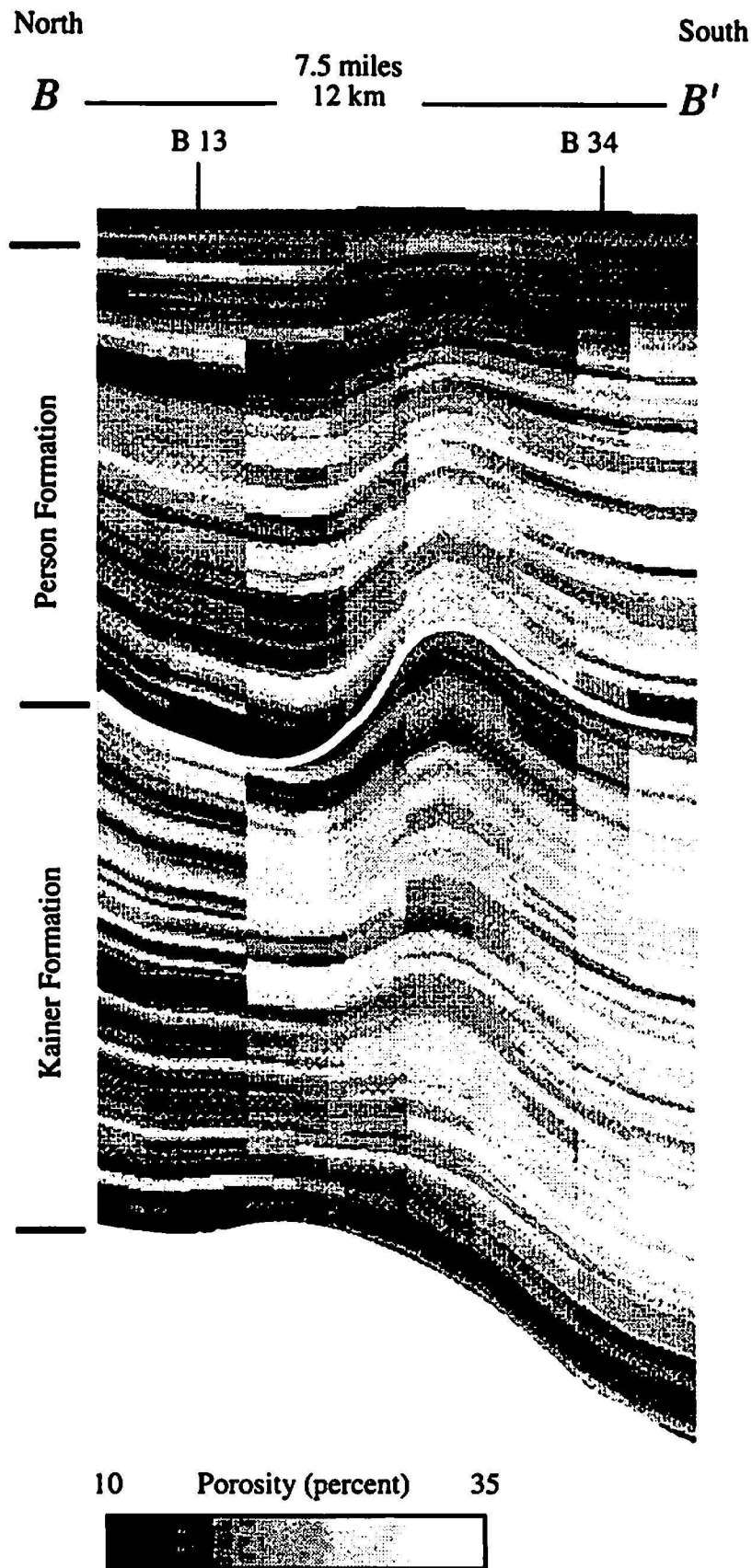


Figure 23. West-east porosity cross section B-B', Bexar County. Location shown in figure 1. Cross section shows porosity calculated by Stratamodel© based on logs shown, as well as data interpolated from surrounding areas.

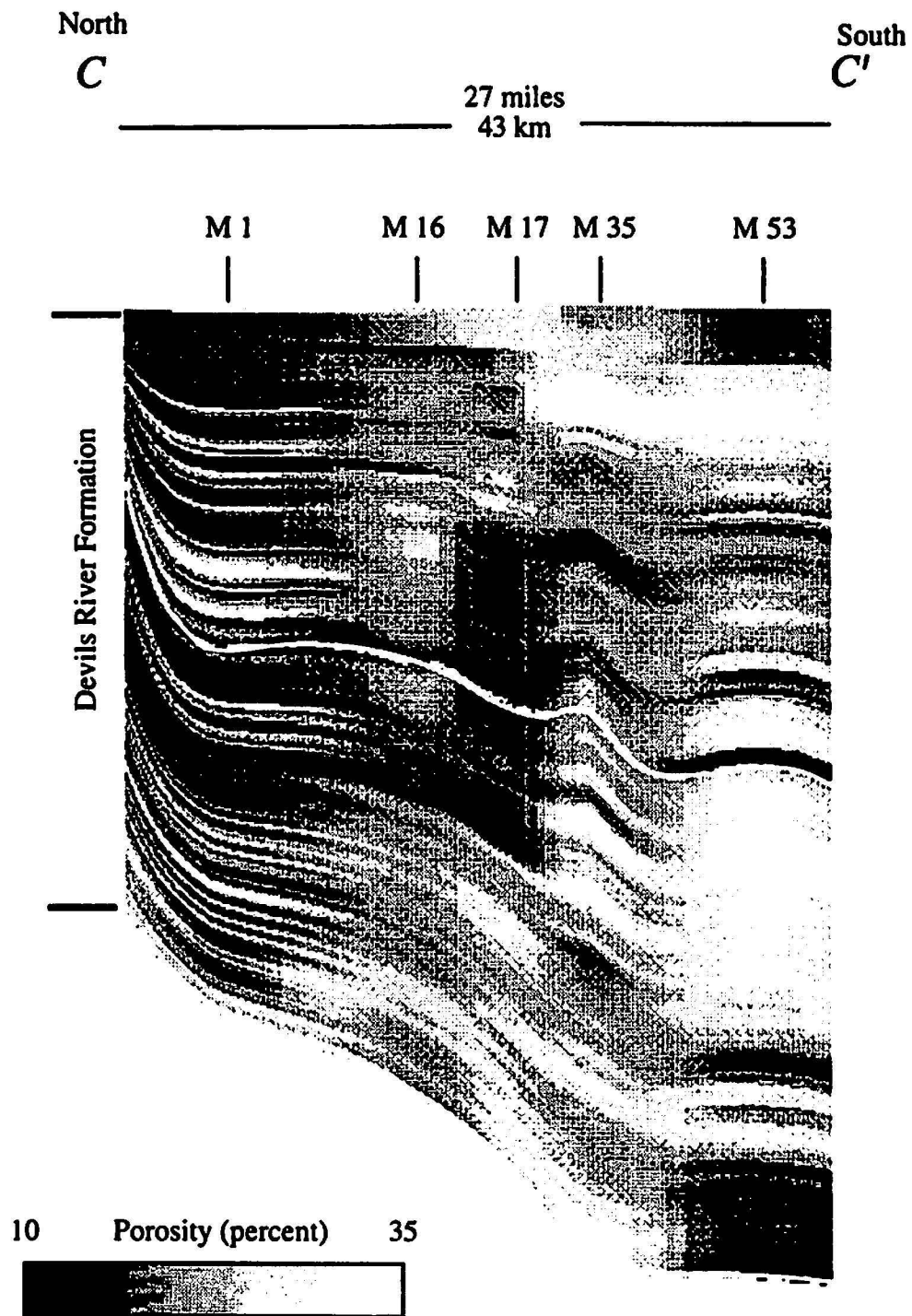


Figure 24. North-south porosity cross section C-C', Medina County. Location shown in figure 1. Cross section shows porosity calculated by Stratamodel© based on logs shown, as well as data interpolated from surrounding areas.

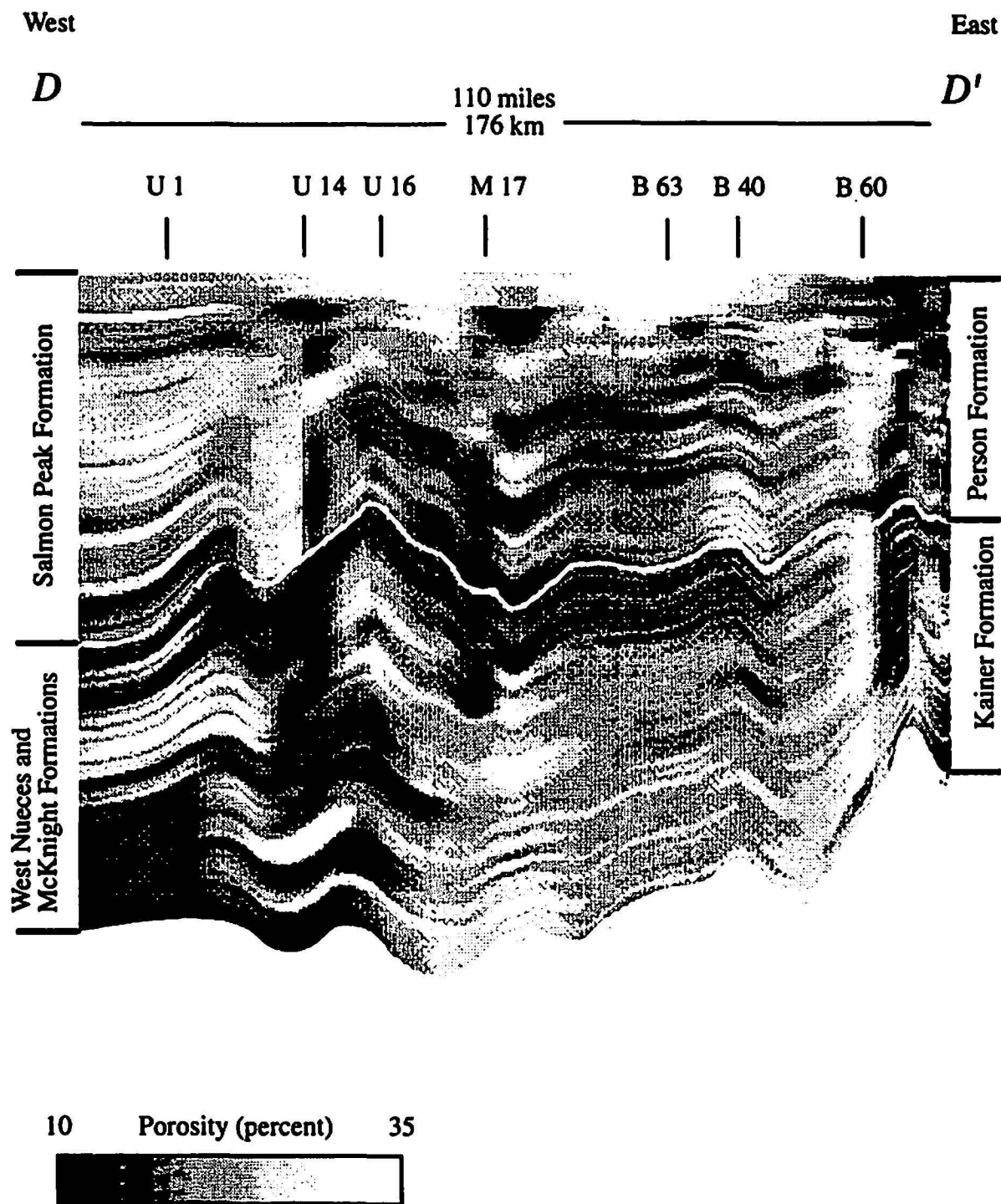


Figure 25. East-west porosity cross section D-D' along length of aquifer. Location shown in figure 1. Cross section shows porosity calculated by Stratamodel© based on logs shown, as well as data interpolated from surrounding areas.

change that could increase porosity. It is possible that fluctuations of the geochemistry along the bad water line have driven diagenesis, resulting in porosity increase. Many of the wells in this area have strong vertical variations in apparent specific conductance on resistivity logs, suggesting that the saline–freshwater interface has a complex, hydrodynamically controlled geometry.

The northern part of the aquifer in Hays, Comal, and northern Bexar Counties also has higher than average porosity. Outcrops from this area show strong diagenetic modification because of dissolution and collapse perhaps related to faulting. Local areas of high and low porosity within the central part of the study area may also reflect the effect of faults and variable flow on porosity development and occlusion.

The total amount of water-filled pore space within the Edwards aquifer is an estimated 215 million acre-feet on the basis of techniques used in this study. Of this, 156.5 million acre-feet are within the confined part of the aquifer, and 58.5 million acre-feet are in the unconfined aquifer. The amount of total porosity is less in the Edwards outcrop, because the upper part of the Edwards has been partly eroded or is unsaturated. These volumes include the total thickness of the Edwards Group (top of Glen Rose to base of Del Rio). The area included in the calculations is geographically bounded by: the bad water line of Brown and others (1992) on the south, the mapped drainage divide at Brackettville on the west, the mapped drainage divide at Kyle on the northeast, and the mapped outcrop limit of the Edwards aquifer on the north. The top of the unconfined aquifer was located at the 1972 potentiometric surface. Water levels that year were average, recording between 651 and 679 ft in the Bexar County J-17 observation well (Brown and others, 1992). In the deep sections of the aquifer in southern Medina County, additional fresh water was recently identified (Schultz, 1992; Schultz and Waugh, 1993; John Waugh, written communication, 1993).

The upper zone of the aquifer (Person-upper Devils River-Salmon Peak Formation) contains an estimated total water-filled porosity of 103 million acre-feet. The lower zone

(Kainer-lower Devils River-West Nueces-McKnight Formations) contains an estimated 112 million acre-feet.

Analysis of Water-Level Response to Atmospheric Pressure Changes

Data on water-level fluctuations were provided for 17 wells, but only 9 could be used to estimate storativity (table 3). Water-level fluctuations at these 9 wells matched the atmospheric pressure changes well (figs. 26 through 28). Data from the other 8 wells were not used for various reasons: equipment malfunction, a float insensitive to small water-level fluctuations, an unexplainable trend, barometric efficiency calculation greater than 1, or an apparent lack of water-level response to atmospheric pressure change. Barometric efficiency greater than 1 probably indicates additional noise (such as pumping effects, recharge, or discharge) that was not removed from the water-level hydrograph.

No statistically significant trends in water levels were found at wells TD 69-38-601 in Medina County (fig. 26b) and YP 69-50-302 in Uvalde County (fig. 28b). The linear trends in water levels in the other 7 hydrographs were removed as previously described. In figures 26 through 28, the original hydrographs are shown on the right and the hydrographs with trends removed are shown beneath the record of atmospheric pressure on the left. The atmospheric pressure graph is repeated in each figure to allow for easy comparison with the hydrographs (figs. 26, 27, and 28a). Daily fluctuation in atmospheric pressure and its water-level response is small compared with the effect of major atmospheric pressure changes probably related to frontal air mass movement, which affects the blocky pattern on most hydrographs in figures 26a and 27a. The effect of the major weather front is less apparent relative to daily fluctuation in the hydrographs in figures 27b and 28.

The changes in atmospheric pressure and the coincident water levels were analyzed following the previously described methods. The standard deviation of atmospheric pressure varied between the time segments chosen for comparison (table 3). Short time segments

Table 3. Calculation of specific storage and storativity in the Edwards aquifer on the basis of barometric efficiency and log-based porosity measurements.

County	Well ID no.	Time segment start (day)	Time segment end (day)	Standard deviation water level (ft)	Standard deviation atmospheric pressure (ft)	Calculated barometric efficiency (%)	Porosity (%)	Aquifer thickness (ft)	Specific storage	Storage coefficient
Bexar	AY 68-29-103	3.95	31.99	0.1442	0.1827	78.9	28	475	5.12×10^{-7}	2.43×10^{-4}
Bexar	AY 68-29-103	16	20	0.0415	0.0601	69.1	28	475	5.85×10^{-7}	2.78×10^{-4}
Comal	DX 68-30-208	3.95	31.95	0.0667	0.1827	36.5	25	480	9.89×10^{-7}	4.75×10^{-4}
Comal	DX 68-30-208	16	20	0.0592	0.0601	98.5	25	480	3.66×10^{-7}	1.76×10^{-4}
Bexar	AY 68-37-203	3.36	31.91	0.1789	0.1829	97.8	17	500	2.51×10^{-7}	1.25×10^{-4}
Uvalde	YP 69-37-402	3.82	31.91	0.1695	0.1828	92.7	19	440	2.96×10^{-7}	1.30×10^{-4}
Medina	TD 69-38-601	1.03	31.99	0.0855	0.1803	47.4	18	548	5.48×10^{-7}	3.00×10^{-4}
Medina	TD 69-38-601	16	20	0.0224	0.0602	37.2	18	548	6.98×10^{-7}	3.82×10^{-4}
Medina	TD 68-41-301	3.9	31.91	0.1267	0.1827	69.4	21	550	4.37×10^{-7}	2.40×10^{-4}
Medina	TD 68-41-301	16	20	0.0457	0.0601	76.1	21	550	3.99×10^{-7}	2.19×10^{-4}
Uvalde	TP 69-45-401	3.24	11.57	0.1314	0.1779	73.9	21	510	4.10×10^{-7}	2.09×10^{-4}
Uvalde	TP 69-45-401	5.09	7.3	0.0656	0.0783	83.9	21	510	3.61×10^{-7}	1.84×10^{-4}
Uvalde	TP 69-45-401	7.34	9.8	0.0575	0.0687	83.7	21	510	3.62×10^{-7}	1.85×10^{-4}
Uvalde	TD 69-50-302	1.03	31.99	0.0724	0.1803	40.1	20	660	7.19×10^{-7}	4.75×10^{-4}
Uvalde	TD 69-50-302	16	20	0.0419	0.0602	69.6	20	660	4.15×10^{-7}	2.74×10^{-4}
Uvalde	YP 69-51-406	21.9	24.7	0.0945	0.1585	59.6	20	665	4.84×10^{-7}	3.22×10^{-4}

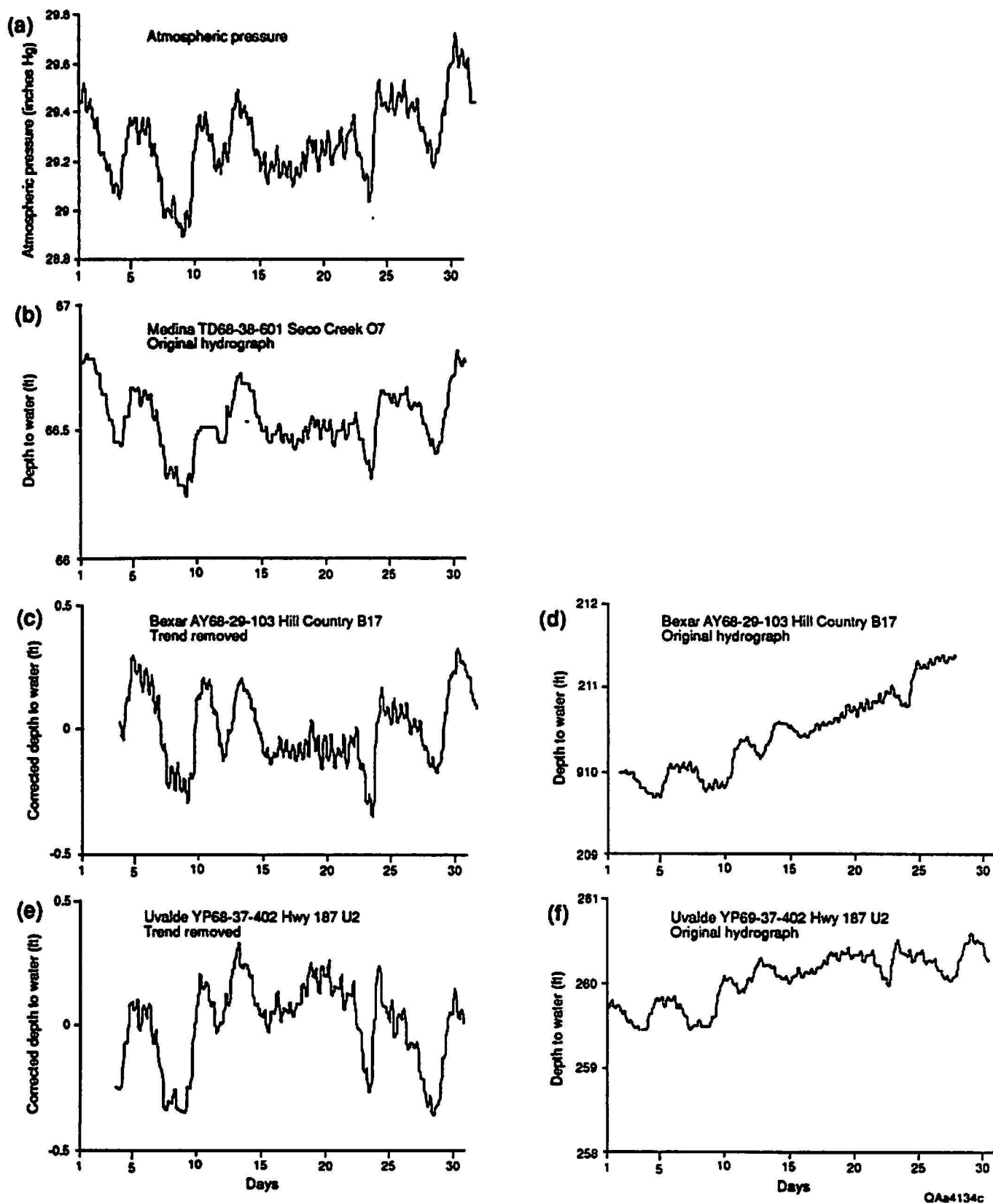


Figure 26. Records of atmospheric pressure (a) and water-level hydrographs (b–f) used to estimate barometric efficiency. Hydrographs (c) and (e) have had linear trend removed from original hydrographs (d) and (f), respectively. Original hydrograph (b) shows no trend. Note difference in vertical scale between left and right columns.

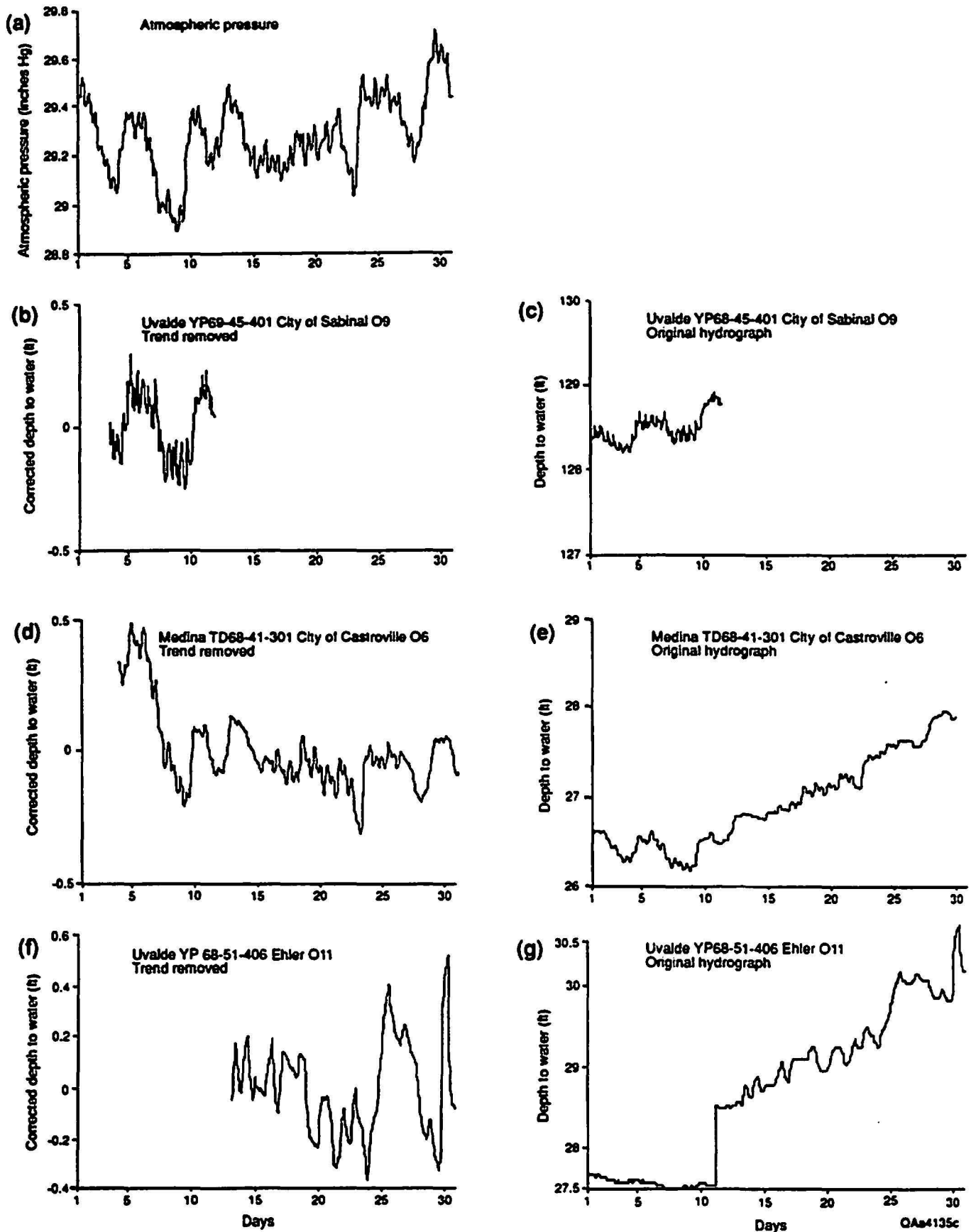


Figure 27. Records of atmospheric pressure (a) and water-level hydrographs (b–g) used to estimate barometric efficiency. Hydrographs (b), (d), and (f) have had linear trend removed from original hydrographs (c), (e), and (g), respectively. Note difference in vertical scale between left and right columns.

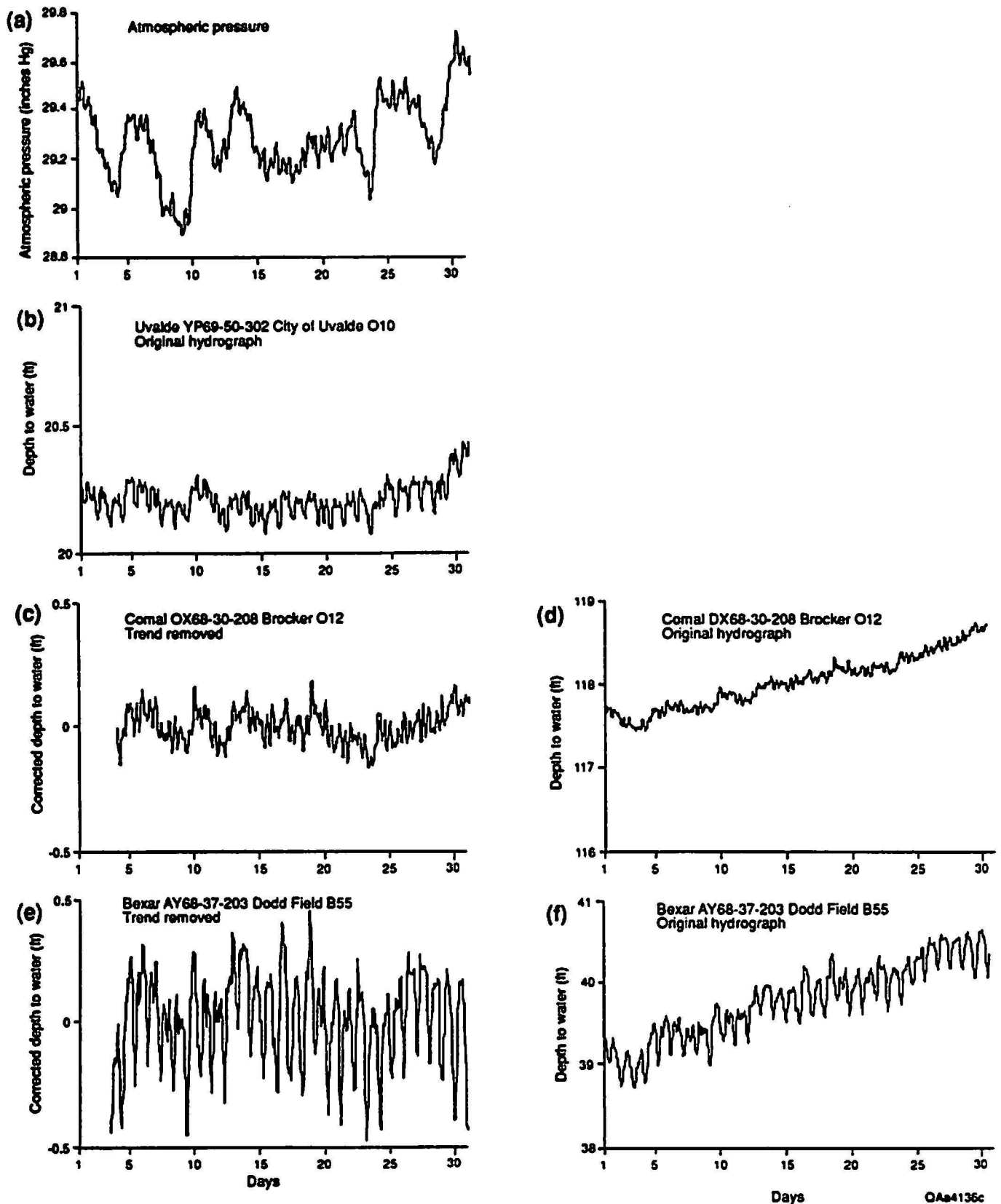


Figure 28. Records of atmospheric pressure (a) and water-level hydrographs (b–f) used to estimate barometric efficiency. Hydrographs (c) and (e) have had linear trend removed from original hydrographs (d) and (f), respectively. Original hydrograph (b) shows no trend. Note difference in vertical scale between left and right columns.

yielded a typical standard deviation of 0.06, and long time segments yielded a typical standard deviation of 0.18. Barometric efficiencies calculated using equation (10) ranged from 0.36 to 0.99 (table 3). At a well with a high value of barometric efficiency, the aquifer matrix is less compressible, the percent of storage attributable to compression of the aquifer matrix is small, and the percent of storage attributable to expansion of water is large (Domenico, 1972). The generally high values of barometric efficiency in Edwards aquifer wells reflect the low compressibility of carbonate rock.

The average porosity of the aquifer at monitor wells was extracted from the log-based porosity interpolated using Stratamodel© (table 3). Barometric efficiency from equation (10) and interpolated average porosity were used to estimate specific storage in equation (13). Water elasticity was assumed to be 300,000 psi, and specific weight of water (ρg) was assumed to be 0.433 psi/ft. Specific storage (S_s) calculated for the wells averaged 2.6×10^{-4} (table 3). The specific storage (S_s) was converted to the storativity (S) by multiplying the former by formation thickness or thickness of the completion interval.

Storativity has not been measured by aquifer tests at any of the wells having water-level hydrographs. It was measured in at least two aquifer tests in Bexar County, at wells AY 68-29-104 ($S = 0.007$) and AY 68-29-410 ($S = 0.00035$) (unpublished data, EUWD). The calculation of storativity at the first well was questionable. Maclay and Small (1986) estimated that average coefficient of storage is between 10^{-4} and 10^{-5} , assuming average formation dimensions and average (20 percent) porosity. The average value of 2.6×10^{-4} , calculated from barometric efficiency and log-based porosity, agrees well with those estimates.

The response of water level in a well to atmospheric pressure changes is small. The effect of the well's water-level fluctuation on pressure change in the aquifer therefore influences only a small radius around the well, limiting the interpretation of hydrologic properties. Additional field tests and data analysis are required to verify whether storativity is representative of local hydrologic properties. Further specific storage measurements with barometric efficiency from the same wells could be used to calculate porosity independently

from log-based measurements. For improved, more precise calculation of porosity, water-level hydrographs should be measured at all wells where storativity has been determined from aquifer tests.

In summary, barometric efficiency of wells within the confined part of the Edwards aquifer can be approximated by calculating the standard deviation of data in the time series, after significant trends are removed. It is important to inspect different segments of the time series to confirm that the barometric efficiency is accurate and unbiased by extraneous noise. The amplitudes of water-level and atmospheric pressure fluctuations can be determined more precisely using harmonic or Fourier analysis to filter out noise, although trends unrelated to the barometric response still need to be removed. More sophisticated time-series analysis might be justified once additional field-test data have been collected to determine storativity.

DISCUSSION

This section of the report assesses the accuracy of the estimate of total water-filled porosity, discusses what the estimate of total in-place water volume means, and presents examples of how the data set can be used.

Reasonable matches were obtained between porosity measurements of core plugs and porosity calculations from neutron and resistivity logs. These matches indicate that calibration was reasonably successful and that various porosity log types and qualities can be combined to yield a functional porosity measurement. Porosity calibration can be erroneous because of (1) unidentified changes in pore-water salinity, (2) overestimation of karst or fracture porosity because of borehole damage, (3) inaccuracies in calibration assumptions, and (4) areas of high and low porosity not penetrated by logs. In particular, high estimates near the base of the Edwards Group may reflect either enhanced porosity because of dolomitization or karstic dissolution, or erroneous high porosity because of saline pore fluids. High estimates of porosity at the top of the Edwards Group may be similar to the diagenetically enhanced high porosity

measured in core in rudist grainstones in this position. The thickness and amount of porosity in some of the very porous intervals at the top of the aquifer, however, might be overestimated by logs because of borehole damage.

This study provides a detailed assessment of the maximum amount of water in place in the Edwards aquifer on the basis of a large data set and a reproducible method. This study's estimate of 215 million acre-feet of total water-filled pore volume, however, is not a direct measure of how much water can or should be produced from the aquifer. The total resource depends on social, ecological, and economic variables as well as many physical variables including, but not limited to, specific retention or amount of water retained against the force of gravity after drainage of the unconfined aquifer, distributions of storativity and permeability, water quality, and annual variations in recharge rate.

Maclay (1989) estimated that 25 to 55 million acre-feet of water in the Edwards is circulating in pore space or drainable by gravity (R. W. Maclay, personal communication, 1993). This is, of course, substantially lower than this study's calculation that there is a total of 215 million acre-feet of water in storage. Maclay and Small (1976) used capillary-pressure tests from the freshwater zone to show that in low-porosity intervals, very high pressures are required to force mercury into the pores. Water in these small and poorly interconnected pores would be retained in the rock by surface tension, or capillary attraction, and be unrecoverable by drainage. More porous samples accepted more mercury at lower pressures; a higher percentage of water in these pores is mobile. Maclay and Small (1976) estimated that only 25 to 50 percent of pore space drains by gravity in the most permeable part of the Edwards and little of the water-filled matrix drains in low-permeability sections such as the Georgetown Formation. Permeability measurements made during this study suggest that porosities above 10 percent generally correspond to permeabilities of greater than 10 md. Exceptions are found in areas with abundant small pores, such as the Salmon Peak Formation in the Maverick Basin and the Person and Kalner Formations south of the bad water line. Applying a 10-percent porosity cutoff to the model only reduces the total water-filled porosity by about 1 percent,

mainly in the West Nueces and McKnight Formations in the Maverick Basin and in thin transgressive units on the platform. In addition, some thin intervals where logs yield high porosity might be artifacts produced by borehole damage. Application of a 50-percent porosity cutoff to eliminate these intervals reduces the total water-filled porosity by another 2 percent. The 3-percent of total water-filled volume that is in rock with less than 10-percent and more than 50-percent total porosity is 7 million acre-feet.

This total amount of stored water represents the long-term accumulation of the volumetric difference between recharge and discharge. Storage increases when recharge exceeds discharge and decreases when recharge is less than discharge. For the period 1934 to 1992, average annual recharge of 677,700 acre-feet was not significantly different from average annual discharge of 647,300 acre-feet to springs and wells (Technical Advisory Panel, 1990; data for 1934 to 1992 from Brown and others [1992] and Steve Walthour, personal communication [1993]). Recharge to the Edwards is controlled by rainfall in the catchment area; there does not appear to be induced recharge from perennial streams by the drawdown of water level in the aquifer (Woodruff and Abbott, 1989; Technical Advisory Panel, 1990). Under drought conditions, pumpage and spring flow can markedly exceed recharge. When this occurs, water is being taken out of storage. In 1956, when water levels were at their historical low during a long drought, more than 2 million acre-feet of water were removed from storage when net discharge exceeded recharge (Garza, 1976). When discharge exceeds recharge and removes water from storage, water levels drop and the volume of spring discharge decreases.

The model and data developed in this study have many potential uses as an aquifer management tool. For example, as previously shown, water volume can be calculated for confined and unconfined parts of the aquifer, and for the aquifer above and below the regional dense member. In addition, water volume can be calculated for various geographic areas such as counties, watersheds, and subregions of the aquifer. The detailed data set compiled in this study can be built upon and modified to incorporate additional well-log data, permeability estimates, and the results of future hydrologic research.

One example of the use of the porosity model produced by this study is updating estimates of in-place water volume as additional data become available and verified. For example, in the deep sections of the aquifer in southern Medina and northern Frio Counties, additional fresh water was identified (Schultz, 1992) and recently confirmed by test drilling (John Waugh, personal communication, 1993). Taking the bad water line of Schultz (1992) in place of that by Brown and others (1992), compared in figures 1 and 2, yields a net gain of 15 million acre-feet of in-place water in Medina and Frio Counties and a net loss of 3.5 million acre-feet in Uvalde County.

A second example of the use of the porosity model is the estimation of water volume between different water levels in the unconfined part of the aquifer, for example, between the 1984 and 1992 potentiometric surfaces. The 1984 water levels record the Edwards potentiometric surface at a very low elevation (John Waugh, written communication, 1993). The 1992 water levels record the Edwards potentiometric surface at its highest recent elevation. These surfaces were added to the cellular model and the volume of water in the unconfined aquifer between these surfaces was calculated. The difference in volume of water contained in the unconfined aquifer between the two potentiometric surfaces is 6.9 million acre-feet, which is the maximum amount of water expected above the 1984 potentiometric surface. This is only 3 percent of the total water in storage throughout the aquifer. Most of the water stored in the Edwards, therefore, lies below the elevation of the 1984 potentiometric surface.

The total amount of water in storage in 1992 must equal the total amount of water in storage in 1984 plus the net addition from recharge. Between 1984 and 1992, recharge was 9.85 million acre-feet and discharge (wells and springs) totaled 6.92 million acre-feet (Brown and others, 1992; Steve Walthour, personal communication, 1993). The amount of error in these values is unknown. Their difference, however, suggests a net gain of 2.93 million acre-feet of water in the aquifer, which is 42 percent of the total water volume calculated between the 1984 and 1992 potentiometric surfaces. This suggests that the specific retention of the

unconfined part of the Edwards aquifer is 58 percent of porosity. Specific retention is the fraction of the total water-filled pores in the unconfined aquifer that is not recoverable because water exists in discontinuous or poorly interconnected pore space and because some water is held in the rock by surface tension or capillary attraction. This is consistent with the interpretation by Maclay and Small (1976) that at least 50 percent of pore space is not drainable by gravity.

The total water volume calculated using the 1972 potentiometric surface as the upper boundary of the unconfined aquifer gives an average volume or average capacity to the extent that 1972 was an average water year. The range in capacity about this average value might be approximately half of the total volume of calculated pore space in the unconfined aquifer between the 1984 and 1992 water-table surfaces, that is, half of 6.9 million acre-feet. Therefore, one could say that the estimate of total water in storage is 215 ± 3.5 million acre-feet. This 1.6-percent uncertainty because of water-level fluctuation is probably less than the total amount of error in porosity calculation.

Changes in the volume or mass of water physically present in the unconfined part of the Edwards aquifer occur via the filling and draining of pore space. Prolonged ground-water production in excess of recharge would cause pores to drain, water levels to decline, and some wells in the upper reaches of the unconfined aquifer to go dry. Changes in water level in the confined aquifer, however, do not reflect change in the amount of water in pore space, which remains full of water, but reflect a change in water pressure as water fills and drains from the unconfined aquifer in the Edwards outcrop. Pumping that removes water from storage in the confined aquifer will cause a drawdown of water pressure and induce water to flow from the unconfined to the confined parts of the aquifer. The confined Edwards can be recharged rapidly because of its high permeability. Storativity and permeability determine the amount and distribution of water-level decline in the aquifer at a given rate of pumping. These physical variables as well as social, ecological, and economic variables might limit the recovery of stored water.

Pumpage of water at rates that exceed annual recharge results in a drop of water level, first by bleeding off pressure in the confined aquifer, and eventually, if the water level drops below the top of the Edwards aquifer, by draining porosity. Only a small amount of water is released from storage in the confined aquifer with drawdown of water pressure. Water is released from storage in the confined part by the expansion of water and the minute compression of the aquifer matrix as water pressure decreases. The volume of water that can be produced with a given amount of water-level decline can be estimated from the relation

$$V = S A \Delta h \quad (14)$$

where

V = volume of water,

S = storativity,

A = aquifer area, and

Δh = change in water level.

Assuming an average S of 2.6×10^{-4} as estimated from water-level hydrographs, a 100-ft (30-m) change in water level over the entire confined aquifer (2,005 mi² [5,133 km²]) would yield only 33,400 acre-feet of water. More than this amount of water is produced annually from the confined part of the Edwards aquifer, which indicates that water moves into the confined part of the Edwards from the recharge zone.

Residence time is the average duration of water in an aquifer and is estimated by dividing total water volume in storage by the recharge rate. At a recharge of approximately 677,700 acre-feet/yr, residence time is approximately 317 years. This means that ground water in the Edwards aquifer is replaced on average every 317 years. This average value is consistent with data on the activity of carbon-14 (¹⁴C) and tritium (³H) radioactive isotopes in Edwards ground water (Pearson and Rettman, 1976). The reciprocal of residence time is the fraction of the stored ground water that enters and leaves the aquifer in a given year—0.3 percent in the Edwards' case.

In summary, there is a large volume of ground water in storage. This study's estimate of 215 million acre-feet of stored water, however, does not describe a previously unrecognized resource that might be developed, nor does it imply more water for development than previously thought. Pumpage in excess of the recharge rate takes water out of storage for as long as the overdraft continues without mitigation and eventually decreases water pressure in the confined aquifer to a level below that which would continue to deliver water to springs at the discharge end of the aquifer.

ADDITIONAL STUDIES

This study outlines a number of significant problems that could be addressed by building on the results of this study:

(1) Permeability distribution

This study expands the data base of interpreted porosity logs and shows the three-dimensional stratigraphic control on porosity in the aquifer. If relationships between porosity and permeability can be developed for the variable carbonate rocks of the Edwards aquifer, this three-dimensional porosity data might be used as the basis of a detailed model of stratigraphically controlled matrix permeability. Many questions regarding aquifer dynamics, such as the interrelation of ground-water production, recharge, water-level change, and spring flow, could be addressed more accurately if the permeability distribution were known in detail. The vertical heterogeneity and lateral connectivity of the porous zones identified by this study are important components of the permeability distribution.

(2) Storativity

Techniques using barometric efficiency to calculate storativity used in this study should be validated using aquifer tests with observation wells. If the accuracy of the results is confirmed, water-level hydrographs along with the porosity data set developed in this study will provide a cost-effective method of estimating storativity across the confined aquifer. In addition, porosity

might be calculated indirectly from measured storativity and a water-level hydrograph and compared to the geophysical log-based porosity estimate. The comparison might help evaluate karstic and fracture porosity.

(3) Aquifer boundaries

The porosity model is least accurate for the outcropping part of the Edwards, which is not well represented by the data set obtained in this study. Log suites collected in the upper part of the aquifer when water levels are high would provide a useful extension of the data base. Coupled geological analysis of outcrops and subsurface formation structure, shallow high-resolution three-dimensional seismic studies, and hydrologic testing would provide additional detailed information needed to accurately assess water resources and to model ground-water flow in the unconfined part of the Edwards aquifer. Comparison of flow in porous matrix to flow in fractured and karstic rock above and below the water table in the unconfined aquifer are needed to better constrain and locate recharge to the aquifer.

Data are sparse in the western part of the study area. The rock fabric in the most porous parts of the Salmon Peak Formation should be examined to determine if it has fairly small pores and relatively low permeabilities, as in the Salmon Peak core examined in this study. Because of the high porosities exhibited, the stratigraphic and hydrologic characteristics of the hydrologic divide near Brackettville in Kinney County is important.

Multiple zones of fresh and more saline water have been observed within research wells in the freshwater-bearing part of the Edwards Group, including the South Medina well. Additional studies that integrate geochemistry and hydrology are needed to explain stratigraphic controls on water quality and the present geometry of the saline-freshwater interface. Such studies have been made of the northern, fault-bounded part of the aquifer and also are needed along the southern boundary of the freshwater zone and at the base of the aquifer. Resistivity logs examined during this study show that the boundary of the freshwater aquifer is irregular in the vertical as well as the map-view dimensions. The complex and dynamic relation between the saline-freshwater interface and water pressure in the aquifer

may influence water quality in wells near the bad water line (Technical Advisory Panel, 1990). In addition, sharp decreases in resistivity in the lower part of the Edwards aquifer suggest that cross-formational leakage of saline water from the Glen Rose Formation may occur at some locations. This could be especially significant in the thin, unconfined part of the aquifer.

(4) Models of ground-water flow and transport

The amount of ground water that can be produced from different areas of the Edwards aquifer for given amounts of water-level decline should be predicted using a numerical model of transient ground-water flow that includes accurate estimates of storativity, recharge rate, and stratigraphically and structurally controlled distributions of porosity and permeability. Simulations of ground-water flow under a range of aquifer management scenarios can provide the data needed to support decisions concerning the social, ecological, and economical issues involved in using the aquifer's resources. Existing hydrologic models incorporate geological complexity associated with faults in the Edwards but do not include vertical variations in permeability. Adding detail on the regional distribution of storativity and the stratigraphic distribution of porosity and matrix permeability, as outlined above, should increase the accuracy with which numerical models predict how much water can be produced from the Edwards for a given amount of water-level decline. Such improved models also could be used to interpret hydrologic characteristics of faults and the extent to which ground-water resources might occur in local or semi-isolated compartments. Furthermore, the three-dimensional porosity data generated in this study could be used in model simulations to study the movement of the saline-freshwater interface and the transport of contaminants in ground water and to develop better understanding of the hydrologic and stratigraphic controls on water quality.

CONCLUSIONS

An accurate estimate the total porosity of the Edwards aquifer requires systematic, rigorous methods that recognize geologic controls on porosity distribution. This geologically complex,

prolific, and important aquifer will be studied for many years. Therefore, this analysis uses a data base to store porosity, log, and stratigraphic data that can be modified to include results of future investigations and new well data. This study incorporates acquisition of data, construction of a data base, construction of a log-based stratigraphic model, calibration of porosity log response to core analysis, and interwell interpolation of log-determined porosity using Stratamodel© SGM three-dimensional modeling software.

This study generated five products: (1) a revised estimate of the log-determined matrix porosity in the Edwards aquifer, (2) a GIS ARC/INFO data base that includes all data accumulated during the course of the study, (3) a three-dimensional stratigraphic model of the internal stratigraphy of the Edwards aquifer, (4) a cell-based porosity distribution within the aquifer, and (5) a demonstration of the use of water-level fluctuation to measure hydrologic properties and degree of confinement in the aquifer.

The porosity of the Edwards aquifer varies on a fine scale from low values of 4 to 12 percent in highstand facies to high values of 20 to 42 percent in grainstones and leached subtidal dolostones. Average porosities in the aquifer vary in response to depositional facies and diagenesis. High average porosities are recognized in the north part of the aquifer in Hays, Comal, and northern Bexar Counties. The southern part of the aquifer on both sides of the saline-freshwater interface in south Medina and Bexar Counties has higher than average porosity. The western part of the aquifer in the outcrop of the Salmon Peak Formation of Kinney and Uvalde Counties is also characterized by high porosity. Porosity for the entire aquifer averages 21.7 percent.

The volume of water in the confined aquifer inside the study area is 156.5 million acre-feet. Average storativity of the confined aquifer was calculated from barometric efficiency and interpolated porosity as 2.6×10^{-4} . The average volume of water in the unconfined part of the aquifer is 58.5 million acre-feet. Of this, 6.9 million acre-feet are in the upper part of the unconfined aquifer, falling between the maximum historic water level in the aquifer and the potentiometric surface at the time Comal Springs became intermittently dry.

ACKNOWLEDGMENTS

This work was performed for and funded by the Edwards Underground Water District under Contract No. 93-04-F0. Core plug porosity/permeability analysis was carried out by Core Petrophysics, Incorporated of Midland, Texas. Thin sections were prepared by Bart Kelly, BEG Core Research Center. Figures were drafted by Joel L. Lardon, Maria E. Saenz, and Richard L. Dillon. Editing was by Jeannette Miether, word processing by Susan Lloyd, and pasteup by Jamie H. Coggin and Margaret L. Evans. Dianne Spinney provided GIS support.

REFERENCES

- Abbott, P. L., 1973, The Edwards limestone in the Balcones Fault Zone, south-central Texas: The University of Texas at Austin, Ph.D. dissertation, 122 p.**
- _____ 1974, Calcitization of Edwards Group dolomites in the Balcones Fault Zone aquifer, south-central Texas: *Geology*, v. 2, p. 539-362.**
- _____ 1975, On the hydrology of the Edwards Limestone, south-central Texas: *Journal of Hydrology*, v. 24, p. 251-269.**
- Anderson, R. Y., Dean, W. E., Kirkland, D. W., and Snider, H. I., 1972, Permian Castile varved evaporite sequence, West Texas and New Mexico: *Geological Society of America Bulletin*, v. 83, p. 59-86.**
- Bates, R. L., and Jackson, J. A., eds., 1987, Glossary of geology: Alexandria, Virginia, American Geological Institute, 788 p.**
- Brown, D. S., Petri, B. L., and Nalley, G. M., 1992, Compilation of hydrologic data for the Edwards aquifer, San Antonio area, Texas, 1991, with 1934-91 summary: San Antonio, Texas, Edwards Underground Water District, Bulletin 51, 169 p.**

- Brown, T. E., Waechter, N. B., Rose, P. R., and Barnes, V. E., 1983, San Antonio sheet, Geologic Atlas of Texas: The University of Texas at Austin, Bureau of Economic Geology, scale 1:250,000.
- Carr, M. M., 1987, Facies and depositional environments of evaporites of the lower Cretaceous McKnight Formation, Maverick Basin, southwest Texas: The University of Texas at Arlington, Master's thesis, 144 p.
- Collins, E. W., in press, Fracture zones between overlapping en echelon fault strands, outcrop analogs within the Balcones Fault system: Shreveport, Louisiana, Gulf Coast Association of Geological Societies Transactions.
- De la Garza, Laura, and Slade, R. M., 1986, Relations between areas of high transmissivity and lineaments—the Edwards aquifer, Barton Springs segment, Travis and Hays Counties, *in* Abbott, P. L., and Woodruff, C. M., Jr., eds., The Balcones Escarpment, Central Texas: Geological Society of America annual meeting, p. 1–144.
- Domenico, P. A., 1972, Concepts and models in groundwater hydrology: New York, McGraw-Hill, 405 p.
- Driscoll, F. G., 1986, Groundwater and wells: St. Paul, Minnesota, Johnson Division, 1089 p.
- Dunham, R. J., 1962, Classification of carbonate rocks according to depositional texture, *in* Ham, W. E. (ed.), Classification of carbonate rocks: American Association of Petroleum Geologists Memoir 1, p. 62–84.
- Ellis, P. M., 1986a, Diagenesis of the Lower Cretaceous Edwards Group in the Balcones Fault Zone area: The University of Texas at Austin, Ph.D. dissertation, 327 p.
- _____ 1986b, Post-Miocene carbonate diagenesis of the Lower Cretaceous Edwards Group in the Balcones Fault Zone area, south-central Texas, *in* Abbott, P. L., and Woodruff, C. M.,

- Jr., eds., *The Balcones Escarpment, Central Texas: Geological Society of America annual meeting*, p. 101–114.
- Ewing, T. E., and Wilbert, W. P., eds., 1991, *Geology of the Edwards aquifer, description and recommendations: South Texas Geological Society Reprint*, v. 1, variously paginated.
- Fieseler, R. G., Jasek, J., and Jasek, M., 1978, *An introduction to the caves of Texas: Texas Speleological Survey, Guidebook No. 19*, 115 p.
- Freeze, R. A., and Cherry, J. A., 1979, *Groundwater: Englewood Cliffs, New Jersey, Prentice-Hall, Inc.*, 604 p.
- Garza, Sergio, 1966, *Ground-water resources of the San Antonio area, Texas: a progress report on studies 1960–64: Texas Water Development Board Report 34*, 31 p.
- Hammond, W. W., Jr., Longley, Glenn, Pavlicek, D. J., and Ozuna, G. B., 1986, *Hydrology of the Edwards aquifer: San Antonio, Texas, Geological Society of America field trip*, 46 p.
- Hovorka, S. D., 1992, *Halite pseudomorphs after gypsum in bedded anhydrite—clue to gypsum-anhydrite relationships: Journal of Sedimentary Petrology*, v. 62, p. 1098–1111.
- Hvorslev, M. J., 1951, *Time lag and soil permeability in ground-water observations: Vicksburg, Mississippi, U.S. Army Corps of Engineers, Bulletin No. 36*, 50 p.
- Jacob, C. E., 1940, *On the flow of water in an elastic artesian aquifer: American Geophysical Union Transactions*, v. 21, p. 574–586.
- Klemt, W. B., Knowles, T. R., Elder, G. R., and Sleh, T. W., 1975, *Ground-water resources and model applications for the Edwards (Balcones Fault Zone) aquifer: Texas Water Development Board Report*, 93 p.

- Kruseman, G. P., and De Ridder, N. A., 1983, Analysis and evaluation of pumping test data (3d ed.): Wageningen, The Netherlands, International Institute for Land Reclamation and Improvement, Bulletin 11, 200 p.
- Lucia, F. J., 1983, Petrophysical parameters estimated from visual descriptions of carbonate rocks: a field classification of carbonate rock pore space: *Journal of Petroleum Technology*, v. 35, no. 3, p. 629–637.
- Maclay, R. W., 1989, Edwards aquifer in the San Antonio region: its hydrogeology and management: *South Texas Geological Society Bulletin*, p. 11–28.
- Maclay, R. W., and Land, L. F., 1988, Simulation of flow in the Edwards aquifer for the San Antonio region, Texas, and refinement of storage and flow concepts, U.S. Geological Survey Water-Supply Paper 2336-A, 48 p.
- Maclay, R. W., Rettman, P. L., and Small, T. A., 1980a, Hydrochemical data for Edwards aquifer in the San Antonio area, Texas: Texas Department of Water Resources, LP-131, 27 p.
- Maclay, R. W., and Small, T. A., 1976, Progress report on geology of the Edwards aquifer, San Antonio area, Texas, and preliminary interpretation of borehole geophysical and laboratory data on carbonate rocks: U.S. Geological Survey Open-File Report 76-627, 60 p.
- _____ 1986, Carbonate geology and geohydrology of the Edwards aquifer in the San Antonio area, Texas: Texas Water Development Board Report 296, 90 p.
- Maclay, R. W., Small, T. A., and Rettman, P. L., 1980b, Water-level, recharge, discharge, specific-capacity, well-yield, and aquifer-test data for the Edwards aquifer in the San Antonio area, Texas: Texas Department of Water Resources, LP-133, 83 p.
- _____ 1981, Application and analysis of borehole data for the Edwards aquifer in the San Antonio area, Texas: Texas Department of Water Resources, LP-139, 88 p.

- Marquardt, G. L., and Elder, G. R., 1979, Records of wells, chemical analyses, and water levels of selected Edwards wells, Bexar County, Texas: Texas Department of Water Resources, Report 237, 458 p.
- Miller, B. C., 1983, Physical stratigraphy and facies analysis, Lower Cretaceous Maverick Basin and Devils River trend, Uvalde and Real Counties, The University of Texas at Arlington, Master's thesis, 217 p.
- Ogden, A. E., 1986, Hydrogeological and hydrochemical investigations of the Edwards Aquifer in the San Marcos area, Hays County: Southwest Texas State University, Edwards Aquifer Research and Data Center Report, 364 p.
- Ogden, A. E., Spinelli, A. J., and Horton, J., 1985a, Hydrologic and hydrochemical data of the Edwards aquifer in Hays and Comal Counties: Southwest Texas State University, Edwards Aquifer Research and Data Center Report No. R2-85, 83 p.
- _____ 1985b, Hydrologic and hydrochemical data of the Edwards aquifer in Hays and Comal Counties: Southwest Texas State University, Edwards Aquifer Research and Data Center Report No. R1-85, 102 p.
- Pearson, F. J., Rettman, P. L., Jr., 1976, Geochemical and isotopic analyses of waters associated with the Edwards Limestone aquifer, Central Texas: U.S. Department of the Interior Geological Survey Report, 35 p.
- Peck, A. J., 1960, The water table as affected by atmospheric pressure: Journal of Geophysical Research, v. 65, no. 8, p. 2383–2388.
- Proctor, C. V., Jr., Brown, T. E., Waechter, N. B., Aronow, S., Pieper, M. K., and Barnes, V. E., 1979, Seguin sheet, Geologic Atlas of Texas: The University of Texas at Austin, Bureau of Economic Geology, scale 1:250,000.

Proctor, C. V., Jr., Brown, T. E., McGowen, J. H., Waechter, N. B., 1988, Austin sheet, Geologic Atlas of Texas: The University of Texas at Austin, Bureau of Economic Geology, scale 1:250,000.

Reeves, R. D., 1978, Chemical and bacteriological quality of water at selected sites in the San Antonio area, Texas, August 1968-January 1975: San Antonio, Texas, Edwards Underground Water District, 122 p.

Rose, P. R., 1972, Edwards Group, surface and subsurface, Central Texas: The University of Texas at Austin, Bureau of Economic Geology Report of Investigations No. 74, 198 p.

Schlumberger, Ltd., 1989, Log interpretation principles/applications: Houston, Texas, Schlumberger Educational Services, variously paginated.

_____ 1993, Porosity Index from neutron, Table C-18.

Schultz, A. L., 1992, Using geophysical logs in the Edwards aquifer to estimate water quality along the freshwater/saline-water interface (Uvalde to San Antonio, Texas): Edwards Underground Water District Report No. 92-03, 46 p.

_____ 1993, Defining the Edwards aquifer freshwater/saline-water interface with geophysical logs and measured data (San Antonio to Kyle, Texas): Edwards Underground Water District Report No. 93-06, 81 p.

Schultz, A. L., and Waugh, J. R., 1993, Utilizing geophysical log interpretation to determine water quality in the Edwards aquifer of South Texas (abs.): Association of Engineering Geologists, 36th annual meeting, p. 70.

Senger, R. K., and Kreitler, C. W., 1984, Hydrogeology of the Edwards aquifer, Austin area, Central Texas: The University of Texas at Austin, Bureau of Economic Geology Report of Investigations No. 141, 35 p.

- Senger, R. K., Collins, E. W., and Kreitler, C. W., 1990, Hydrogeology of the northern segment of the Edwards aquifer, Austin region: The University of Texas at Austin, Bureau of Economic Geology Report of Investigations No. 192, 58 p.
- Sieh, T. W., 1975, Edward (Balcones Fault Zone) aquifer test well drilling investigation: Texas Water Development Board, Water Availability Division, 117 p.
- Smith, C. I., 1964, Physical stratigraphy and facies analysis, Lower Cretaceous limestones, Edwards Plateau, West Texas: Houston, Texas, Shell Development Company, EPR Special Report No. 45, 138 p.
- Technical Advisory Panel, 1990, Technical factors in Edwards aquifer use and management, *in* Krier, C. T., and Smith, Terral, co-chairs, committee report to the 72nd Legislature: Austin, Texas, Special Committee on the Edwards aquifer, variously paginated.
- Waechter, N. B., Lozo, F. E., Jr., and Barnes, V. E., 1977, Del Rio sheet, Geologic Atlas of Texas, Robert Thomas Hill Memorial Edition: The University of Texas at Austin, Bureau of Economic Geology, scale 1:250,000.
- Warren, J. K., 1982, The hydrological setting, occurrence, and significance of gypsum in late Quaternary salt lakes in South Australia: *Sedimentology*, v. 29, p. 609–637.
- Wagh, John, 1993, Unpublished maps of 1989 and 1993 water-level data.
- Weeks, Edwin, 1979, Barometric fluctuations in wells tapping deep unconfined aquifers: *Water Resources Research*, v. 15, no. 5, p. 1167–1176.
- Wermund, E. G., Cepeda, J. C., and Luttrell, P. E., 1978, Regional distribution of fractures in the southern Edwards Plateau and their relationship to tectonics and caves: The University of Texas at Austin, Bureau of Economic Geology Geological Circular 78-2, 14 p.

Woodruff, C. M., 1989, Lineaments and the Edwards aquifer—Barton Springs segment, Travis and Hays Counties: Southwest Texas State University, Edwards Aquifer Research and Data Center Report No. R1-89, 45 p.

Woodruff, C. M., and Abbott, P. L., 1986, Stream piracy and evolution of the Edwards aquifer along the Balcones Escarpment, Central Texas, *in* Abbott, P. L., and Woodruff, C. M., Jr., eds., The Balcones Escarpment, Central Texas: Geological Society of America annual meeting, p. 77–100.

GLOSSARY*

Acre-feet — amount of water that would cover one acre (43,560 ft²) to a depth of one foot (approximately 326,000 gal.).

Aquifer — a formation, group of formations, or part of a formation that both transmits and stores water in pore space and contains sufficient saturated permeable material to yield economic quantities of ground water to wells and springs.

Aquifer test — a field method for determining permeability and storativity on the basis of withdrawal of measured quantities of water from or addition of water to a well and measurement of resulting changes in hydraulic head in the aquifer.

Argillaceous — containing or largely composed of clay-sized particles or clay minerals.

Barometric efficiency — ratio of the response of water level in a well in a confined aquifer to change in atmospheric pressure (dimensionless).

*Modified from definitions given in Driscoll (1986) and Jackson and Bates (1987).

Borehole — a generally cylindrical hole in the earth made by drilling for the purpose of extracting liquids such as ground water and petroleum or for measuring subsurface geologic characteristics.

Capillary pressure test — a laboratory method for determining porosity and pore size distribution of rock samples, usually small cylinders taken from core obtained from a borehole.

Confined aquifer — an aquifer in which ground water is isolated from the atmosphere and bounded above and below by (confining) beds of low permeability that retard movement of water into or out of the aquifer, in which water is added to or released from storage in pore space by change in water pressure rather than by filling or draining of pore water; the confined part of the Edwards aquifer lies entirely in the subsurface and is confined by the overlying Del Rio Clay and the underlying Glen Rose Formation.

Confined ground water — subsurface water in a confined aquifer; the division between confined and unconfined ground water is gradational; confined water is called artesian water where the potentiometric surface or the aquifer is above land surface and flowing wells or springs are present.

Dedolomitization — diagenetic process by which dolomite in contact with ground water containing very small ratios of dissolved magnesium to calcium is replaced by calcite, usually increasing in porosity.

Diagenesis — chemical and physical changes undergone by a sediment after its deposition and burial, usually involving compaction and mineral solution and precipitation, exclusive of metamorphism at elevated temperature and pressure.

Discharge — loss or removal of ground water from an aquifer such as by movement to surface water in springs and seeps at topographically low elevations, pumping from wells, evaporation at a shallow water table, or transpiration by plants.

Dolomitization — diagenetic process by which calcite (CaCO_3) is wholly or partly converted to dolomite ($\text{CaMg}(\text{CO}_3)_2$).

Effective porosity — percentage of the bulk volume of a rock that is occupied by pore spaces that are interconnected and through which subsurface fluid can move; effective porosity, therefore, is less than total porosity.

En echelon — an overlapping or staggered arrangement, for example, of faults, in which the orientation of individual features is at an angle to that of the zone as a whole.

Geographic Information System — computer programs with which spatial data are compiled, sorted, retrieved, analyzed, transformed, and displayed.

Harmonic (Fourier) analysis — a method for determining frequency and amplitude characteristics of observed periodic data by comparison with a mathematical function consisting of an infinite series of summed sine and cosine terms.

Heterogeneity — nonuniformity in structure or composition with properties, for example, permeability and porosity, that vary with position.

Highstand — interval of time during one or more cycles of relative change of sea level when sea level is at its highest level above the shelf edge.

Hydraulic head — a representation of the potential energy per unit weight of ground water, consisting of gravitational, pressure, and velocity components and expressed in units of length; hydraulic head is determined in an unconfined aquifer by the elevation at which water is observed in a borehole and in a confined aquifer by the pressure of ground water and the elevation of the measurement point.

Hydrograph — time record of the fluctuation of hydraulic head of ground water as monitored in a borehole.

Hypersaline — excessively saline, with salinity substantially greater than that of sea water.

Intertidal — depth zone in a marine environment between high water and low water.

Karst — a type of topography that is formed by solution of limestone, gypsum, and other rocks by ground water and that is characterized by sinkholes and caves; also the process of solution of limestone, gypsum, and other bedrock that enlarges pore space in the subsurface in a karst environment; also the resulting rock characteristics.

Matrix — the solid skeleton of a porous medium: a granular matrix is an assembly of solid mineral grains separated and surrounded by pores, voids, or interstices; matrix porosity is the fine porosity between crystals or grains as contrasted with larger fractures and vugs.

Moldic pores — pores resulting from the removal, usually by solution, of an individual constituent of a rock, for example, a fossil skeleton.

Neutron log (scaled/unscaled) — recording of induced neutron reactions measured versus depth in a borehole, especially sensitive to hydrogen content.

Permeability — property or capacity of a granular or fractured medium for transmitting a fluid, which relates the rate of fluid flow to the imposed gradient in hydraulic head (units of L/T); used in this report as a synonym for hydraulic conductivity, which depends not only upon the properties of the porous medium but also upon the kinematic viscosity of the fluid.

Porosity — ratio of the bulk volume of a rock that is occupied by pore space or interstices, whether isolated or interconnected; usually stated as a percentage.

Potentiometric surface — an imaginary two-dimensional surface representing the total (static) hydraulic head of ground water of constant density and defined by the levels to which water will rise in a cased borehole open to the aquifer.

Recharge — the addition of water to the zone of saturation in an aquifer; also the amount of water added.

Resistivity log — recording of electrical resistivity of rock and contained fluids measured versus depth in a borehole.

Rudist — a bivalved mollusk belonging to the superfamily Hippuritacea, characterized by an inequate shell, usually attached to a substrate and forming mounds or reefs during the Cretaceous period.

Sabkha — a supratidal environment of sedimentation formed under arid to semiarid conditions on restricted coastal plains and characterized by evaporite-salt, tidal-flood, and eolian deposits.

Specific storage — storativity per unit thickness of an aquifer, with dimensions of [1/L].

Storativity — volume of water released from or taken into a column of aquifer with unit cross-sectional area under unit decline in hydraulic head (dimensionless); also called storage coefficient.

Subtidal — depth zone in a marine environment below low tidal level and below the intertidal zone.

Supratidal — depth zone in a marine environment just above high tide level and above the intertidal zone.

Transgressive — produced by a relative rise of sea level that brings offshore, typically deep-water environments to areas formerly occupied by nearshore, typically shallow-water conditions.

Unconfined aquifer — an aquifer where the water table forms the upper boundary and is exposed to the atmosphere through openings in overlying material, in which water is added to or released from storage by filling or draining of pore space; the unconfined part of the Edwards aquifer mainly lies within the geologic outcrop of the Edwards Group.

Well log — recording of measured or computed physical, chemical, or electrical characteristics of a rock section measured versus depth in a borehole.